8-2010

Seasonal Energy and Water Balance of a *Phragmites Australis*-Dominated Wetland in the Republican River Basin (Southwestern Nebraska, USA)

Gregory J. Cutrell
University of Nebraska - Lincoln, greg.cutrell@gmail.com

Acknowledgements

I would like to thank the Nebraska Environmental Trust (NET), the Nebraska Water Resources Advisory Panel (WRAP), and the University of Nebraska Rural Initiative for providing funding for this project, as well as the School of Natural Resources at the University of Nebraska-Lincoln (UNL) for funding my research assistantship. I would like to thank and acknowledge my committee: John Lenters (major advisor), Dean Eisenhauer, Ayse Irmak, and Erkan Istanbulluoglu. The principle investigators that established this project are Durelle Scott, Erkan Istanbulluoglu, and John Lenters, and without them, this Thesis would not be possible.

I would like to acknowledge that this study could not have been completed without the help of many people. Before arrival on this project, hours of hard work was put into testing and setting up instrumentation by Durelle Scott, Kyle Herrman, Evren Soylu, Tiejun Wang, Steven Walters, Kenneth Von Buettner, and John Lenters. I like to thank Betty Walter-Shea, David A. Wedin, Bryan Leavitt, and the other faculty and graduate students in the School of Natural Resources for the comments, information, and critiques that were given to me throughout my time at UNL. I would also like to acknowledge Shashi Verma, Andy Suyker, Dan Hatch for providing the eddy covariance data from the Mead site, as well as the High Plains Regional Climate Center for the AWDN data, the National Climatic Data Center (NCDC) for the COOP climate data, and the U.S. Geological Survey for the Landsat-5TM imagery. I would also like to thank Don Brown from Campbell Scientific and both Martin Veenstra and Victor Cassella from Kipp & Zonen for the technical help with instrumentation. I am very grateful of the help

from Evren Soylu and Steven Walters in the field throughout the 2009 growing season, as without them, this study could not have been completed. I am also very grateful for the guidance, education, and help from my advisor John Lenters, without whom I would have not have become the scientist and researcher I am today. Finally, I would like to thank my family and fiancée Erin Ball for always supporting me throughout my time at UNL.

Table of Contents

List of Figures

List of Tables

List of Acronyms and Symbols

a	atmospheric air
A	area
AM	April and May monthly averages
AWDN	Automated Weather Data Network
BREB	Bowen Ratio Energy Budget (W m^{-2})
c	canopy
$C_{\langle E \rangle}$	mass transfer coefficient (-)
$C_{\langle H \rangle}$	heat transfer coefficient (-)
Cp	specific seat (J kg^{-1} °C^{-1})
C_n^2	structure parameter of the refractive index of air ($m^{-2/3}$)
C_T^2	structure parameter of temperature (K^2 $m^{-2/3}$)
D	aperture diameter (m)
d	zero-displacement height (m)
Δz	change in depth (m)
DGPS	Differential Global Position System
DOY	Day Of Year
dr	inverse square of the earth-sun distance (astronomical units)

dx	transect Length (m)
e	vapor pressure (Pa)
EC	Eddy-covariance
E_{sun}	mean solar exoatmospheric irradiance (W m^{-2} $ster^{-1}$ μm^{-1})
ET	evapotranspiration (mm day^{-1})
ET_{ref}	reference evapotranspiration
EVATION	EVApoTranspiratION
Fr	fraction of vegetation
f_T	universal stability function (-)
g	gravitational acceleration (~9.8 m s^{-2})
GW_{net}	net groundwater flux
h	height (m)
H	sensible heat flux (W m^{-2})
LE	latent heat flux (W m^{-2})
H	sensible heat flux (W m^{-2})
JJA	June/July/August monthly averages
K	volumetric heat capacity (M Jm^{-3} K)
K	temperature in Kelvin
k_v	van Kármán constant (=0.4)
l	latent heat of vaporization (MJ kg^{-1})
L	spectral radiance (W m^{-2} $ster^{-1}$ μm^{-1})
LAI	Leaf area index
L_{mo}	Monin-Obukhov length (m)
Lw	downward longwave radiation (W m^{-2})
LAS	Large Aperture Scintillometer
N	Harbeck area relationship
$NDVI$	Normalized Difference Vegetation Index
NIR	spectral reflectance in Near-Infrared spectrum
P-T	Priestley-Taylor equation
P	precipitation
p	pressure (Pa)
PET	Potential EvapoTranspiration
ΔQ	change in water storage (m)
QC	Quality Control
Q_{cal}	quantized calibration pixel
r	planetary reflectance
r	correlation coefficient
RED	spectral reflectance in red spectrum
RH	Relative Humidity (%)
Rn	net radiation (W m^{-2})
R_{net}	Net overland waterflow
$\Delta S/\Delta t$	heat storage rate (W m^{-2})
s	soil
S	slope of saturation vapor pressure ($kPaC^{-1}$)
SigDemod	variance of electromagnetic intensity ($Volts^2$)
SigPUCn2	scaled structure parameter of the refractive index ($Volts^2$)

SO	September and October monthly averages
Sw	downward shortwave radiation (W m^{-2})
ΔT	change in air temperature (°C)
T	air temperature (°C or K)
T^*	temperature scale (K)
u_*	friction velocity (m s^{-1})
veg	vegetation
w	water
z_{LAS}	effective height (m)
z_o	roughness length (m)
α	Priestley-Taylor constant (1.26)
β	bowen ratio (-)
ρ	density (kgm^{-3})
σ	Stephan Boltzmann constant (W m^{-2} K^{-1})
σ_{lhI}^2	variance of natural logarithm of intensity fluctuations
γ	psychometric constant (k Pa C^{-1})
τ	albedo (-)
θ_s	solar zenith angle (degrees)

Chapter 1

General Introduction

In 1943, the states of Colorado, Nebraska, and Kansas signed the Republican River Compact to define the allocation of the water within the Republican River basin. Since then, the agriculture economy has grown throughout Nebraska, bringing along with it irrigation to maximize crop yield. The number of registered wells increased from 1200 in 1936 to approximately 100,000 in 2005 (Flowerday et al., 1998; Hovey, 2005). From 1999 to the present, Nebraska has faced legal challenges from Kansas over the excessive use of water within the basin. One important outcome of these challenges has been the resolution that Nebraska's water allocation will not just be limited to surface water withdrawals, but rather groundwater pumping in Nebraska and its effect on the Republican River flow will also be considered (State of Kansas v. State of Nebraska and State of Colorado, 2000).

Under pressure from Kansas to shut down irrigation wells and pay $73 million in 2007 for damages due to the breach of the compact, Nebraska attempted to increase streamflow in the Republican River by removing invasive plant species along the riparian corridors of the Republican (and Platte) River. Nebraska legislature passed a bill (Legislative Bill 701) allotting $2 million each year for the removal of various invasive species (*Phragmites australis*, or common reed, *Tamarix ramosissima Ledeb*, or saltcedar, and *Elaeagnus angustrifolia L*, or Russian olive) along the riparian areas of the Republican River during 2007 and 2008.

This current study is part of a larger project to better understand the effects of removing *P. australis* on the carbon balance, water quality and quantity, and stream ecology within the Republican and Platte River basins. Earlier work has already found that *P. australis* sequesters significantly more carbon than native vegetation (and open water areas), and so the removal of *P. australis* is not necessarily a good idea from the perspective of the carbon sequestion (Walters, 2010). Also, it was found in a controlled greenhouse study and field scale herbicide treatment of riparian vegetation, that the use of herbicides in an isopropylamine salt form resulted in an increased ammonium flux that could adversely impact adjacent aquatic ecosystems (K. Herrman, personal communication, 8 July 2010).

For the purposes of this thesis, the main goal is to calculate the rate of evapotranspiration from *P. australis* in a riparian wetland setting within the Republican River basin (Chapter 2) and thereby examine the potential "water savings" effect of removing *P. australis* from the riparian corridors. In general, one might expect the removal of *P. australis* should increase surface infiltration through decreased plant interception, as well as decrease the amount of transpired water that is withdrawn from the high water table of the riparian zone. The response to vegetation removal, however, ultimately depends on what takes the place of the invasive plant species (e.g., native plants, open water, bare soil), as well as other non-linear effects such as subsequent changes in the water table depth. The removal of vegetation to decrease water loss (i.e., mesquite, salt cedar, giant cane, and other woody species) within riparian corridors has been practiced successfully throughout the southwestern and western US (Jones and Gregory, 2008). It has been found that the removal of mesquite, a small deciduous tree,

in Texas lead to an 11% reduction in ET (Saleh et al., 2008), while daily ET decreased by 0.12 mm when removing salt cedar (Dugas et al., 1998). Contrary to other vegetative removals, Burba et al. (1999a) found that the averaged water evaporation was 8% (0.3 mm day-^{1}) larger than *P. australis* ET. Previous have also found that *P. australis* ET rates can reach 6.9 mm day^{-1} (Smid, 1974), 6.5 mm day^{-1} (Burba et al., 1999), 6.3 mm day^{-1} (Fermor et al., 2001), 5.0 mm day^{-1} (Peacock and Hess, 2004), and 5.8 mm day^{-1} (Zhou and Zhou, 2009). Transpiration studies of *P. australis* have found maximum rates of ~9.5 mm day^{-1} (Sánchez-C et al., 2004) in Spain and 10 mm day^{-1} in Germany (Herbst and Kappen, 1999). Once the ET is estimated for the wetland, the data will be later used to help calibrate and validate a regional water balance model of the Republican River basin and the entire state of Nebraska.

In addition to the "water savings" aspects of this research, we are also interested in understanding the basic energy and water balance of *P. australis* (Chapter 2). The seasonal energy balance can demonstrate how net radiation, heat storage, latent heat, and sensible heat are partitioned over *P. australis* and how they change in response to plant growth and climate variability throughout the year. In terms of instrumentation, we use relatively new technology (a Large Aperture Scintillometer) to directly measure the sensible heat flux, as well as net radiometers and soil/water temperature probes to measure the net radiation and ground heat storage. Latent heat flux is then calculated from the energy balance and converted to a rate of evapotranspiration. In terms of the water balance, the measured ET and precipitation rates are then compared with changes in water level to determine the relative influence of groundwater.

To assess the potential impact of *P. australis* removal, we compare the observed ET rates with those of native plants (using in situ and remote sensing data; Chapter 3), as well as with a hypothetical "open water" surface (using a simple mixed-layer evaporation model; Chapter 4). This provides a preliminary idea of the potential change in ET that might result from the replacement of *P. australis* by at least two other land cover types. Finally, Chapter 5 provides a general summary of the conclusions from this thesis.

Chapter 2

Energy and Water Balance Over *Phragmites australis*

2.1 Introduction

The management of water resources is becoming more important across the world as the population grows and climate changes. The need to improve our understanding of the global and regional water balance is readily apparent, particularly in the presence of changes in land use and climate. Current studies of the water balance include efforts to understand how available surface water resources such as lakes and rivers are changing with climate and human use. Surface water is important for human usages such as drinking water, irrigation, industry, ecosystems, and hydro-power. Lakes and rivers are directly connected with atmospheric processes, but they are also linked to groundwater recharge and aquifers that provide water for drinking and irrigation. Understanding the effects of climate and land use on surface and groundwater resources requires a close examination of both the energy and water balance of the land-atmosphere system.

In regions of the world such as the U.S. Great Plains, irrigated agriculture and other "consumptive uses" play a significant role in the regional water balance. Surface and groundwater supplies have become stressed as agricultural producers strive to increase crop yield in water-limited regions. The Republican River basin, which occupies portions of Colorado, Nebraska, and Kansas (Figure 1), is an example of a region that has been significantly impacted by the use of surface water and groundwater

for irrigation. In response to an extended drought during the 1930's and a devastating flood in 1935, a compact was declared in 1943 among the states within the Republican River basin. The compact designates how the river water should be apportioned by using an availability-to-consumption ratio for each state. Since the compact's initiation, flood and center pivot irrigation has gained widespread use in Nebraska to maximize crop yields and overall agricultural production. Over the decades, Nebraska has continued to drill irrigation wells and has faced legal challenges from Kansas in association with reductions in Republican River streamflow (Kansas Department of Agriculture, 2010). Several studies have investigated the causes for declining streamflow in Nebraska (Szilagyi, 1999; Szilagyi, 2001; Burt et al., 2002; Wen and Chen, 2006). It was found that changing climatic influences such as precipitation and temperature could not explain the decrease in streamflow (Szilagyi, 1999; Wen and Chen, 2006) or runoff depletion (Szilagyi, 2001) and rather caused by human activities such as crop irrigation, change in vegetative cover, water conservation practices, and the construction of reservoirs. It was later determined through statistics and modeling that there was a significant relationship between increasing irrigation wells and decreasing streamflow (Burt et al., 2002; Wen and Chen, 2006).

In an attempt to increase streamflow in the Republican River and improve stream function and biodiversity, the state of Nebraska began removing invasive plant species along of the riparian corridors of the Republican and Platter River in 2007. The intent of this vegetation removal campaign was at least threefold: 1) Decrease consumptive use of water along the Republican River by reducing riparian evapotranspiration, 2) Remove invasive species to help restore native vegetation and biodiversity, and 3) Remove

vegetation along stream channels and bars to improve stream function, ecology, and habitat for birds and other wildlife. Other states have undertaken similar vegetation removal campaigns for similar reasons (Monteiro et al., 1999; Wilcox and Whillans, 1999; Grothues and Able, 2003; Kiviat, 2006; Virginia DCR, 2007). In Nebraska, the primary plant species targeted for removal (primarily through spraying of herbicide) were *Phragmites australis* (Common Reed), *Tamarix* (Salt Cedar), and *Elaeagnus angustifolia* (Russian Olive). All of these plant species (particularly *P. australis*) are prevalent not only in the Republican River basin, but others as well (e.g., the Platte River Basin).

In the current study, we examine the potential "water savings" effect of removing *P. australis* from the riparian corridors of the Republican River basin. This study is part of a broader project that has also examined the impacts of *P. australis* removal on water quality and stream ecology (Herman, 2010; Walters, 2010). Our primary objective here is to understand the consumptive use of water by *P. Australis* – i.e., the rate of evapotranspiration (ET) – in a saturated, wetland environment within the Republican River basin. Doing so requires not only an understanding of the surface water balance, but also the energy balance, as latent heat flux can play a particularly significant role. The surface energy balance can be written as

$$Rn + LE + H = \Delta S, \qquad (1)$$

where Rn is net radiation, LE is latent heat flux, H is sensible heat flux, and ΔS is the total rate of heat storage in the "ground" (vegetation canopy, surface water, soil, etc.) The sign convection in Equation 1 is such that "positive" denotes heat fluxes "into the ground." Equation 1 can be rearranged to solve for the latent heat flux:

$$LE = \Delta S - Rn - H, \qquad (2)$$

which results in estimates of *LE*, so long as *H* can be measured independently (e.g., through eddy covariance estimates or large aperture scintillometery). Often the sensible heat flux is estimated in conjunction with the Bowen ratio through

$$H = \beta * LE, \qquad (3)$$

which in combination with Equation 1, leads to the Bowen Ratio Energy Budget (BREB) estimate of latent heat flux:

$$LE = -\frac{Rn - \Delta S}{1 + \beta}. \qquad (4)$$

The Bowen ratio is then estimated independently through surface air temperature and vapor pressure gradients (Fritschen, 1966; Guo and Schuepp, 1994; Lenters et al., 2005).

Previous studies have used various methods and instrumentation to determine the rate of ET for *P. australis*, such as the BREB method (Smid, 1975; Burba et al., 1999; Sánchez-C et al., 2004; Peacock and Hess, 2004), a phytometer (Fermor et al., 2003), measurements of sap flow (Moro et al. 2002), and the eddy-covariance (EC) method (Zhou and Zhou, 2009). Jia et al. (2009) also applied a model based on the energy budget using MODIS satellite data to simulate the rate of ET from *P. australis* over the Yellow River Delta in China. It is important to note that regional variations in vegetation, climate, and water availability play an important role in determining the rate of ET in studies such as these. For example, while the study by Burba et. al (1999a) was also conducted in Nebraska, it was located in a wetland in the Sandhills, where the climate, vegetation, and soil type is slightly different. Some of the other studies were conducted in significantly different locales (e.g., England, China, Spain, and Czechoslovakia).

In the current study, we use a Large Aperture Scintillometer (LAS), which calculates H directly, to then calculate LE from Equation 2. For comparison purposes,

we also estimate ET rates using the Priestly-Taylor formula, which is essentially a simplified version of the BREB method (Equation 4). While the EC method is a popular and well-tested methodology for measuring ET, the EC method is not suitable in areas of significant spatial heterogeneity (such as narrow riparian systems with varying vegetation height) and often has problems with energy balance closure (Twine et al., 2000). LAS systems have been tested against EC systems over homogenous and heterogeneous land types and have been found to be a reliable and accurate method for estimating ET (Chehbouni et al., 2000; Hoedjes et al., 2002; Meijinger et al., 2006; Ezzahar et al, 2007; Kleissl et al., 2008).

The primary goal of this study is to estimate the rate of ET from *P. australis* during the 2009 growing season for a riparian wetland in south central Nebraska. We are also interested in understanding the relative roles of meteorology and vegetation phenology on ET rates, the seasonal variability in the surface energy and water balance, and the impacts of herbicide spraying on ET rates. (The wetland was sprayed in mid July of 2009 to assess the impact of vegetation removal. In addition to the late season response during 2009, we are continuing to monitor the wetland through the 2010 growing season to assess the longer-term impacts of vegetation removal.) The site description, instrumentation, methodology, and quality assurance techniques are discussed in sections 2.2-2.5. The energy budget results and the basic climatology of the site during the 2009 season is discussed in section 2.6, followed by discussion and conclusions in section 2.7.

2.2 Site Description

Our wetland study site is located approximately 16 kilometers east of Cambridge, Nebraska and 600 meters north of the main stem of the Republican River (Figure 1). The wetland is located at an elevation of 640 meters above mean sea level in a predominantly agricultural watershed. A sparse stand of cottonwood trees surrounds the wetland, which is relatively long and narrow (approximately 1000 meters in length, and varying in width from about 5 meters in the western end to 60 meters in the central and eastern portions). The wetland receives some flowing water from an exposed spring in the far western edge but otherwise experiences very little surface flow, with most of the water entering and leaving through groundwater seepage. Significant irrigation occurs in the surrounding fields during portions of the summer, and water is also occasionally transferred out of the east end of the wetland through an ephemeral stream during periods of higher water level. The surface is occupied by 52% of the invasive *Phragmites australis* (Common Reed), 31% native *Typha latifolia* (Cattail), 8% native *Juncus effuses* (Common Rush), and 9% open water. The plant community is very tall and dense in most areas, with *P. australis* growing to approximately 4.2 meters at its maximum height. The wetland soil is mostly comprised of clay.

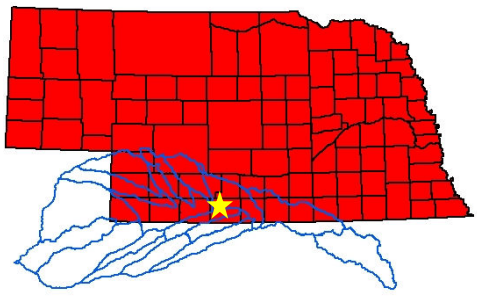

Figure 1. Location of the study site (star) in south-central Nebraska (red) within the Republican River basin (blue). The site latitude and longitude are 40°17.91' N and 99°57.90' W.

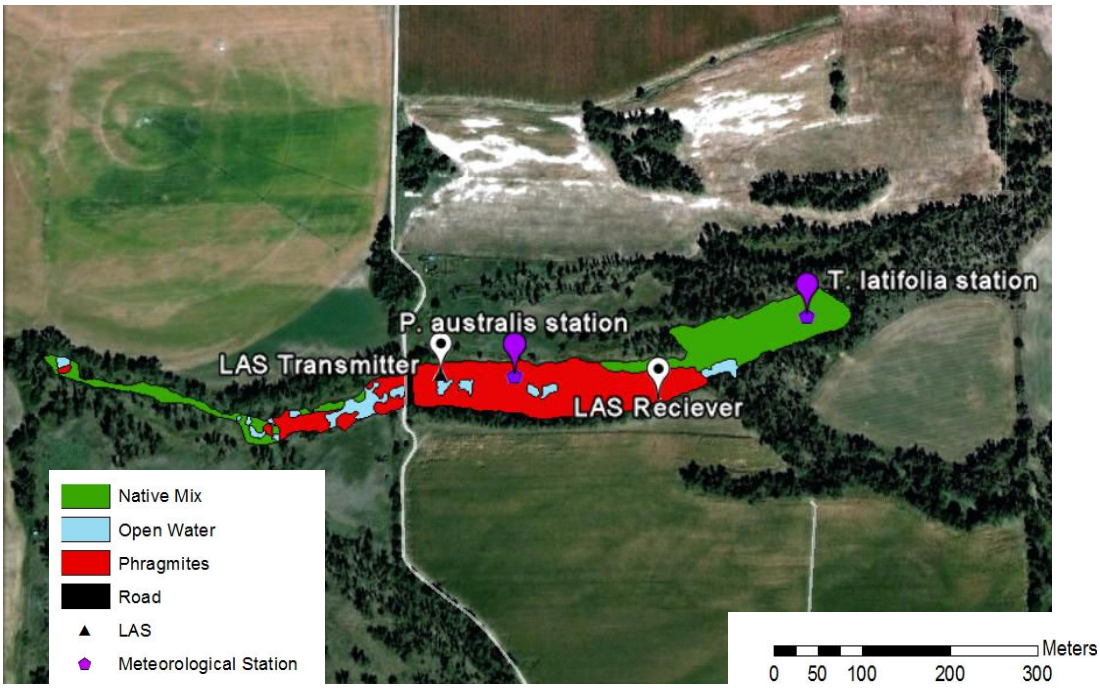

Figure 2. Wetland map showing land cover classification and locations of the LAS transmitter, LAS receiver, and two meteorological stations.

2.3 Instrumentation

A meteorological tower located near the midpoint of the invasive *P. australis* vegetation (see Figure 2) was installed in the wetland to monitor the surface energy and water balance, as well as basic meteorology. The tower is 6.3 meters tall at its maximum height and located in a dense *P. australis* area 20 meters away from the northern edge and 40 meters away from the southern edge of the wetland. The meteorological station consists of a Campbell Scientific CR3000 datalogger, barometric pressure sensor (Setra 278), net radiometer (Kipp & Zonen CNR2), pyranometer (Kipp & Zonen CMP3), propeller anemometer (R.M. Young 05106 marine version), precision infrared temperature sensor (Apogee IRR-P), tipping bucket rain gauge (Texas Electronic TE525MM), two ventilated temperature/relative humidity probes separated vertically by

1.8 m (R.M. Young 41372VC with NIST temperature calibration to 0.01 °C), and a non-aspirated temperature/relative humidity sensor within the vegetation canopy (Vaisala HMP45C). Table 1 lists the measurements heights and maximum uncertainty for each of the various instruments. A digital camera (Campbell Sci. CC640) and measurement rod with 10-cm gradations were also installed to estimate the daily plant height and weather conditions. Periodic LAI measurements of the *P. australis* were made over the course of the growing season using an LAI-2000 (LI-COR Biosciences).

Measurement	**Height (m)**	**Maximum uncertainty**
Wind speed	6.3	1 % or ($\geq \pm 0.3$ ms^{-1})
Wind direction	6.3	± 3°
Upper aspirated temperature/RH	5.9	± 0.01 °C, ± 4% RH
Lower aspirated temperature/RH	4.1	± 0.01 °C, ± 4% RH
Canopy temperature/RH	2.2	± 0.4 °C, ± 3% RH
Net radiation	5.0	± < 10% daily
Radiometric surface temperature	5.0	± 0.5 °C
Incoming solar radiation	5.8	± 10% daily
Barometric pressure	3.2	± 2.5 hPa
Digital camera	4.9	NA
Rainfall rate	4.2	+0,-5% (20 to 30 mm/hr)
Soil/water temperature	~0.5 to -0.75	± 0.2 °C
Soil specific heat	NA	5%
Thermal conductivity	NA	5%

Table 1. Measurement heights (m) of the meteorological instruments at the *P. australis* station relative to the soil/water interface. Also shown are the estimated maximum uncertainties (from manufacturer specifications).

Two sets of continuous water level measurements were obtained in the wetland using a Level TROLL 300 transducer (In-Situ, Inc.) and an SR50A sonic ranging sensor (Campbell Scientific). Six HOBO temperature probes (U23-003 2x External Temperature Data Logger; Onset Computer Corporation) were installed on stakes and driven into the ground near each of the two meteorological stations to measure the soil and water heat storage rates. Three probes measured water temperature at +15 cm, +45 cm, and the

surface (i.e., floating), while three probes measured soil temperature at -15 cm, -45 cm, and -75 cm depth. Finally, a KD-2 PRO (DECAGON) was used to measure the specific heat and thermal conductivity of the soil.

A Kipp & Zonen Large Aperture Scintillometer (LAS), which consists of a transmitter and receiver, was installed in the *P. australis* portion of the wetland to measure sensible heat flux. The LAS was aligned along a transect that placed the meteorological station at roughly the midpoint of the cross-section (Figure 2). The transmitter was mounted in the wetland on a steel tower at a height of 4.8 meters above the soil/water interface, while the receiver was mounted on a tripod on the north bank of the wetland at a height of 4.2 meters. The LAS receiver measured the fluctuations in beam intensity, which were then recorded at one-second intervals by a Campbell Scientific CR1000 datalogger and averaged to ten-minute values. Computer software provided by Kipp & Zonen (known as "EVATION" – from "EVApoTranspiratION") was used to calculate sensible heat flux in conjunction with ten-minute data from the *P. australis* meteorological and soil monitoring stations (i.e., the upper and lower air temperature, upper relative humidity, barometric pressure, wind speed, heat storage rate, and net radiation).

All measurements from the *P. australis* and *T. latifolia* meteorological stations were sampled every ten seconds and averaged to 10-minute, hourly, and daily means. Daily minimum and maximum values were also recorded. The HOBO soil/water temperature sensors were set to sample every 20 minutes, while the Level TROLL 300 transducer sampled at 15-minute intervals. Occasional spurious data points in the HOBO temperature record were removed and a 3-sample running mean was applied to smooth

the time-series before calculating rates of temperature change for use in the heat storage equation.

2.4 Methodology

2.4.1 *Surface Energy Budget*

In this study, we apply the surface energy balance (Equation 1) and LAS-based measurements of sensible heat flux (Equation 2). Net radiation is measured with a Kipp & Zonen CNR2 net radiometer, while the rate of heat storage in the wetland is measured using multiple temperature sensors at various heights through the canopy, water, and soil column (Figure 3). Although heat storage in the vegetation canopy is often ignored, it is estimated here for the completeness since *P. australis* is very tall and dense. The total rate of heat storage in the wetland ($\Delta S/\Delta t$) is calculated as the sum of the heat storage from four separate layers: 1) the vegetation/air canopy (with variable vegetation height), 2) the water layer (also of variable height), 3) the upper 60-cm soil layer, and 4) deep soil heat flux beneath the 60-cm depth layer. As diagrammed in Figure 3, each layer contains 1-2 temperature sensors, with the water layer having a floating sensor at the water surface. The soil temperature sensors are separated by a fixed 30-cm interval, and a deep soil heat flux is calculated from the temperature gradient across the bottom two layers. Measurements of soil volumetric heat capacity where made at five locations throughout the wetland and when averaged together yielded a value of 3.435 (assumed constant through the various soil layers). A single Vaisala HMP45C (mounted in a radiation shield) was used to measure the canopy air temperature.

Mathematically, the rate of total heat storage change in the wetland can be written as

$$\frac{\Delta S}{\Delta t} = \left(\frac{\Delta S}{\Delta t}\right)_{canopy} + \left(\frac{\Delta S}{\Delta t}\right)_{water} + \left(\frac{\Delta S}{\Delta t}\right)_{uppr\ soil} + \left(\frac{\Delta S}{\Delta t}\right)_{deep\ soil}, \qquad (5)$$

where

$$\left(\frac{\Delta S}{\Delta t}\right)_{canopy} = \left(\rho_{\langle w\rangle} \cdot h_{\langle a\rangle} \cdot Cp_{\langle a\rangle} \cdot \frac{\Delta T_{\langle a\rangle}}{\Delta t}\right) + \left(biomass_{\langle veg\rangle} \cdot Cp_{\langle veg\rangle} \cdot \frac{\Delta T_{\langle veg\rangle}}{\Delta t}\right), \qquad (6)$$

and

$$\left(\frac{\Delta S}{\Delta t}\right)_{water} = \left(\rho_{\langle w\rangle} h_{\langle w\rangle} \cdot Cp_{\langle w\rangle} \cdot \frac{\Delta T_{\langle w\rangle}}{\Delta t}\right), \qquad (7)$$

and

$$\left(\frac{\Delta S}{\Delta t}\right)_{soil} = \left(h_{\langle s\rangle} \cdot VHC_{\langle s\rangle} \cdot \frac{\Delta T_{\langle s\rangle}}{\Delta t}\right), \qquad (8)$$

and

$$\left(\frac{\Delta S}{\Delta t}\right)_{deep} = K \cdot \left(\frac{\Delta T_{\langle 75cm-45cm\rangle}}{\Delta z_{\langle 75cm-45cm\rangle}}\right), \qquad (9)$$

where $s, w, a,$ and veg represent the soil, water, air, and vegetation parameters, ρ (kg m^{-3}) is the density, h (m) is the height of the storage layer, VHC (MJ m^{-3} K) is the volumetric heat capacity of the soil, Cp (MJ k g^{-1} °C^{-1}) is the specific heat of for $s, w, a,$ and veg, K (W m^{-1} °C^{-1}) is the soil thermal conductivity, $\Delta T/\Delta t$ is the temporal rate of change in temperature, $\Delta T/\Delta z$ (m) is the vertical temperature gradient, and brackets indicate a depth-weighted vertical average. VHC and Kwere derived from five soil samples with a mean and standard deviation for $VHC$of 3.435 and 0.298 MJ k g^{-1} °C^{-1} of 0.995 and 0.219 W m^{-1} °C^{-1} for K.

Although the specific heat for *P. australis* was not measured directly, a value of 2700 J kg^{-1} $°C^{-1}$ for general vegetation was used (Thom, 1975; Moore and Fisch, 1986; Chen et al., 2007; Higuchi et al., 2007). The fresh vegetation biomass was estimated from measurements of maximum dry biomass, leaf area index (LAI), and an average percent water content of 86% at full growth (Smart and Bingham, 1974; Pelleschi et al., 1997). To represent the *P. australis* phenology, a polynomial fit from the LAI was used to scale the maximum fresh biomass accordingly throughout the growing season. The maximum dry biomass (measured at the end of the season) was found to be 5018 g m^{-2} (average of five samples).

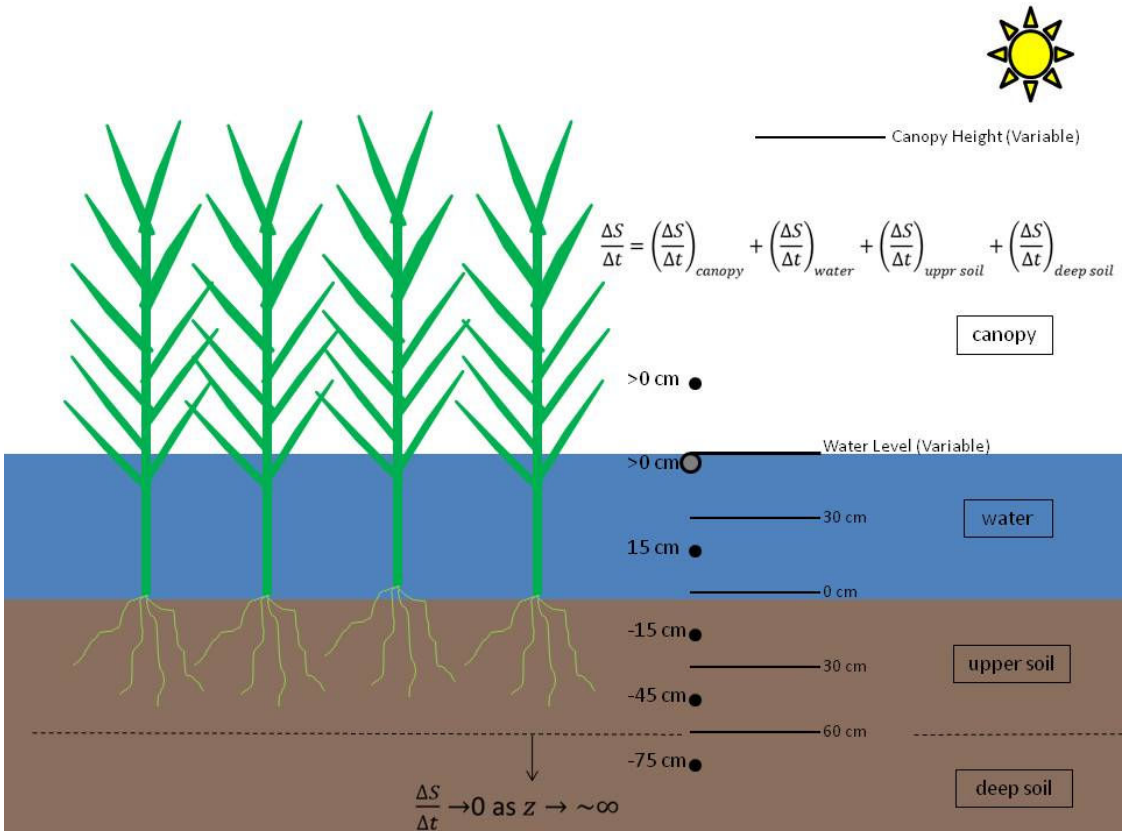

Figure 3. Illustration of the methodology used to calculate the heat storage of the wetland. Black dots represent fixed temperature sensors, gray dot represents the variable surface water temperature float, and the black lines represent the layers boundaries for each sensor.

2.4.2 *Large Aperture Scintillometer Theory*

As discussed above, we use an LAS system to directly estimate the amount of sensible heat flux from the wetland (rather than the Bowen ratio method, for example). Given the significant role of the LAS instrument in this study, we take some time to discuss the basic theory of these measurements. The LAS measures atmospheric scintillations that are caused by changes in the index of refraction of air due to the turbulent fluctuations in air temperature and water vapor. The scintillations measured by the LAS are expressed as the "structure parameter" of the refraction of air (C_n^2), which represents the turbulence of the atmosphere. The relationship between C_n^2 and the variance of the natural log of beam intensity (σ_{lnI}^2) is:

$$C_n^2 = 1.12\sigma_{lnI}^2 D^{\frac{7}{3}} dx^{-3}, \quad (10)$$

where D (m) is the aperture diameter and dx (m) is the transect length. Once C_n^2 ($m^{-2/3}$) is calculated internally in the LAS receiver unit, the structure parameter of temperature C_T^2 ($K^2\ m^{-2/3}$) can be solved from C_n^2 since temperature related effects have a much larger influence on scintillations than humidity for scintillometers in the near-infrared range, (Wesely, 1976),

$$C_n^2 \approx \left(\frac{-0.78 \cdot 10^{-6} p}{T^2}\right)^2 \cdot C_T^2 \left(1 + \frac{0.03}{\beta}\right)^2, \quad (11)$$

where β, defined in Equation 3 is the Bowen ratio to help correct for humidity related scintillations, p (Pa) is the pressure, and T (K) is the temperature measured at the *P. australis* station. Depending on the strength of H and LE, the Bowen ratio can be large (>2) when $H >> LE$, or small (<0.5) when $LE >> H$. If β is small, the humidity parameter

has the potential to cause significant scintillations, and Equation 11 is needed. If the Bowen ratio is large, then the equation can be simplified to

$$C_n^2 \approx \left(\frac{-0.78 \cdot 10^{-6} p}{T^2}\right)^2 \cdot C_T^2 , \qquad (12)$$

For our purposes, Equation 13 is used since the Bowen ratio is generally small over the vegetation-dominated wetland.

Using the Monin-Obukhov similarity theory to represent the height at which convectively driven turbulence dominates over mechanically driven turbulence, the momentum of *H* can be calculated with general meteorological measurements by (Wyngaard et al. 1971).

$$\frac{C_T^2 (z_{LAS} - d)^{\frac{2}{3}}}{T_*^2} = f_T \left(\frac{z_{LAS} - d}{L_{mo}}\right), \qquad (13)$$

where d (m) is the zero-displacement height, z_{LAS} (m) is the effective height of the scintillometer beam above the surface (Hartogensis et al., 2003), T_* (K) is the temperature scale, L_{mo}(m) the Monin-Obukhov length, and f_T is the universal stability function for stable and unstable periods (De Bruin et al., 1993). It is important to note that there has been no agreement on the calculation of the stability function during stable periods (Kipp & Zonen, 2007). Hartogensis et al. (2003) also found that *H* was very sensitive to z_{LAS}, and measuring z_{LAS} as accurately as possible is essential for accurate *LE* values. Since the vegetation distribution below our LAS beam is very homogenous, the zero-displacement height can be calculated by d=0.1 $\cdot$ h_{veg}. T_* is defined by

$$T_* = \frac{-H}{\rho c_p u_*} , \qquad (14)$$

and

$$L_{mo} = \frac{u_*^2 T}{g k_v T_*} \ , \qquad (15)$$

where ρ (kg m^{-3}) is the density of air, k_v the van Kármán constant (=0.4), g the gravitational acceleration (~9.8 ms^{-2}), and u_* (ms^{-1}) is the friction velocity. Computer software (known as "EVATION") was provided by the LAS manufacturer to calculate H based on the above theoretical considerations. EVATION begins by assuming an initial value for β, and once H has been calculated, LE is then estimated from the energy balance, after which the initial β is then replaced with a "new" β. The program is ran iteratively for every ten minute interval until the difference between the initial and "new" β is less than a one percent, after which the final H is then calculated.

It is also important to note that the saturation of the LAS can occur on occasion (i.e. H is becomes so strong the measured scintillations level off and eventually decrease). The degree of saturation depends on path length, height of beam above the ground, aperture size, and other variables. Such instances typically occur when there is a large amount of atmospheric turbulence, and the strength of the received intensity is weakened. The relation between H and the scintillation strength becomes non-existent and the LAS method becomes no longer useful (Kohsiek et al., 2006). This theory has been discussed in depth and experimented by (Clifford et al. 1973; Wang et al. 1978) and tested in the field by Kohsiek et al. (2006).

2.4.3 *Priestley-Taylor Equation*

For comparison with the LAS-derived energy balance, we also estimated ET rates using the simpler Priestley-Taylor (P-T) method (Priestley and Taylor, 1972). As discussed previously, the P-T formula is based on simplifications to the BREB method

(which was not found to work well for our site due to the weak vertical vapor pressure gradients). The P-T equation is generally used to estimate potential evapotranspiration (PET) in conditions over a saturated surface under conditions of minimal advection, which was found during most of growing season. An advantage of the P-T equation is that the only required measurements needed are temperature, atmospheric pressure, net radiation, and the heat storage rate. We calculated P-T ET rates on a daily basis under the follow relationship:

$$PET = \alpha \cdot \left[\frac{S}{(S+\gamma)}\right] \cdot (Rn - S), \qquad (16)$$

where α=1.26, S (kPaC^{-1}) is the slope of saturation vapor pressure curve, and γ (kPaC^{-1}) is the psychometric constant. The P-T constant of 1.26 compares well with the average value of 1.3 found by Burba et al. (1999a) for a *P. australis* wetland during early and peak growth stages. Although wind and humidity are neglected in the P-T relationship, the results tend to be highly correlated with the more complex Penman-Monteith equation, since temperature is used in both formulas (Utset et al., 2004). It has also been found that daily to ten-day P-T averages provide reasonable estimates of ET over shallow lakes and ponds when compared to the energy balance method (Stewart and Rouse, 1976; De Bruin and Keijman, 1979; Rosenberry et al., 2004).

2.4.4 *Water Balance*

The water balance is used in this study to provide additional verification of the calculated ET rates through comparison with changes in water level. The water budget calculations also allow us to assess the relative significance of other water balance

components such as precipitation and groundwater seepage. Similar to the energy balance, the water balance can be expressed as

$$P - ET + GW_{net} + R_{net} = \frac{\Delta L}{dt}, \qquad (mm/day) \qquad (17)$$

where P is precipitation rate, GW_{net} is the net flux of groundwater and R_{net} is the overland flow into/out of the wetland, and $\Delta L/dt$ is the rate of change in water level. Note that Equation 17 neglects surface inflow and outflow, which is assumed to be negligible for the study wetland (relative to the other terms). During periods of limited influence from precipitation and groundwater, one should find that the rate of ET closely matches the rate of decline in water level. Graphs of cumulative P – ET can also be compared with water level to assess the variation in net groundwater flux through time.

2.5 Data Quality and Uncertainty

Given the many factors involved in calculating ET from the energy budget method, it is important to assess the quality of the various data sources, to quantify the uncertainty in each of these sources, and to estimate the impact of these uncertainties on the final ET calculations. Table 1 lists the estimated maximum uncertainty for many of the measured variables, but additional sources of error need to be considered as well, particularly those that relate to the calculation of sensible heat flux. For example, LAS-derived sensible heat flux values are sensitive to the height of the LAS above the canopy, which is also an input parameter in the data processing software, EVATION. Since this height varies with the height of the vegetation, it is important to assess the precision with which the plant height must be specified and how often it should be updated in the calculations over the course of the growing season. In this section, we examine these and

other sources of uncertainty, as well as the net impact of all potential errors on the resulting energy balance calculations. We also discuss the various methods that are used to identify, remove, and gap-fill certain erroneous data points – not only for the sensible heat flux, but other variables as well.

A comparison of measurements between both meteorological stations within the wetland revealed a period of erroneous air temperature measurements from the upper sensor at the *P. australis* station from June 14 – July 23. Since the temperature gradient between the upper and lower sensor over the *P. australis* is needed for the calculation of sensible heat flux, an accurate gap-filling method was needed. Various 10-minute data regressions were created for the vertical temperature gradient (during periods of "good" data only) to determine if there were any ancillary meteorological variables that could serve as a suitable proxy. To account for seasonality, only data a month before and after the erroneous period were used in the scatter plots. It was found that net radiation had the best relationship with the vertical temperature difference (r^2=0.66), and a 2nd order polynomial fit (Figure 4) was used to fill in the data gap. To check the accuracy of the new gap-filling algorithm, the observed and "derived" temperature differences were compared during the period of good data (one month prior and after the data gap). It was found that the RMS difference between the two datasets was approximately 0.80 °C. Typical vertical temperature differences range from about -5 to +3 °C (Figure 4), so the gap-filling procedure leads to an estimation error of approximately 16% or larger. However, since the LAS data processing software requires only the sign of the temperature gradient (not the magnitude) to calculate sensible heat flux, the method used here for filling gaps in the air temperature data are likely to be more than adequate.

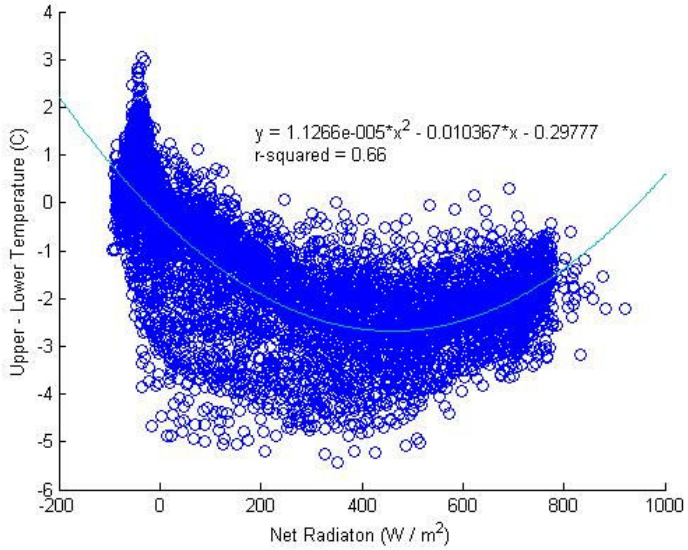

Figure 4. Scatter plot of the upper-lower air temperature difference (°C) vs. net radiation (W m^{-2}). Each data point represents a 10-minute average during the period of May 14-August 23 (with the "bad" period from July 14-July 23 excluded from the analysis). A 2nd order polynomial fit to the data is also shown.

To examine the sensitivity of the LAS-derived sensible heat flux to the specified plant height, the EVATION program was run through multiple iterations over the course of the growing season, changing only the input plant height (by 0.5-m increments from 1.5 to 4.5 m). Sensible heat flux values from various runs were compared with those of the mean plant height of 3.0 m. It was determined that an uncertainty of ± 1.5 m in the input plant height results in an RMS difference of 15.8 W m^{-2} in the sensible heat flux values, whereas an uncertainty of ±0.5 reduces the RMS difference to 5.1 W m^{-2}. Considering that the measured height of the *P. australis* (as determined from digital photos of the vegetation and measurement stake) of the *P. australis* varies considerably over the course of the year (1.9-4.2 m), this analysis shows that the plant height change within EVATION must be considered throughout the growing season. To account for this, EVATION was run five times at fixed plant heights of 2.0, 2.5, 3.0, 3.5, and 4 m.

The daily values of measured plant heights were used to determine which EVATION output should be used, based on which plant height was closest to the observed value (i.e., to the nearest 0.5 m).

After accounting for the changes in vegetation height, the LAS-derived sensible heat flux values were examined to identify any glaring anomalies. Graphs of the mean diurnal cycle (Figure 5a) revealed that there was a systematic tendency for erroneously high sensible heat flux values to occur in the early morning and late evening hours (around the times of sunrise and sunset). The sensible heat flux values were also much more variable during these hours of the day, and the anomalous values typically lasted for about 1-3 hours. An examination of ancillary meteorological variables and other components of the energy balance offered no reason to believe that the observed spikes in sensible heat flux were physically plausible or real. Rather, we suspect that the erroneous values are simply an artifact of the strong changes in atmospheric stability (and index of refraction) that often occur around sunrise and sunset. As such, an algorithm was developed to identify and remove these morning and evening spikes in sensible heat flux. The quality control algorithm is comprised of two parts. The first part provides an effective "first cut" at removing approximately 70% of the erroneous spikes, while the second part removes some remaining spikes in the evening that were missed by the first iteration. In the process of investigating the reasons for the sunrise/sunset spikes, it was found that the variance of the electromagnetic intensity (as measured by LAS variable "SigDemod") and the scaled structure parameter of the refractive index of air ("SigPUCn2") were significantly higher than normal during these periods. As such, the product of these two metrics (at 10-minute timescales) was used to create a quality-

control (QC) flag (*f* = *SigDemod* * *SigPUCn2*) for identifying sensible heat flux anomalies around sunrise and sunset (see Figure 5c). The distribution of *f* values during "non-spike" hours (namely 8:00-15:00 and 21:00-3:00 local standard time) was used to identify the "normal" range of *f* values that one might expect to see. Monthly values of the 90th percentile from this distribution were then applied as cut-offs during potential sunrise (4:00-7:00) and sunset hours (16:00-20:00). *f* values that exceeded this cut-off were then flagged, and the sensible heat flux values were set to "missing data." In all, approximately 7% of the 10-minute sensible heat flux values were removed as a result of this procedure (23% when referring to only the sunrise/sunset periods). Figure5c and 5d show the mean diurnal cycle of the quality control flag, *f*, as well as the number of 10-minute values that exceeded the 90th percentile. Note the "spike" in high *f* values during the sunrise/sunset periods, which are the only time periods for which anomalous values were actually "removed." Figure 5a and 5b also shows the mean diurnal sensible heat flux values before and after this initial quality control procedure. The sunrise "spike" has largely been eliminated, while the sunset anomalies have been greatly reduced (though not eliminated.)

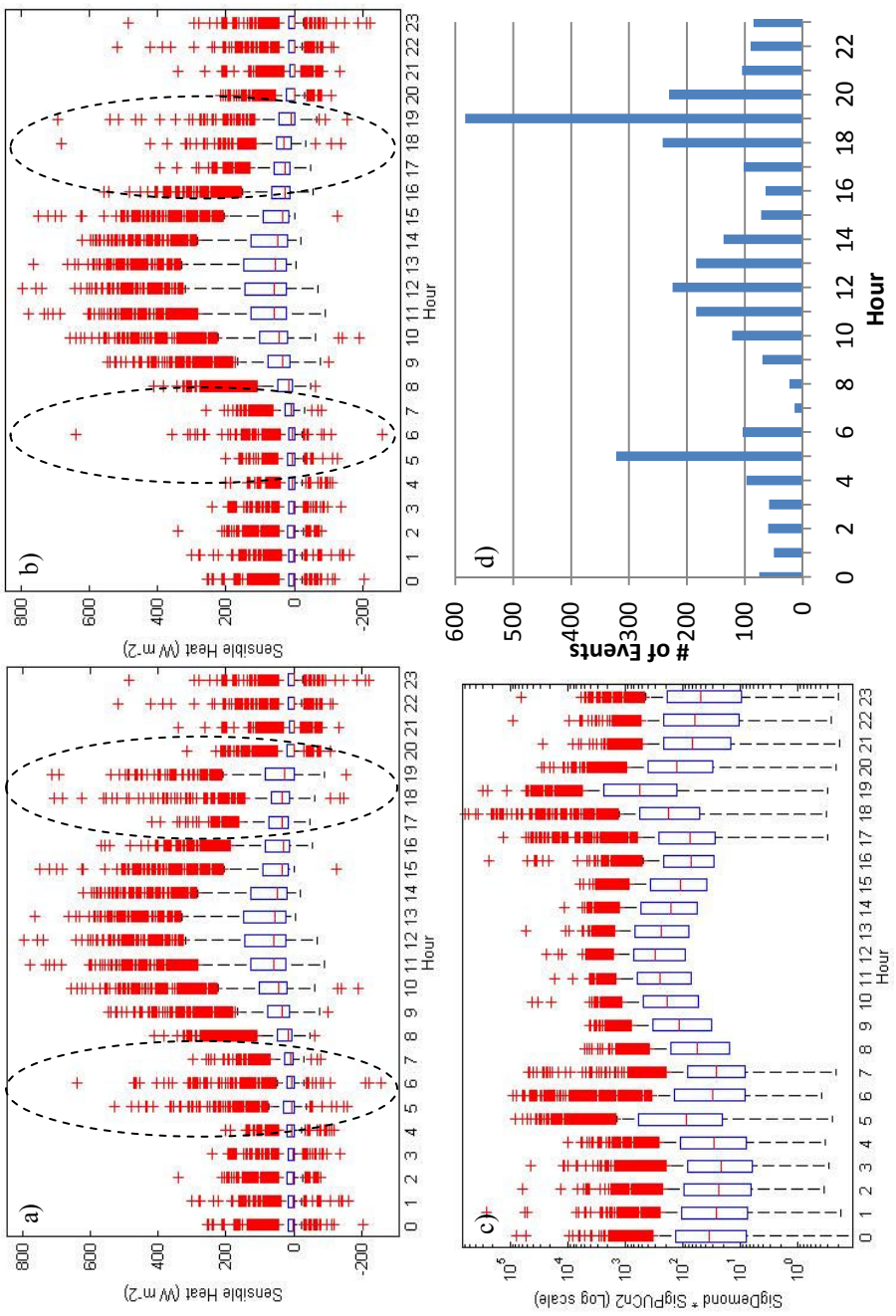

Figure 5. A box-and-whisker plot of the average growing season diurnal *SH* flux (W m^{-2}) a) before and b) after the first QC, as well as the c) QC flags (SigDemod*SigPUCn2). In each plot, the central mark is the median, the edges of the box are the 25th and 75th percentiles, the whiskers extend to the most extreme data points not considered outliers, and outliers are plotted individually (red crosses). Figure d) illustrates the number of 10-minute QC flags that exceed the 90th percentile during the growing season.

A second QC method was needed to further correct the remaining high values of sensible heat flux at sunset. No ancillary variables similar to the QC flag, *f*, were found to adequately identify these remaining heat flux anomalies, and so a simple cutoff value was applied to the sensible heat fluxes themselves. The cutoff value was determined for each month of the growing season on an hour-by-hour basis, using the 90-95th percentiles as the appropriate cut off (depending on the prevalence of sunset heat flux anomalies). In all, only 2.5% of the remaining sensible heat flux values between the hours of 16:00 and 19:00 were removed using this procedure. The final mean diurnal cycle of the growing season sensible heat flux, after apply applying both QC methods, shows that the anomalous sunrise and sunset spikes have been effectively removed (Figure 6).

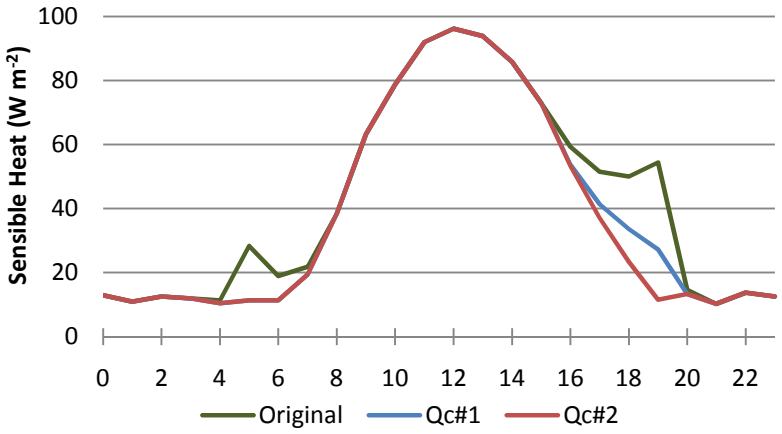

Figure 6. The non-quality controlled (QC) average growing season diurnal heat flux (green short dash), after the first QC method (Qc#1) (long blue dash), and after the second QC method (Qc#2) (red solid line).

In order to fill the data gaps that were created by the above QC procedure, regressions between the (good) sensible heat flux values and other ancillary atmospheric variables were created. For unstable periods (lower air temperature > upper air temperature), it was found that the product of net radiation and wind speed ($g = Rn * U$)

produced the best overall regression with the 10-minute sensible heat flux values (Figure 7a). This regression was subsequently split into periods of positive *Rn* (roughly daytime), and negative *Rn* (nighttime) to create two separate relationships (see Figure 5b and 5c). The $Rn > 0$ regression was further divided into April and a May-October time periods (not shown) to account for significantly higher sensible heat fluxes during the month of April. The correlation coefficients (r) for the $Rn > 0$ regression ranged from 0.72 (for May-October) to 0.86 (for April), while the r value for $Rn < 0$ was found to be -0.52. Finally, for stable periods (which occurred primarily at night), it was found that a simple regression with wind speed provided the best approximation for sensible heat flux ($r = -0.72$; Figure 7d), and so this relationship was used to fill the data gaps during stable periods.

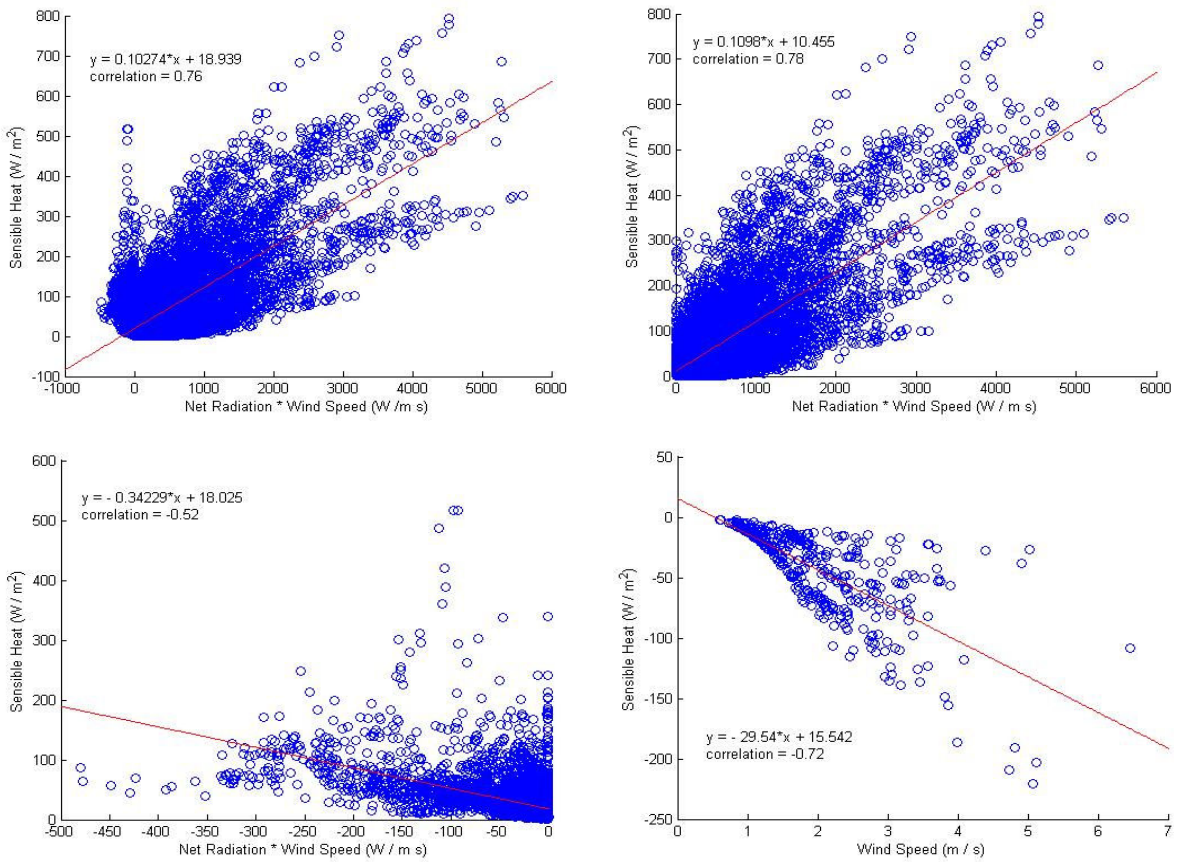

Figure 7. April–October regression between 10-minute values of sensible heat flux (y-axis) and the product of net radiation and wind speed (Rn * U) for a) all unstable periods, b) unstable periods with Rn * U > 0, c) unstable periods with Rn * U < 0, and d) stable periods. Note that the regression in d) is versus wind speed only, not Rn * U. Linear regressions, their equations, and the r^2 values are also shown for each plot.

Prior to deploying the LAS and meteorological station at our wetland site in the Republican River basin, a short deployment was initiated in Mead, Nebraska (in April of 2008), at an Ameriflux research site utilized by colleagues at the University of Nebraska (S. Verma, A. Suyker, and others). This site has been collecting eddy covariance (EC) and energy balance data in managed ecosystems (e.g., rainfed and irrigated maize and soybean), and we used this opportunity to undertake a comparison between the LAS- and EC-derived sensible heat fluxes (and other energy balance components). Previous comparisons of these two methods have suggested that LAS-derived sensible heat fluxes may be systematically higher than those derived from EC measurements, in some cases by up to 21% (e.g., Randow et al., 2008; Kleissl et al., 2008). Data collected at the Mead, NE site were compared over a 38-day period using hourly mean radiative, sensible, latent, and soil heat fluxes (measured with two Hukseflux heat flux plates and soil temperature sensors). Both sets of instruments were mounted on towers or tripods above a large, homogenous open field (rainfed maize/soybean rotation) with sufficient (and similar) fetch. The soil was not tilled and was essentially bare at this time of year, with some low stubble left over from the previous growing season.

Comparison of the hourly sensible heat flux from the LAS and EC systems revealed an r-squared value of 0.95, with the LAS derived fluxes being 29.6% higher than the EC estimates (based on the slope of a linear regression). Similar between the two systems of the available energy (net radiation minus ground heat flux) found only a 0.2% difference, leading to an underestimation of LAS-based latent heat flux compared to the EC system. It is important to note that EC systems often suffer from a lack of energy balance closure (Wilson et al., 2002; Twine et al., 2000), and the dataset collected

at Mead is no exception. We found that the "residual" of the EC-derived energy balance was approximately 28.4 % of the net radiation, which is not an insignificant bias. To account for this, we applied a series of three "adjustments" to the EC data: 1) no adjustment, 2) applying the EC-derived residual entirely to the sensible heat flux to force energy balance closure, and 3) apportioning the residual between the sensible and latent heat fluxes according to the measured Bowen ratio (which is assumed to be correct) to force energy balance closure (similar to Twine et al., 2000). The resulting EC-derived sensible heat flux values from adjustment #2 were 16.6% higher than the LAS-derived values, with an r^2 of 0.93. Adjustment #3, on the other hand, resulted in EC-derived sensible heat flux values that were 4.2 % lower than the LAS-derived values. Thus, we conclude from this comparison that an effective overall "bounds" on the LAS-derived sensible heat fluxes ranges from a maximum value of ~17% higher than the "observed" value to ~30% lower than the observed value. One could also argue that the "most likely" value of LAS-derived sensible heat flux corresponds to the Bowen ratio-apportioned EC flux value, which is 4.2 % lower than the observed. For the purposes of this study, however, we assume that the observed sensible heat flux values from the LAS are "correct," and we apply the above maximum error bounds to assess the impact of this potential uncertainty on the resulting evapotranspiration estimates.

The final error bounds for the ET estimates were calculated by adding the various component errors in quadrature (which assumes that the errors are random and independent). This includes uncertainties in the heat storage rate ($\Delta S/dt$), Rn, and H. Since the water storage term constitutes the majority of the heat storage rate, the uncertainties from the soil and canopy heat storage have largely been ignored. The

HOBO temperature sensors have a measurement resolution of 0.03 °C (which reduces to approximately 0.01 °C when averaging over multiple sensors). To be conservative, we also assume a factor-of-ten uncertainty due to the use of only a single soil/water temperature probe in the wetland, which increases the temperature uncertainty to approximately 0.1 °C. Together with Equation 8, the heat storage uncertainty was then calculated using an average water density, water level, and specific heat for the growing season. Due to the increase in temporal averaging, the resulting hourly heat storage uncertainty of 40.7 W m^{-2} decreases to daily and 5-day uncertainties of 1.7 W m^{-2} and 0.34 W m^{-2}. It can be seen in Figure 8 that as the average heat storage temporal averaging is increased (i.e. hourly to daily), the "spread" within the heat storage will then decrease and thus decrease the uncertainty. Similarly, for calculating the uncertainty in the mean diurnal heat storage term, the raw hourly uncertainty was reduced by the square root of the number of days used in the diurnal average. Taking into account all sources of error (*Rn,* $\Delta S/dt$, and *H*), we find that the RMS uncertainty in the hourly and daily latent heat flux is 54.0 W m^{-2} and 21 W m^{-2}, or 34.0% and 16% of the mean value. Subsequent figures of ET include error bars that reflect the above uncertainty analysis.

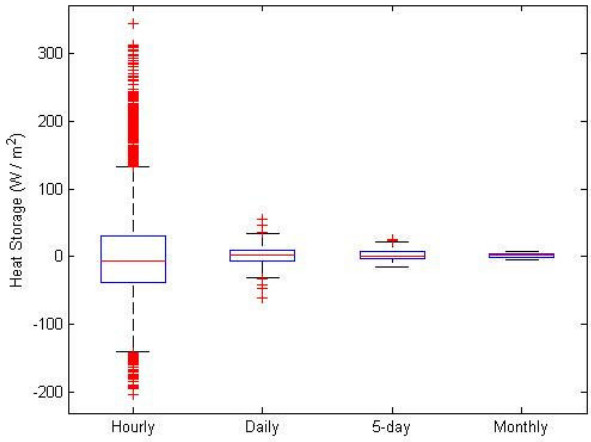

Figure 8. A box-and-whisker plot for the hourly, daily, 5-day, and monthly heat storage rate averages.

2.6 Results

2.6.1 *30-Year Climatology and 2009 Conditions*

To provide some context for the energy and water balance analysis, we first discuss the local climatic conditions that exist at the wetland study site. The atmospheric conditions are discussed both in terms of the long-term climatology, as well as the meteorology that occurred during the 2009 field season. The long-term climatic data for the wetland were obtained through the National Climatic Data Center (NCDC) from a National Weather Service Cooperative Observer Program (COOP) station in Beaver City, Nebraska. The COOP station (number 250640) is located 21 kilometers to the southeast of the wetland and has been in operation since 1931. We present data from the past 30 years (1979-2008) to represent the mean climate, while data from the meteorological station in the *P. australis* portion of the wetland and Beaver City are used to illustrate the atmospheric conditions during 2009.

Much of the western Republican River basin is located in a semi-arid climate, but our study wetland is positioned near the "average" U.S. boundary between humid and semi-arid climates. Although the interannual variability is high, the most recent 30-year climatology from Beaver City would classify the climate as humid continental (according to the Köppen scheme). The mean annual maximum, minimum, and average daily temperatures at Beaver City are 20.4 °C, 3.3 °C, and 11.9 °C, respectively, and the region receives, on average, 605 mm of precipitation annually (685 mm of snowfall). Monthly mean values of temperature and precipitation from the wetland and Beaver City during the growing season are shown in Figure 9. The "growing season" typically begins in

mid-April (after the last spring freeze) and lasts until the first freeze in mid-October. During 2009, the beginning and ending dates occurred around April 11 and October 3, respectively, and is how we choose to define the "growing season" for the purposes of this study. Both May and July of 2009 were characterized by well-above-normal precipitation at the wetland site (Figure 9). June, July, and August were also cooler at the wetland site in 2009, as compared to the Beaver City climatology. Interestingly, however, the monthly mean air temperature at Beaver City for July of 2009 was significantly warmer than at the wetland site. We suspect that this is related to the wet conditions and high latent heat flux that exist in the wetland and the surrounding irrigated fields – a difference that is likely to be most evident during the height of the growing season.

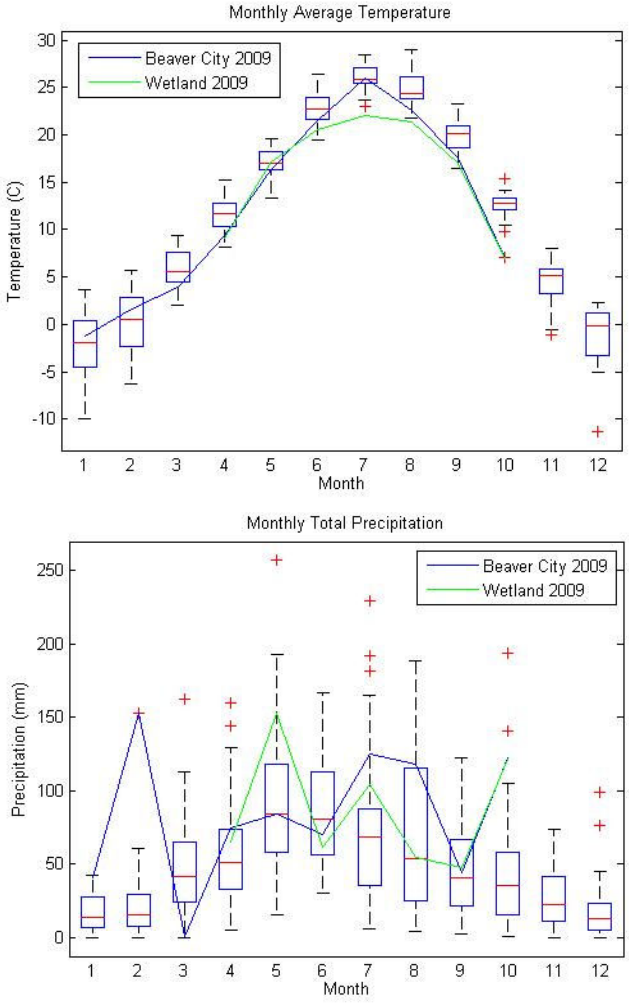

Figure 9. 2009 monthly mean air temperature (°C) and monthly total precipitation (mm), as well as a box-and-whisker plot of the 30-year mean climatology for the study location. The 2009 data are taken from the wetland meteorological station (green) and the Beaver City COOP station (blue), while the 30-year averages are from the COOP station.

Daily precipitation, water level, air temperature, surface water temperature, relative humidity, and wind speed are shown in Figure 10. The water level increased from the beginning of the growing season until late June, after which it steadily decreased until September and then leveled off through the end of the growing season. Daily air temperatures are much more variable than the wetland water temperatures, but they

generally oscillate about similar mean values through mid June. For the remainder of the year, however, the air temperature is notably warmer than the water temperature (particularly from mid June to mid August). This is likely due to the strong insulating effect of the tall *P. australis* vegetation (and associated high latent heat flux), as well as the cooling influence of groundwater and soil heat flux.

Daily mean wind speeds at the wetland site were generally strongest during April, May, and October, in association with extratropical storms and frontal activity (Figure 10d). Prevailing wind directions in the spring tended to be out of the northwest or southeast (Figure 11), while winds during June–September were predominantly easterly and much weaker (with occasional northwesterly winds that were stronger, but less common). Even though the anemometer at the wetland station is mounted at a height of over 6 m (above the soil/water interface), it is noteworthy that the daily mean wind speeds are generally quite weak (usually less than 1 m s^{-1} during June–September). Daily mean wind speeds at a nearby AWDN station in Holdrege, Nebraska, for example, are typically around 3–4 m/s. We attribute the reduction in wind speeds at our wetland site to the "wind shading" effect of the nearby cottonwood trees, as well as the added wind resistance that occurs in conjunction with the growth of the *P. australis* (up to 4.2-m tall at the height of the growing season).

Figure 12 shows the mean diurnal cycle of air temperature, wind speed, and net radiation for the months of April/May (AM), June/July/August (JJA), and September/October (SO) for the growing season. Air temperatures generally reach their daily maximum around 14:00-16:00 local standard time and daily minimum around 5:00-6:00. Although JJA clearly has the highest daily mean temperature, the diurnal

temperature range of about 12 °C is similar for all three seasons. Wind speed shows a pronounced diurnal cycle during all seasons (weakest during JJA), with maximum wind speeds occurring in the afternoon (12:00-16:00) and minimums occurring from evening to morning (19:00-6:00). Clearly, much of the diurnal variation in temperature and wind is closely tied to the pronounced hourly variations in solar and net radiation (Figure 11c).

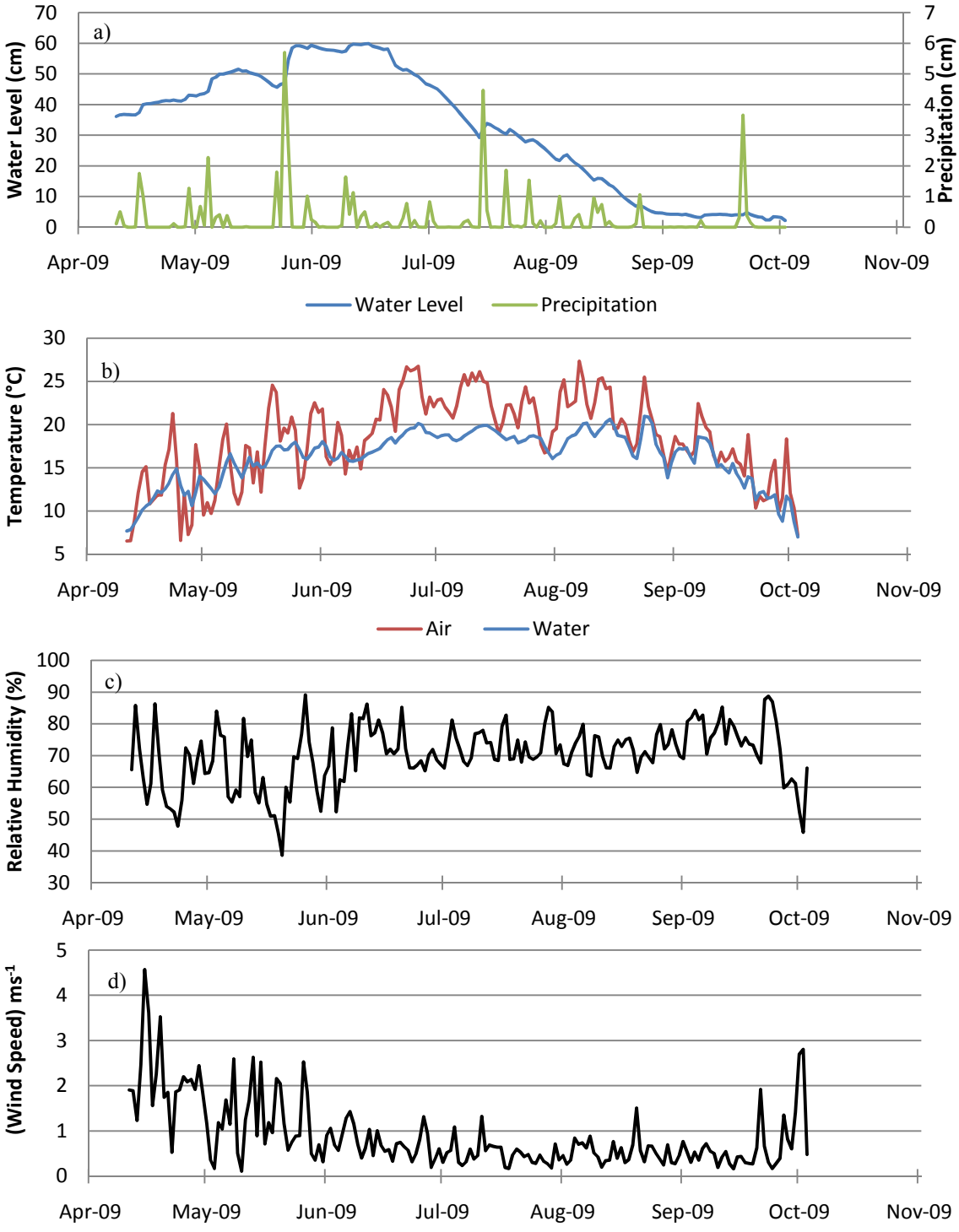

Figure 10. 2009 daily mean a) precipitation (green) and water level (blue), b) air temperature (red) and surface water temperature (blue), c) relative humidity, and d) wind speed from the *P. australis* meteorological station.

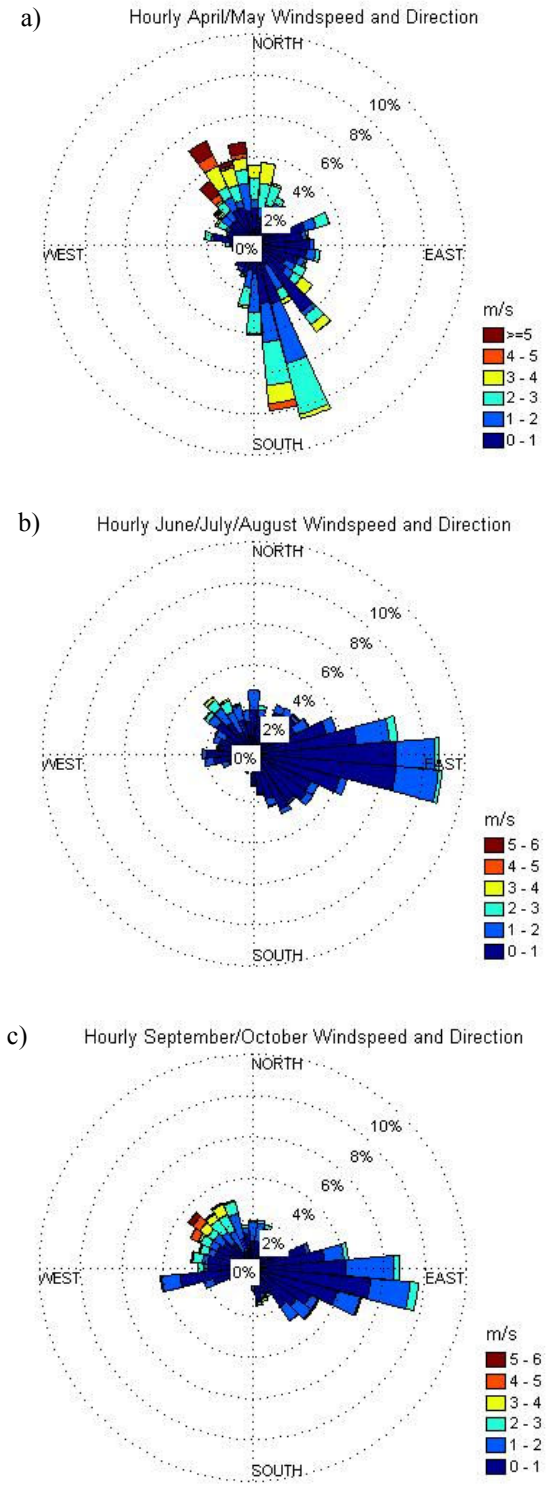

Figure 11: The hourly wind speed (ms^{-1}) and direction (°) for a) April/May (AM), b) June/July/August (JJA), and c) September/October (SO). The AM hourly averages begin on April 11 and average SO ends on October 3.

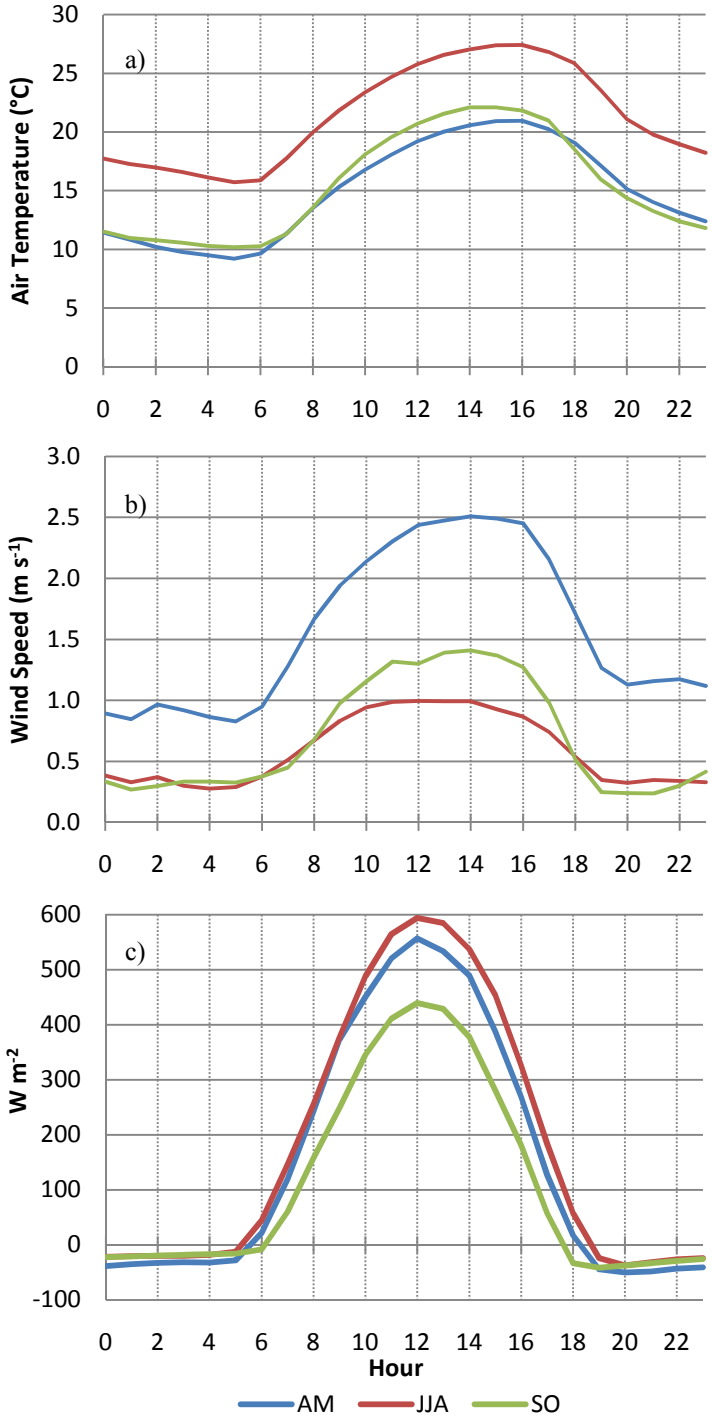

Figure 12. Mean diurnal cycle of: a) air temperature (°C), b) wind speed (m s^{-1}), and c) net radiation (W m^{-2}), as measured at the wetland site during April/May (MAM), June/July/August (JJA), and September/October (SO) of 2009. Each hourly mean represents the average that begins on the hour and includes all measurements until the next hour (1 AM average = 1:00 – 1:59).

2.6.2 *Vegetation Height and Leaf Area Index*

After the winter of 2008/09, a significant amount of dead biomass remained standing in the *P. australis* portion of the wetland. Most of this biomass was derived from the previous growing season (2008), although some could have lingered from previous years as well. New, green shoots of *P. australis* began to emerge from the wetland around April 20, 2009 (i.e., approximately 9 days after the last spring freeze). The *P. australis* grew steadily (but at a decreasing rate of growth) until reaching a maximum height of 4.2 meters in early July (Figure 13). In addition to plant height, leaf area index (LAI) measurements were made five times throughout the growing season with an LAI-2000 (LI-COR Biosciences). The measurements were made along a marked transect through the *P.australis* (at 9 different measurement locations) and represent a bulk LAI for both dead and living biomass (as well as both stems and leaves). The 95% confidence level of the various LAI measurements ranges from ± 0.07 to ± 0.32. Similar to plant height, the LAI increased over the course of the growing season from a minimum of 2.5 on May 27 (the date of first measurement) to a maximum of 5.4 on July 22 (Figure 13). The *P. australis* was then sprayed heavily with herbicide (a mixture of Roundup® and Habitat®) on July 22 (by means of helicopter) to kill the vegetation and monitor the response. From visual observations, the *P. australis* appeared slightly browner in the weeks subsequent to spraying, and the LAI was observed to decline to a value of 4.46 on August 6, although the decline could have occurred from nature senescence (Figure 13). The growing season officially ended in early October after a hard freeze. At this time, three plots within the wetland with an area of 0.2 m^2 and one plot with an area size of 0.4 m^2 of dry biomass were collected and weighed, yielding an average value of 5018 g m^{-2}.

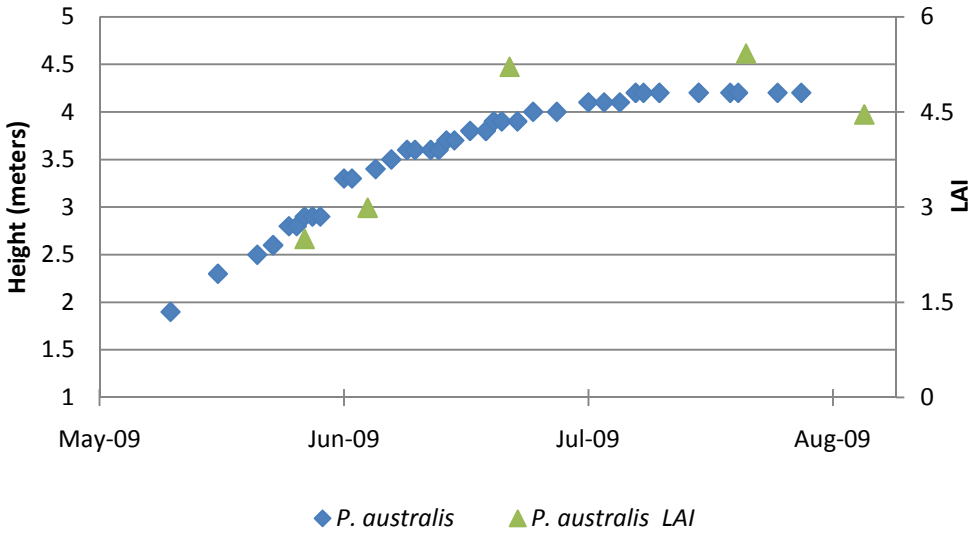

Figure 13. *P. australis* observed plant height (diamond) and LAI (triangle).

2.6.3 *Surface Radiation Balance*

Radiative heat fluxes at the earth's surface (particularly incoming solar radiation) are important drivers of the land surface energy balance. A 5-day running mean of incoming solar radiation, incoming longwave radiation, net longwave radiation, and net radiation is found in Figure 14. From April to May, the incoming solar radiation (SW) beings to increase until late June, thereafter slowly decreasing until the end of the growing season. The strong changes in magnitudes during the early season are due to significant cloud cover from the passage of extratropical cyclones and fronts. Generally, the month of June would receive more incoming SW than May due to the earth/sun proximity, but due to a cloudy June, May received more solar radiation. Another portion of the SW radiation balance is the outgoing SW (not depicted), which is a function of the surface albedo (or reflectance). When the surface albedo increases, more incoming SW energy is reflected into the atmosphere (increase in outgoing SW) which then decreases the total net SW.

The incoming longwave (LW) radiation (a function of the atmospheric temperature) increased and decreased throughout the growing season (Figure 10b). Since net LW is simply the outgoing LW subtracted from the incoming LW, net LW illustrates the LW radiation gradient (ie. temperature gradient) between the surface and atmosphere. As seen in the early parts of the growing season, when the magnitude of net LW increases, more energy is leaving the surface to the atmosphere rather than energy transmitted from the atmosphere to the surface that was observed on the previous day. These fluctuations in net LW occur because the water within the wetland has a higher specific heat than the atmosphere. With water having a higher specific heat, the cold air that occurs after the passage of frontal systems (frequent in April and May) decreases the air temperature more than water and therefore increases the magnitude of net LW. From June to mid-September, there is little fluctuation in net LW, with daily net LW in mid-September reaching a minimum of -5.6 W m^{-2} (air and water temperature closest to equilibrium).

The net radiation (*Rn*), which is sum of net LW and net SW, is strongly influenced by SW radiation since there are small changes in LW radiation magnitude throughout the growing season compared to SW radiation. With daily net LW radiation emitting away from the surface and daily net SW emitting towards the surface, daily *Rn* always acts as available energy for latent and sensible heat fluxes over the wetland. The available energy through *Rn* is greatest from late June through July, which is attributed to the high incoming SW and a relatively small negative net LW.

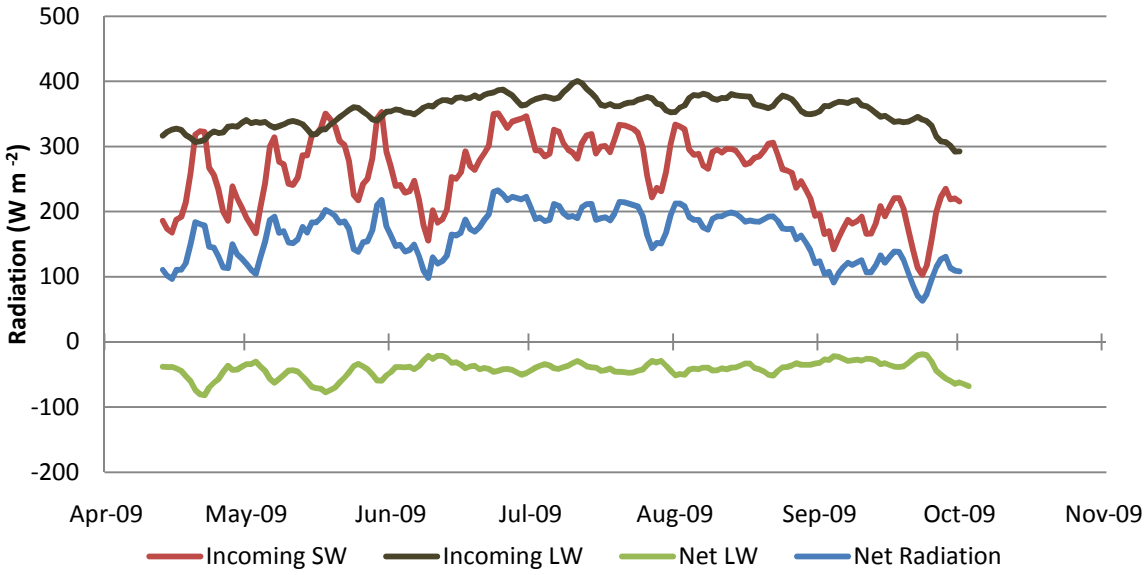

Figure 14. 2009 5-day running mean for incoming solar radiation (red), incoming longwave radiation (brown), net longwave radiation (green), and net radiation (blue) over *P. australis*.

Surface albedo depends on numerous factors, including sun angle, cloud cover, and surface characteristics (e.g., vegetation, soil, water depth). For our study wetland, the 5-day running mean shortwave albedo (5-day outgoing shortwave divided by 5-day incoming shortwave) shows moderate seasonal variation over the course of the growing season in the *P. australis* portion of the wetland (Figure 15). Daily albedo values varied from a minimum of 0.16 on April 17 to a maximum of 0.24 on June 8. We attribute some of this increase in albedo to the greening up and "leafing out" of the *P. australis*, which would help to obscure some of the exposed (and darker) water surface in the wetland. No water albedo measurements were made for this study, but Burba et al. (1999b) found open water albedo values of 0.12 for a similar *P. australis* wetland in central Nebraska. As illustrated in Figure 15, the *P. australis* albedo values subsequently declined later in the season (beginning in late July), presumably in response to reductions in LAI due to senescence and possibly herbicide spraying.

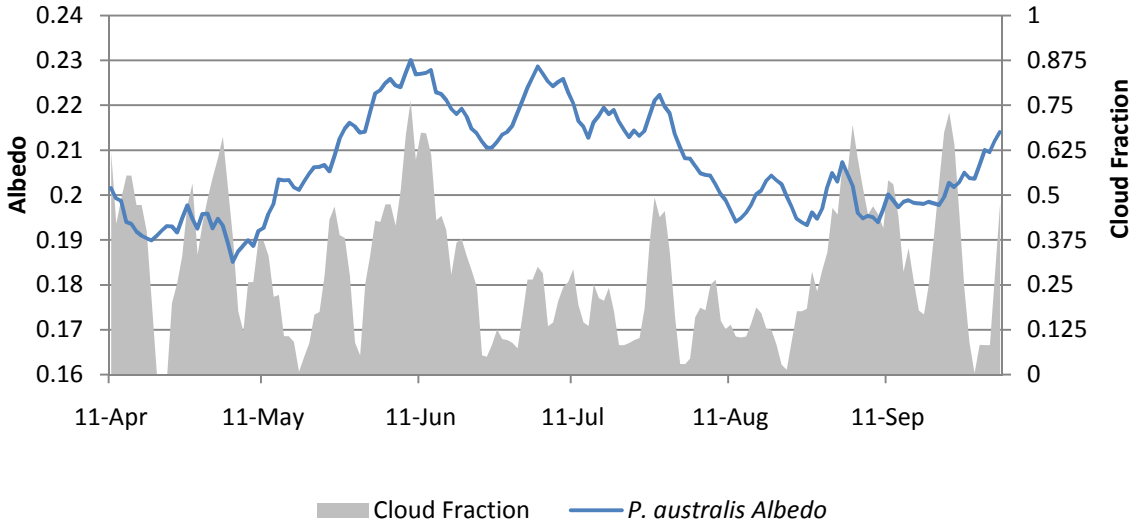

Figure 15. Cloud fraction and *P. australis* surface albedo during the 2009 season. Values are based on 5-day running mean measurements of incoming and reflected solar radiation, as well as theoretical clear sky values of incoming solar radiation for the given latitude and time period (to calculate cloud fraction).

In addition to the seasonal variations in albedo, short-term variations are also evident and are often associated with changes in cloud cover. Specifically, periods of high (low) surface albedo tend to occur under conditions of high (low) cloud cover (Figure 15). It has been found in previous studies (e.g., Lord et al., 1985) that the scattering of diffuse incoming shortwave radiation intercepts more leaf area per unit energy than direct shortwave, thus increasing the shortwave reflectance. The increased reflectance occurs when diffuse radiation is predominant, because the plants are equally illuminated on all sides, and shadows behind the plant leaves are significantly reduced (Guyot and Gu, 1993; Deering and Eck, 1987). Previous studies have also demonstrated the role of LAI and percent vegetation cover in measurements of surface reflectance (e.g., Colwell, 1974). Song (1999) also observed that while background soil had a lower albedo, corn increased in albedo with increasing LAI.

Finally, we note that hourly albedo values show a strong dependence on solar zenith angle. Figure 16 illustrates this for the first four months of the growing season, showing that albedo increases by approximately 50% from mid-day values to morning and evening values. The previously noted increase in albedo from April to July is also evident, with June showing anomalously low values during morning and evening (presumably in association with the higher cloud cover during June). It is interesting to note that this seasonal increase in albedo is contrary to what one would expect based on sun angle alone (with zenith angles being lowest in late June and early July). This helps to reiterate the important role of vegetation phenology and LAI in affecting the seasonal changes in wetland albedo.

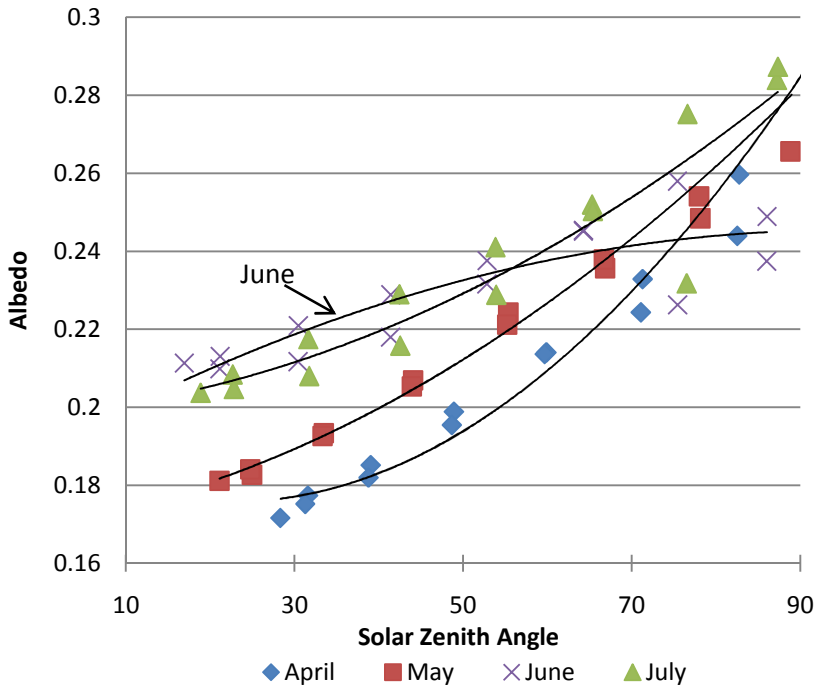

Figure 16. Hourly values of wetland surface albedo as a function of solar zenith angle and month. Black lines represent 2nd-order polynomial fits for each month.

2.6.4 *Heat Storage Rate*

The 5-day running mean of $\Delta S/\Delta t$ of the wetland can be seen in Figure 17 and is affected by the available energy at the water surface, the water temperature (Figure 10b), and water depth (Figure 10a). The average daily air and vegetation heat storage reached a maximum of 0.58 of the total 15.78 W m^{-2} and 1.65 of 7.79 W m^{-2}. The water in the wetland was found to be the largest heat storage of the wetland, thus the water level was most important in the calculation of $\Delta S/\Delta t$. If the water level is high, more energy is stored and released from the water and less energy transferred to the soil. Consequently, if the water level is low, less energy can be stored in the water and more energy is transferred and released to the soil. The maximum and minimum daily $\Delta S/\Delta t$ of the water was 51.7 of 55.9 W m^{-2} and -67.0 of -61.3 W m^{-2} during late April and early May. $\Delta S/\Delta t$ of the wetland reached a daily maximum and minimum average of 56.0 and -61.3 W m^{-2} on April 25 and May 6. The trend throughout the growing season illustrates that on average daily $\Delta S/\Delta t$ sequestered energy at the beginning of the growing season and then released more energy towards the end (Figure 18). The $\Delta S/\Delta t$ of the canopy (sum of the air and vegetated $\Delta S/\Delta t$) were included in the total heat storage ($\Delta S/\Delta t$) of the wetland due to the dense and tall vegetation, but was not included in Figure 17 due its overall small fluxes.

Each month's average diurnal $\Delta S/\Delta t$ varied along with the percent of energy used from net radiation. In May during the early growth of vegetation, maximum $\Delta S/\Delta t$ for the growing season sequestered 177 W m^{-2} of the available net radiation (570 W m^{-2}) at 13:00. Once the vegetation reached its peak in July, the heat storage only used 40 of 597 W m^{-2} at 13:00. While the average net radiation between May and July were only 5%

different, due to a larger canopy, decreased water level, and increased latent heat flux, the percent of available energy partitioned in these months changed from 33 to 7%. In September during senescence, the heat storage reached 88 of 405 W m^{-2} at 11:00, with the partitioning increasing to 22%. Diurnally averaged *Rn* was never less than $\Delta S/\Delta t$ during nighttime, therefore sensible and/or latent heat were the sinks of the available energy from $\Delta S/\Delta t$ that was released from the wetland. The diurnal cycle for the months of April/May (AM), June/July/August (JJA), and September/October (SO) are shown in Figure 22. In AM when *P. australis* was in early growth and the water temperature was relatively cool, the diurnal cycle of the heat storage followed the same trend as net radiation. The AM diurnal trend occurred because *P. australis* is transpiring little water vapor, hence most of the available energy is proportioned into *H* and $\Delta S/\Delta t$. Once the *P. australis* began to transpire and water temperature reach a maximum, the magnitude of $\Delta S/\Delta t$ of the wetland in JJA decreased during the daytime and nighttime. As the *P. australis* senesced (lower ET) and water level reached a seasonal low, the water began to release more energy into the atmosphere than sequester. The phase shift in SO is likely caused by lower *Rn*, an earlier sunset, and lower water level. *LE* and *H* during SO also reaches a monthly maximum after the peak net radiation, which would allow less energy to be partitioned into heat storage in the afternoon.

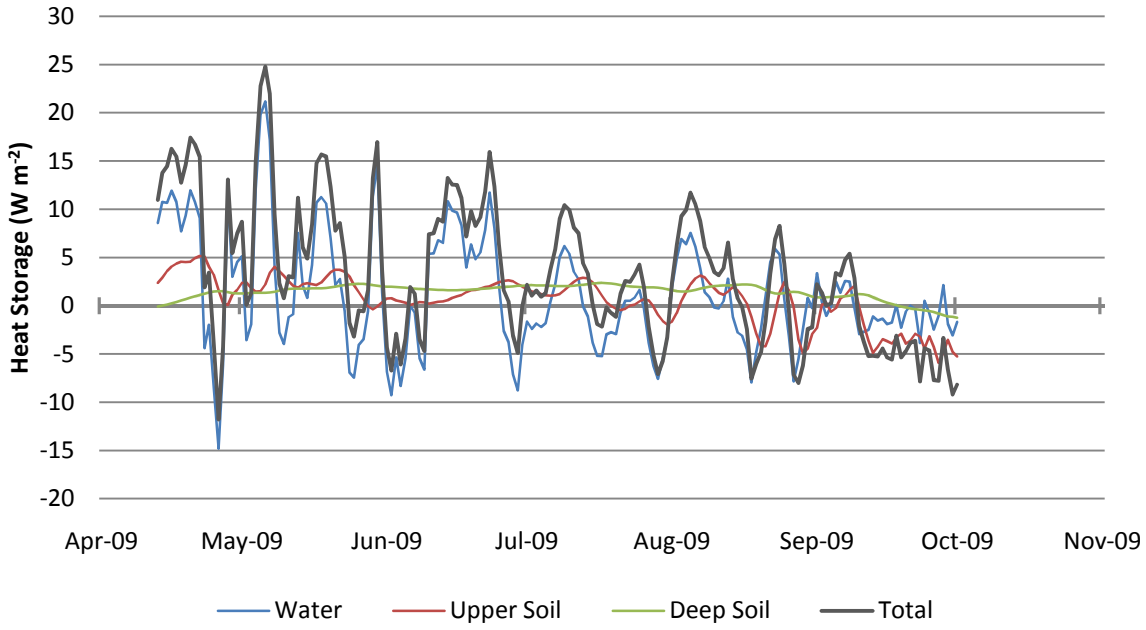

Figure 17. The growing season five day running mean heat storage (W m^{-2}) for water (blue large-dashed line), upper soil (red small-dashed line), lower "deep" soil (green cross-dashed line), and total storage (solid line) at the *P. australis* site.

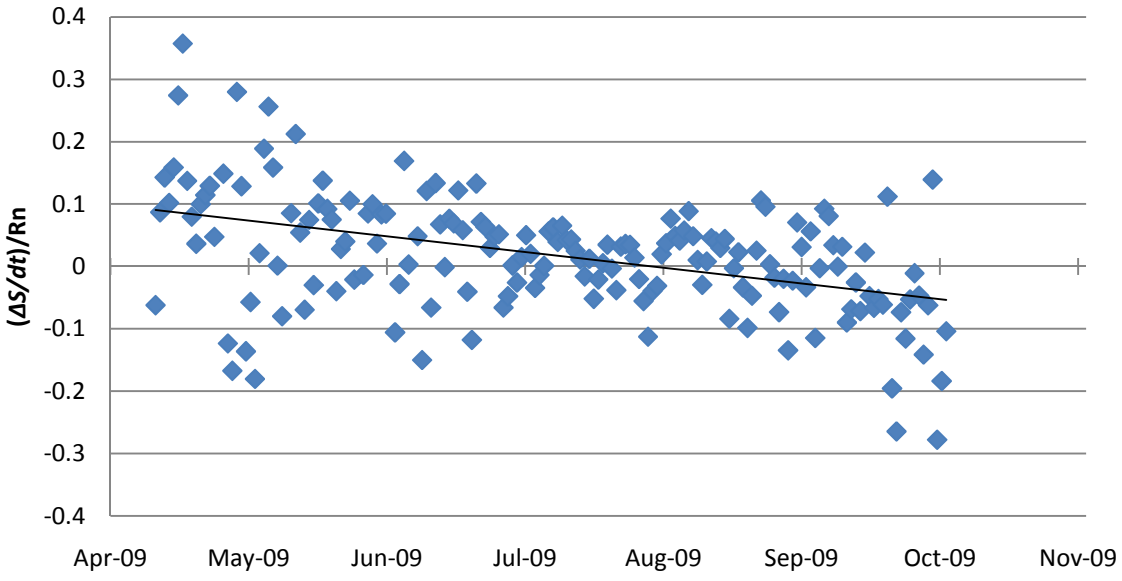

Figure 18. Ratio of daily heat storage rate and net radiation with a linear trend line fit for the growing season.

2.6.5 *Sensible Heat Flux*

The sensible heat flux varied in magnitude throughout the growing season with the highest fluxes at the beginning of the season and the lowest fluxes during full vegetation (Figure 21). *H* reached an average daily maximum of 199.0 W m^{-2} in mid-April with no vegetation, and a daily minimum of 5.5 W m^{-2} in late June with full vegetation. The daily ratio of available energy (Rn-$\Delta S/\Delta t$) partitioned into *H* throughout the growing season can be seen in Figure 19. Two days in April used more available energy from *Rn* and $\Delta S/\Delta t$, therefore those days had more condensation (releasing of latent heat). *H* acquired almost all available energy during April and as vegetation grew, less energy was partitioned into *H* until it reached a daily minimum of 0.02 - 0.18 from late-June to mid-August (Figure 19). Once the vegetation began to senesce, more available energy was again partitioned into *H*.

The average diurnal fluctuations of *H* generally began to increase shortly after *Rn* increased at sunrise (Figure 22). Each month's average diurnal maximum of *H* occurred at the *Rn* maximum or shortly afterwards. April comprised of the largest diurnal *H* of 225 W m^{-2} at 14:00, while July's maximum was only 40 W m^{-2} at 12:00. Generally, after *H* reached a maximum, it decreased along with net radiation until approximately zero. On average throughout the growing season, the nighttime *H* was positive from the water releasing energy due to the surface being warmer than the air temperature. The energy released from the surface created unstable conditions where the lower temperature is greater than the upper above the canopy. Finally, it can be seen in Figure 22 that as the growing season progressed from AM to JJA, the amplitude of *H* decreased, then after July the amplitude begins to increase again through SO.

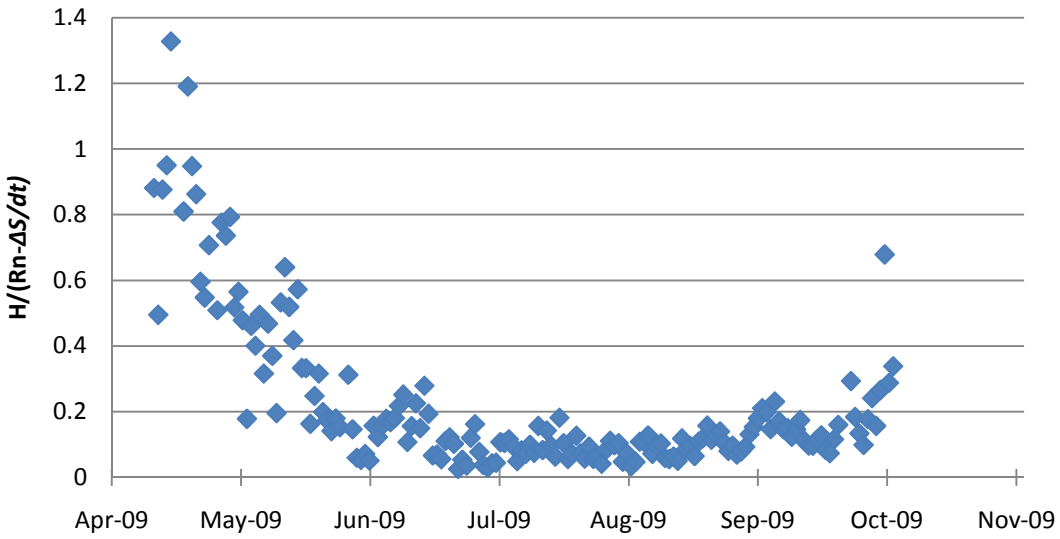

Figure 19. Ratio of sensible heat flux and available energy (net radiation minus heat storage rate) throughout the growing season.

2.6.6 *Latent Heat Flux and Evapotranspiration*

The 5-day average daily latent heat flux and evapotranspiration for the growing season is found in Figure 20 and the 5-day running mean is found in Figure 21. *LE* began to increase at the beginning of the growing season and continued to until late June. After May, the amount of available energy portioned into *LE* varied between 80 and 97% until mid-August, where during this period the atmospheric conditions mostly affected the ability for *P. australis* to transpire and not the plant growth (as seen from April-May). By the end of senescence, *LE* only used ~60% of the available energy. With the *P. australis* sprayed on July 22, there appeared to be minimal influence from the herbicide treatment on the ratio of available energy used by *LE*, but rather the slow decline of energy used was probably due to natural senescence.

Diurnally on average, *LE* increases and decreases along with net radiation throughout the day. As seen in Figure 22, the monthly diurnal averages change throughout the year with increasing *LE* from April-May to June-August and then decreasing towards September-October. Burba et al. (1999a) found that the *LE* maximum occurred about 1-2 hours after the peak in *Rn*, while the maximum diurnal *LE* for this study occurred at peak *Rn* to an hour afterward. With the diurnal maximum of *LE* and *Rn* occurring during the same time, it can be inferred that the vegetated surface was more response to the available energy rather than the maximum wind and vapor pressure gradient (strong driver of open water evaporation) that occurs later in the afternoon. The average diurnal nighttime *LE* for all months throughout the growing season was generally a sink of energy. An exception to *LE* being a sink was during July from 19:00-3:00, when the diurnal average *LE* was -3 to -29 W m^{-2}. Throughout the growing season, the bulk amount of *LE* shifted from the first half of the day in April/May, to approximately mid-day during the peak growth months (June-August), and then after mid-day by September/October. This can be accounted for by the energy sequestered and released by $\Delta S/\Delta t$ of the wetland. During the evening hours of 16:00 and 17:00 for September/October, *LE* actually becomes greater than *Rn*, which is due to $\Delta S/dt$ energy that was released from the wetland surface.

The minimum daily averaged *LE* (ET) was -35.6 W m^{-2} (-1.25 mm day^{-1}) on April 14 and the maximum was 233.0 W m^{-2} (8.21 mm day^{-1}) on June 29. The daily maximum ET measured higher than past studies of 6.9 mm day^{-1} (Smid, 1974), 6.5 mm day^{-1} (Burba et al., 1999a), 6.3 mm day^{-1} (Fermor et al., 2001), 5.0 mm day^{-1} (Peacock and Hess, 2004), and 5.8 mm day^{-1} (Zhou and Zhou, 2009). The average daytime and nighttime *LE*

for this study was 242.4 and 6.1 W m^{-2}. The accumulated ET and precipitation throughout the growing season was 771 mm and 470 mm, with a ratio of 1.61. Assuming all upper and lower uncertainty bounds occurred; the accumulated ET maximum and minimums would range between 661 mm (1.4) to 897 mm (1.9).

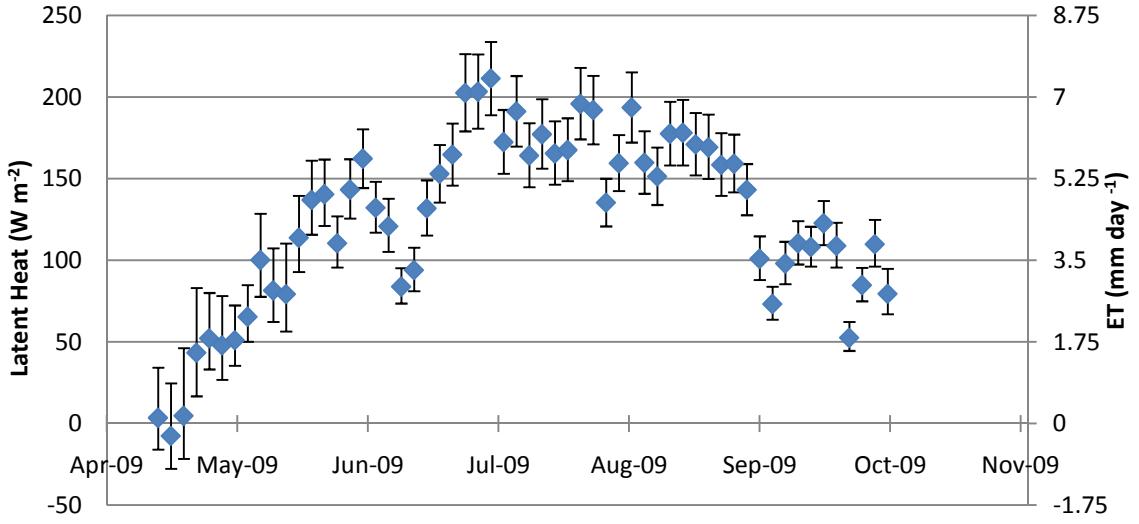

Figure 20. 5-day growing season averages of latent heat flux (W m^{-2}) and evapotranspiration (mm day^{-1}).

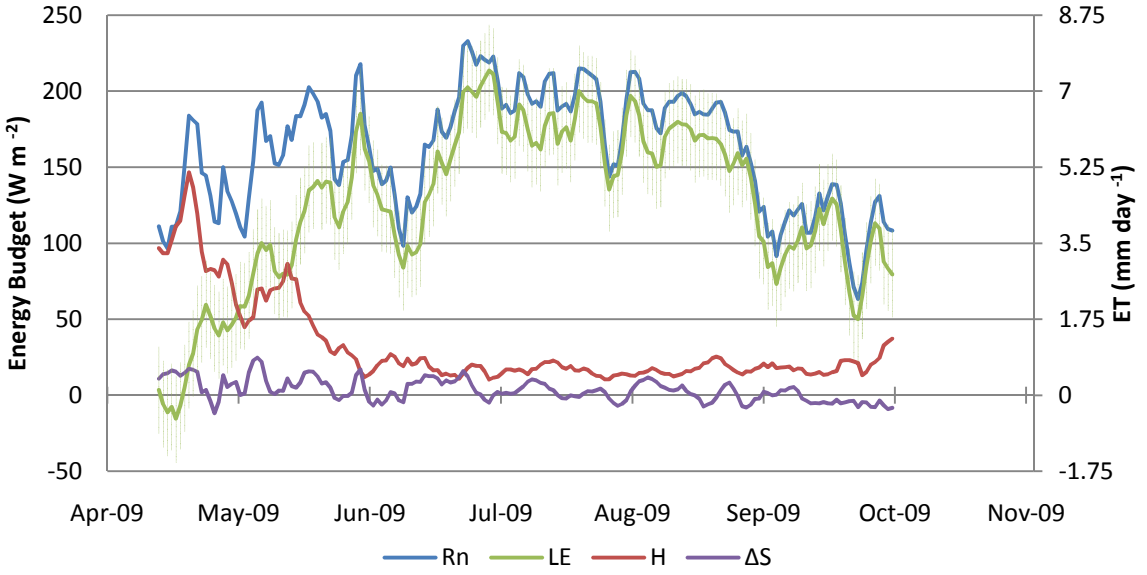

Figure 21. 2009 5-day running means of net radiation (blue), change in heat storage (purple), sensible heat flux (red), latent heat flux (green dashed line), and evapotranspiration (green). The shaded green area represents the uncertainty of latent heat flux.

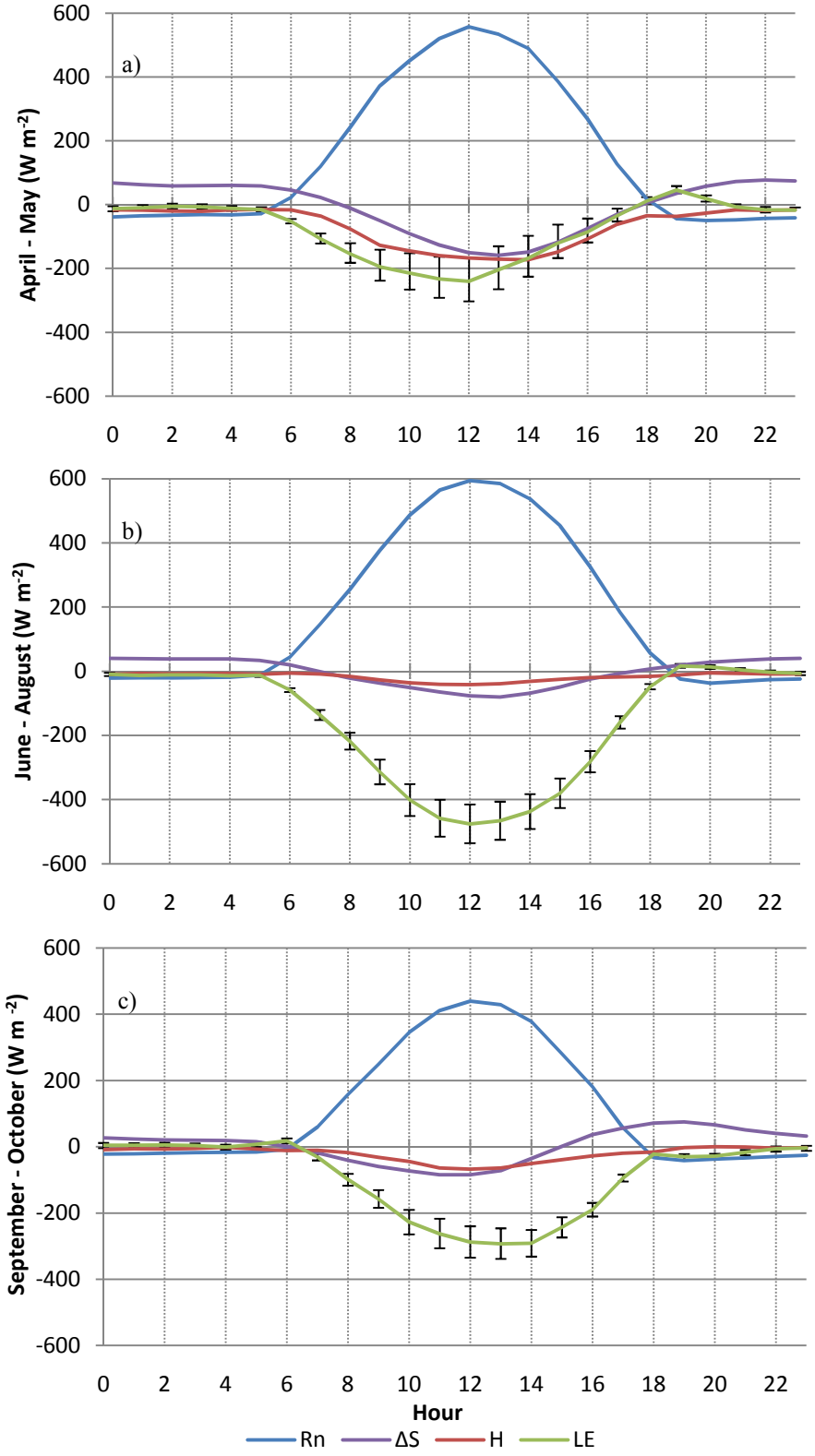

Figure 22. 2009 monthly average of a) April/May, b) June/July/August, and c) September/October diurnal cycles of net radiation (blue), heat storage rate (purple), and sensible heat (red) and latent heat flux (green).

2.6.7 *Priestley-Taylor ET Estimates*

The 5-day running mean for the energy balance and Priestley-Taylor derived latent heat flux and evapotranspiration is seen in Figure 23. The largest deviation between both methods occurred during the early part of the growing season, where afterwards both methods agreed throughout the remaining of the growing season, with an r-squared value of 0.78. If the growing season is broken up before and after June 1 (period when vegetation becomes dominate), the r-squared value is then 0.22 for April 11 to May 29 and 0.97 for June 1 to October 3. The daily average *LE* for P-T was 139 W m^{-2} compared to 124 W m^{-2} from the energy balance derived ET, and the daily accumulated ET from the P-T method was 861 mm, 11% higher than the energy balance derived ET.

A possible reason for the deviation could be that the P-T equation has been found to fail under dry conditions or periods when the wind speed is relatively high (McAneney and Itier, 1996). From the LAS, high advection of sensible heat was measured through most of April and parts of May, which could explain why the P-T equation is not a good estimate during that time period. In conclusion, once the vegetation becomes dominate and the air over the wetland more humid and wind speed decreases, the P-T is a good approximation of the ET for the wetland.

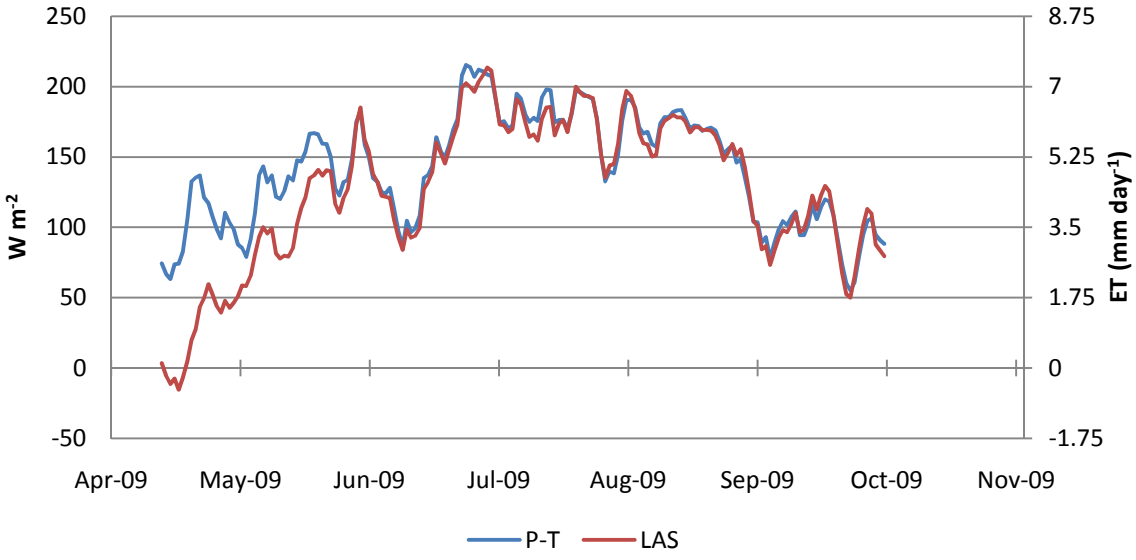

Figure 23. Latent heat (W m^{-2}) and evapotranspiration (mm day^{-1}) five-day running means derived from the Priestley-Taylor equation (dashed) and the LAS energy balance.

2.6.8 *Water Balance*

Precipitation, water level, and accumulated precipitation minus energy balance derived ET (P-ET) for the growing season can be found in Figure 23. To better understand the other water balance components of net groundwater and overland flow, the accumulated P-ET was forced to begin at the water level on April 11. In April, the water level continues to increase through mid-June, while the P and ET stay relatively balanced until mid-June. After mid-June, the water level beings to decrease rapidly until early September when then the water level begins to level off and stay neutral. From mid-June, P-ET also decreases throughout the remaining of the growing season and "crosses" the water level in early August (Figure 23). From this, it can be concluded that the wetland was affect by a net increase in $G_{net} + R_{net}$ from late April to early August (where lines "cross"). Afterwards, there is a net decrease in $G_{net} + R_{net}$ until the end of the growing season. During the net increase of $G_{net} + R_{net}$, two periods of positively

and negatively fluxes affected the water level. From April to June, $G_{net} + R_{net}$was acting towards increasing the water level, and afterwards it was decreasing the water level. Without the net increase of G_{net}throughout the growing season, total accumulated ET may not have been reached in the wetland due to the absent water in the wetland.

It is believed that $G_{net}$is the main cause of increasing and decreasing water level that is not seen in the P-ET, rather than overland flow. From observations, while there is a small spring on the western portion of the wetland, there is no sharp gradient of land surrounded the wetland that would cause large amounts of water to flow into the wetland. It is also known that there are agricultural fields surrounding the wetland, of which flooding and center pivots irrigate the majority of fields that would have an effect on groundwater during July and August. Finally, with the wetland location only 500 meters north of the Republican River, any water that percolates into the catchment soil north of the river would progress south towards the river. A comparison between May 24 and July 15 revels the importance of groundwater fluxes in the wetland. While the change in magnitude between the water level and accumulated *P*-ET are similar on July 15, the water level has a greater percent change on May 24 than the accumulated *P*-ET. This difference is probably due to the small spatial extent of the July 15 rain event, but May 24 consisted of a more widespread event, which would have had a greater influence on the groundwater flow through the catchment through percolation. Due to the importance of groundwater in this region, piezometers have been placed around the wetland to measure the groundwater influx and discharge.

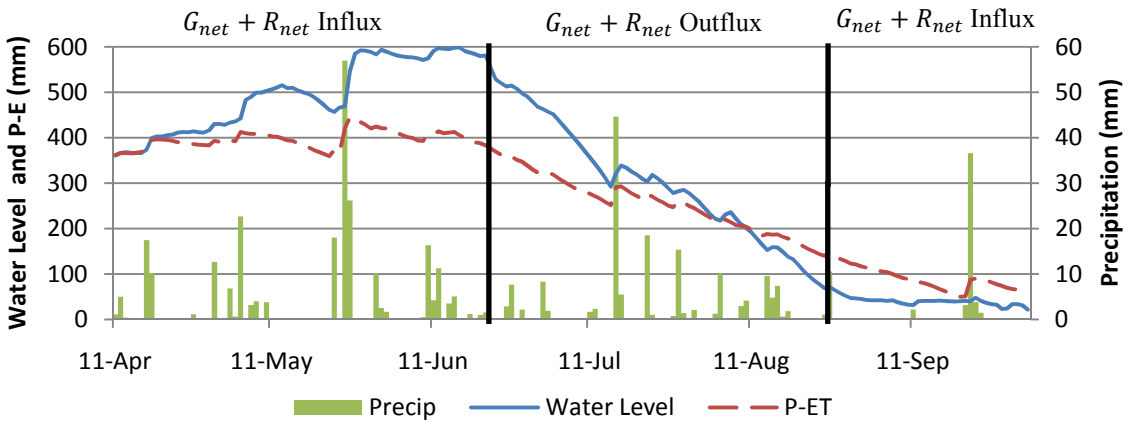

Figure 24. Daily precipitation (mm), wetland water level (mm), and precipitation minus LAS evapotranspiration (mm). Black lines represent the periods of net groundwater and overland flow influx and discharge.

2.7 Discussion and Conclusions

A energy balance study was conducted in a wetland over *Phragmites australis* in southwest-central Nebraska in 2009. A Large Aperture Scintillometer (LAS) system was used to calculate sensible heat flux (*H*) and then calculate the residual latent heat flux (*LE*) using the earth's energy budget. The supplement measurements of net radiation (*Rn*) and heat storage rate ($\Delta S/\Delta t$) were also directly calculated in the *P. australis* location. The Priestley-Taylor (P-T) was used as an additional method to calculate ET, along with the water balance to determine the influences of groundwater on the water storage of the wetland. The growing season was defined from April 11 to October 13, while both May and July of 2009 were characterized by well-above-normal precipitation and August-October was cooler than normal. *P. australis* emerged from the water surface approximately April 20 and grew to a maximum height of 4.2 meters in early July. The Leaf Area Index (LAI) ranged from 2.5 on May 27th to 5.42 on July 22nd.

July consisted of the highest monthly incoming shortwave radiation of 296 W m^{-2} and net radiation of 192 W m^{-2}. Due to a cloudy June, May received more incoming radiation (275 W m^{-2}) than June (264 W m^{-2}). The daily albedo ranged from 0.16 to 0.24 and the daily to weekly variations were found to be related to the cloud cover. The increased cloud cover resulted in higher diffuse radiation which in turn increased the ratio of reflected shortwave to incoming radiation due to the equally illumination on all sides of the plant leaf. A seasonal albedo increased due to the *P. australis* LAI increasing and less shortwave radiation reaching the lower albedo water surface. Finally, diffuse and direct radiation was found play an important role to determine how much net radiation reaches the surface. Factors such as background (water/soil) albedo, LAI, DIFN, leaf orientation, zenith angle, and leaf reflectance will make each vegetated surface uniquely different in its response to seasonal albedo.

The heat storage rate was calculated by finding the heat storage in the deep soil, upper soil, water, and vegetated canopy. With a total heat storage daily maximum and minimum average of 56.0 and -61.3 W m^{-2},the water storage was the most significant energy source and sink of the $\Delta S/\Delta t$ with a maximum and minimum daily storage of 51.7 and -67.0 W m^{-2} during late April and early May. The monthly average diurnal $\Delta S/\Delta t$ reached a maximum in May (177 W m^{-2}) and a minimum in July (40 W m^{-2}) where the *Rn* partitioned in $\Delta S/\Delta t$ changed from 33 to 7%. The $\Delta S/\Delta t$ monthly diurnal cycle also varied over the growing season due to the changes of net radiation, water level, water temperature, and latent heat flux. *Rn* was never less than the heat storage at night, indicating sensible and/or latent heat must have been the sink of the available energy from $\Delta S/\Delta t$ that was released from the wetland. Finally, $\Delta S/\Delta t$ began the growing season

by sequestering more energy than releasing and towards the end of the growing season $\Delta S/\Delta t$ was releasing more energy than sequestering.

H varied in magnitude throughout the growing season with the highest fluxes at the beginning of the season and the lowest during the full vegetation. *H* reached an average daily maximum of 199.0 W m^{-2} in mid-April with no vegetation, and a daily minimum of 5.5 W m^{-2} in late June with full vegetation. *H* acquired the majority of available energy during April and May, and then decreased to 0.2-18% from late-June to mid-August. On average throughout the growing season, since the water surface was warmer than the air temperature, nighttime *H* was negative (flux from surface to the atmosphere) due to the water releasing energy.

The latent heat flux was the largest sink of available energy once the vegetation began to reach approximately three meters in height. After May, the amount of available energy portioned into daily *LE* varied between 80 and 97% until mid-August, and by the end of senescence daily *LE* only used ~60% of the available energy. Although observations during 2010 reveled that *P. australis* had been killed due to the herbicide spraying, there was no strong evidence that the spraying on July 22 caused an unnatural decrease in *LE* during the 2009 season. The bulk *LE* occurred in the first half of the day in April/May and shifted to the later half in September/October due to $\Delta S/\Delta t$. During September/October the diurnal daytime average *LE* became larger than net radiation due to the release of energy from the heat storage. The daily maximum was 233.0 W m^{-2} and 8.21 mm day^{-1} on June 29, and the average daytime and nighttime *LE* was 242.4 and 6.1 W m^{-2}. The average rate of *LE* during the growing season was 124 W m^{-2} (4.4 mm day^{-1}) and the ratio of accumulated ET (mm) to precipitation (mm) was 771 to 410 (1.61).

Assuming all upper and lower uncertainty bounds occurred; the accumulated ET maximum and minimums would range between 661 mm (1.4) to 897 mm (1.9).

The Priestley-Taylor agreed well with the energy balance derived ET after June 1, but during the beginning of the growing season the P-T method overestimated ET. The daily average *LE* for the P-T equation was 139 W m^{-2} compared to 124 W m^{-2} estimated from the LAS, and the daily accumulated ET from the P-T method was 861 mm, 11% higher than the energy balance derived ET. In conclusion, once the vegetation becomes dominate and the air over the wetland more humid and wind speed decreases, the P-T is a good approximation of the ET for the wetland.

It was concluded that precipitation and ET were not the only factors acting on the water storage of the wetland and a net increase of water storage from groundwater was observed. From April 11 to mid-June there was a net influx from groundwater and overland flow into the wetland, afterwards a net outflux until early September, and then another net influx through the end of the growing season. It is believed that the groundwater is the major factor acting on the wetland water storage besides P and ET. To further understand the importance of groundwater piezometers have been placed around the wetland to measure the groundwater influx and discharge. Nonetheless, without the influence of groundwater and/or overland flow on the water storage, the accumulated ET may not have been reached.

Chapter 3

Comparison of Energy Balance between *Phragmites australis* and Native Vegetation (*Typha latifolia*)

3.1 Introduction

One possibility after the removal of *P. australis* is that a native plant species, like *Typha latifolia*, will move in and replace the invasive *P. australis*. The purpose of this chapter is to compare the ET rates between *P. australis* and *T latifolia* and estimate the "water saved" if *T. latifolia* replaces *P. australis*. Therefore, it is important to estimate the evapotranspiration rates between both vegetations. Understanding the differences between heat storage and the atmospheric conditions between both vegetations are also desired and could help explain ET differences between both vegetations. Finally, a comparison of the energy balance derived ET, Priestley-Taylor, and remote sensing for *Phragmites australis* will be conducted. The methodology for the surface energy budget, LAS, and the Priestley-Taylor can be found in Chapter 2.4. The instrumentation and methodology is presented in section 2, results in section 3, and the discussion and conclusions are found in section 4.

3.2 Methodology

3.2.1 *In-Situ (Measurements)*

Two meteorological towers were installed in the wetland to monitor the surface energy and water balance, as well as basic meteorology. One station is located near the in the invasive *P. australis* vegetation (refer to Chapter 2.3), while the other station is positioned at the eastern end of the wetland amongst the native *T. latifolia* (see Figure 2). The *T. latifolia* tower is 4.9 meters in height and located in the eastern portion of wetland surrounded by trees greater than 30 meters away from the station on the north, east, and south sides (Figure 2). Both stations consists consist of the same instruments described in Chapter 2.2 with the exceptions the *T. latifolia* station was not equipped with a non-aspirated temperature/relative humidity sensor within the vegetation canopy, a pyranometer, or a water level sensor. The instrumentation height comparison for both stations is found in Table 2. The *T. latifolia* station shut down due to power failures from April 17 – April 23 and from May 2 – May 8. Refer to Chapter 2.3 for information regarding the water and soil temperatures, as well as the specific and thermal conductivity of the soil.

	***P. australis* Station (m)**	***T. latifolia* Station (m)**
Wind speed	6.3	5.1
Wind direction	6.3	5.1
Upper aspirated temperature/RH	5.9	4.2
Lower aspirated temperature/RH	4.1	2.4
Net radiation	5.0	3.2
Radiometric surface temperature	5.0	3.2
Atmospheric pressure	3.2	2
Rainfall rate	4.2	1.6

Table 2. Measurement heights (m) of the meteorological instruments at the *P. australis* and *T. latifolia* stations relative to the soil/water interface.

3.3.1 *Landsat 5TM Remote Sensing*

The Landsat 5TM satellite is one of many remote sensing tools that can be utilized to acquire ET from small to large regions. The Landsat satellite whose image resolution is approximately 30 meter is an earth-observing satellite jointly managed by the National Aeronautics and Space Administration and the U.S. Geological Survey that began in 1972. The use of Landsat for this project is not only to view the difference between native and non-native vegetation, but also to compare the ET rates with measured in-situ rates at the field site. The Landsat imagery was acquired online for row 32 path 30 on five different days for 2009 (USGS). The days and time (Central Standard Time) acquired were April 19 (13:39), June 22 (13:23), July 8 (19:47), July 24 (15:03), and September 26 (14:29). All days no zero cloud cover except for April 19 (7 % cloud cover), of which the clouds did not overlap with the study area. Only the red and near infrared spectral bands were used in this study to calculate ET.

Once the bands were collected for each day, the original files were converted from TIF format to ESRI GRID format for further calculations in ArcGIS. To calculate ET, two values are needed, the normalized vegetation index (NDVI) and the reference ET for the wetland. The spectral radiance and reflectance are needed to calculate NDVI (Chander and Markham, 2003), and the vegetation fraction cover and surrounding weather station data are needed to calculate a reference ET for the wetland (Gillies et al., 1997).

Spectral radiance is the outgoing radiation energy of each band as observed at the top of the atmosphere by the satellite. Equation 18 is used to convert the ESRI GRID bands from digital to spectral radiance:

$$L = \frac{(L_{max} - L_{min}) * (Q_{cal} - Q_{cal\,min})}{(Q_{cal\,max} - Q_{cal\,min})} + L_{min}\,, \qquad (18)$$

where L (W m^{-2} $ster^{-1}$ μm^{-1}) is the spectral radiance at the sensor aperture, L_{max} is the spectral radiance scaled to $Q_{cal\,max}$ (W m^{-2} $ster^{-1}$ μm^{-1}), L_{min} is the spectral radiance scaled to $Q_{cal\,min}$, Q_{cal} is the quantized calibration pixel value (digital number or DN), $Q_{cal\,min}$ is the minimum quantized calibration pixel value (DN=0) corresponding to L_{min}, and $Q_{cal\,max}$ is the maximum quantized calibration pixel value (DN=255) corresponding to L_{max}. Since $Q_{cal\,min}$ is equal to zero for Landsat 5TM, Equation 18 simplifies to

$$L = \frac{(L_{max} - L_{min}) * (Q_{cal})}{(Q_{cal\,max})} + L_{min}\,, \qquad (19)$$

where L_{min} and L_{max} values for bands three and four are (-1.17, 264.0) and (-1.51, 221.0) respectively (C., Gyanesh and B. Markham, 2003).

Once the spectral radiance is found, the reflectance of light at the top of the atmosphere can be converted from the spectral radiance by

$$r = \frac{\pi * L * dr}{E_{sun} * \cos(\theta_s)}\,, \qquad (20)$$

where r (unit less) is the planetary reflectance, L is the spectral radiance at the sensor aperture from Equation 19, dr (astronomical units) is the inverse square of the earth-sun distance, E_{sun} (W $m^{-2}ster^{-1}$ μm^{-1}) is the mean solar exoatmospheric irradiance, and θ (degrees) is the solar zenith angle. For bands three and four, E_{sun} is 1554 and 1036 W $m^{-2}ster^{-1}$ μm^{-1} respectively (C., Gyanesh and B. Markham, 2003). To find dr, the day of year (DOY) is used in

$$dr = 1 + 0.033 * \frac{\cos\,(DOY * 2 * 3.141592654)}{365}\,, \qquad (21)$$

where for 2009, the *DOY* year equals 109, 173, 189, 205, and 269. In our case with flat terrain, θ can be simplified as the sun elevation over the horizon subtracted from 90°. The sun elevation for each *DOY* was found to be 54.74° (109), 64.12° (173), 62.93° (189), 60.75° (205), and 44.28° (269).

After the reflectance for both bands have been calculated, the Normalized Difference Vegetation Index (NDVI) can be solved by using the ratio of reflectance found in Equation 20:

$$NDVI = \frac{(NIR - RED)}{(NIR + RED)}, \qquad (22)$$

where *RED* and *NIR* is the spectral reflectance measurements in the red (0.63 – 0.69 μm) and near-infrared (0.77 – 0.90 μm) regions of the electromagnetic spectrum. *NDVI* ranges from negative -1 to 1, where the higher *NDVI* indicates the higher the fraction of live green vegetation in the imagery cell. From the NDVI, the fraction of vegetation cover (*Fr)* can be found using Equation. 22 by (Gillies et al., 1997)

$$Fr = \left[\frac{(NDVI - NDVI_s)}{(NDVI_{veg} - NDVI_s)}\right]^2, \qquad (23)$$

where $NDVI_s$ and $NDVI_{veg}$ is the NDVI at bare soil and a fully vegetative surface which are used to represent the minimum and maximum *NDVI* values of the Landsat imagery.

Reference ET is the rate at which a moist environment readily vaporizes water from a specific vegetative surface. Reference ET data was obtained from Nebraska's Automated Weather Data Network (AWDN) at the High Plains Regional Climate Center (HPRCC) and uses the Penman-modified equation to calculate reference ET for the crop alfalfa in millimeters per day (mm day^{-1}). The stations of Curtisunta, Holdrege, Holdrege 4N, Lexington, McCook, Minden, and Smithfield, Nebraska were used to calculate the reference ET for the wetland. An inverse distance interpolation was used to incorporate

each stations reference ET for every *DOY*. The distances to AWDN stations were kept below 50 miles from the wetland to represent the best reference ET for the wetland (Figure 25). Once the reference ET was calculated for the wetland, the actual ET for the wetland can be found by

$$ET = Fr * ET_{ref} . \qquad (24)$$

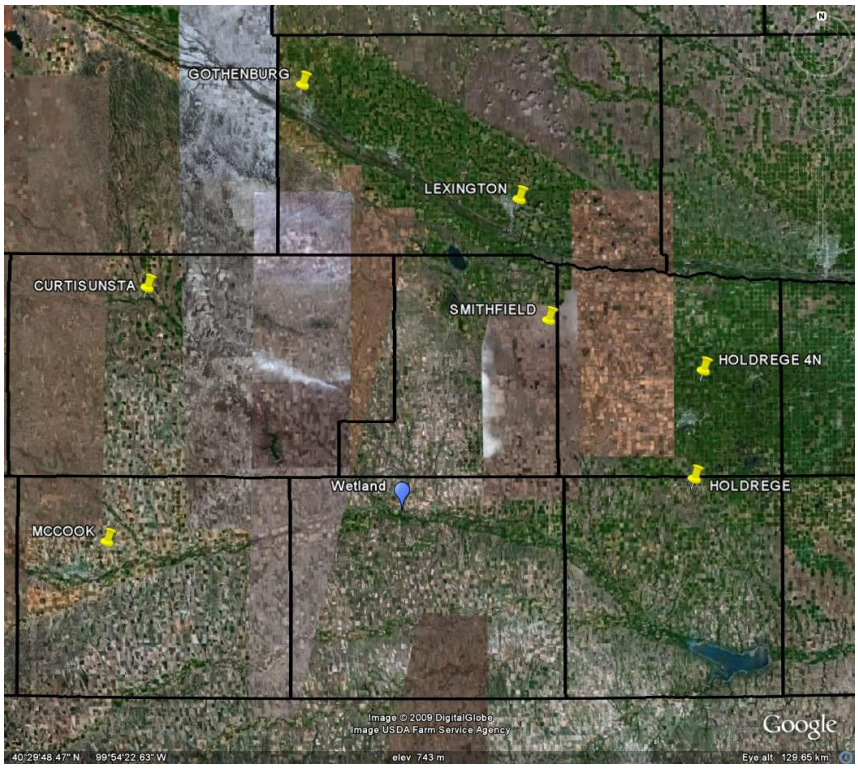

Figure 25. Seven Automated Weather Data Network stations (yellow) used to calculate reference ET for the wetland (blue).

3.3 Results

3.3.1 *Vegetation Height and Leaf Area Index*

Similar to the vegetative information described for *P. australis* in Chapter 2.6.2, the *T. latifolia* began to grow in stands of dead biomass from the previous growing

season. The new shoots of *P. australis* emerged from the wetland water surface approximately two weeks before *T. latifolia*. Both vegetations had a similar growth rate with *T. latifolia* reaching a maximum height of 3.2 meters a week before *P. australis* reached a maximum height of 4.2 meters (Figure 26). The measurements for *P. australis* can be found in Chapter 2.6.2. Although there were no LAI or biomass measurements taken from *T. latifolia* during the 2009 growing season, *T. latifolia* LAI has been measured throughout 2010 (last measurement on July 21), which measured an LAI of 1.3 on May 26 and 3.9 on July 21. Assuming that the *T. latifolia* vegetation is approximately the same for both 2009 and 2010, it can be conclude that *T. latifolia* LAI is ~66% less than *P. australis* in late-May and reduces to ~34% less in mid-July.

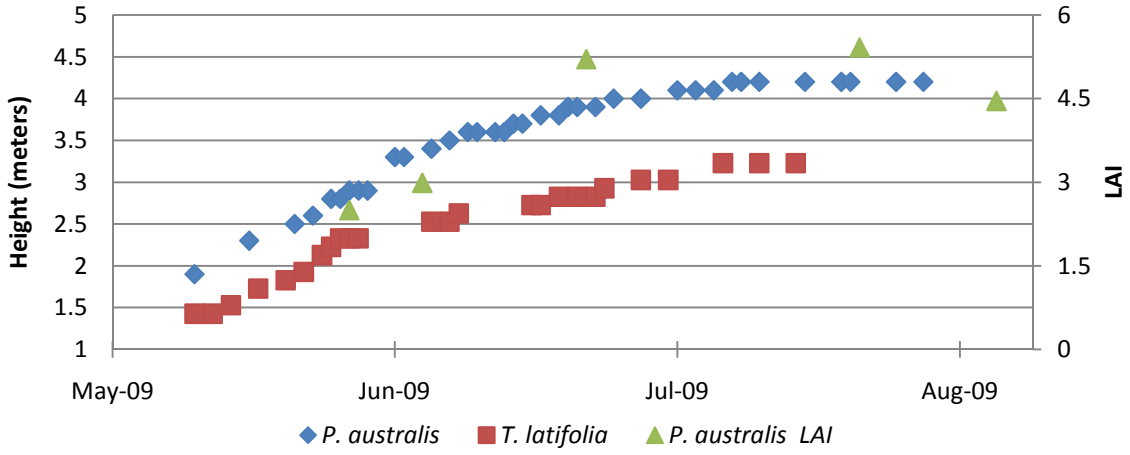

Figure 26. *P. australis* (diamond) and *T. latifolia (square)* observed plant heights and *P. australis* LAI (triangle).

3.3.2 *Meteorological Conditions*

The daily surface meteorological measurements of the water level, precipitation, air temperature, water temperature, relative humidity, and wind speed is found in Figure 27. The water level within the *T. latifolia* was approximately 13 cm lower than *P.*

australis throughout the growing season, resulting with the water level falling below the soil/water interface in *T. latifolia* from late August until the end of the growing season. The *T. latifolia* average temperature above the canopy was 0.2 °C cooler than *P. australis*, which is probably due to the smaller distance between the temperature sensor and the water surface at the *T. latifolia* station. The water temperature was generally warmer within *T. latifolia*, with the largest deviations occurring during July before the last measurement of water temperature was made at the *T. latifolia* station. April and May exhibited periods of multiple days with daily relative humidity below 60% along with wind speeds greater than 2 ms^{-1} (dry air advection) until the end of May, where afterwards wind speed increased and relative humidity decreased. The relative humidity at the *T. latifolia* station was generally higher than *P. australis*, which could in part be due to less air mixing that resulted from the lower wind speed over *T. latifolia* as well as the shorter distance between the water level and temperature sensors. As seen in Figure 27e and described in Chapter 2.6.1, due to the denser trees around the eastern portion of the wetland, the "wind shading" (lower wind speeds) affected was even greater over the *T. latifolia* than over the *P. australis*.

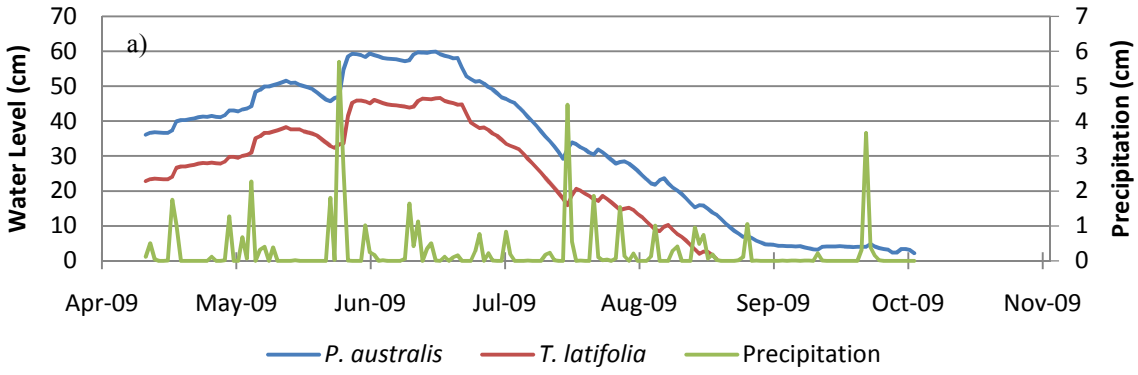

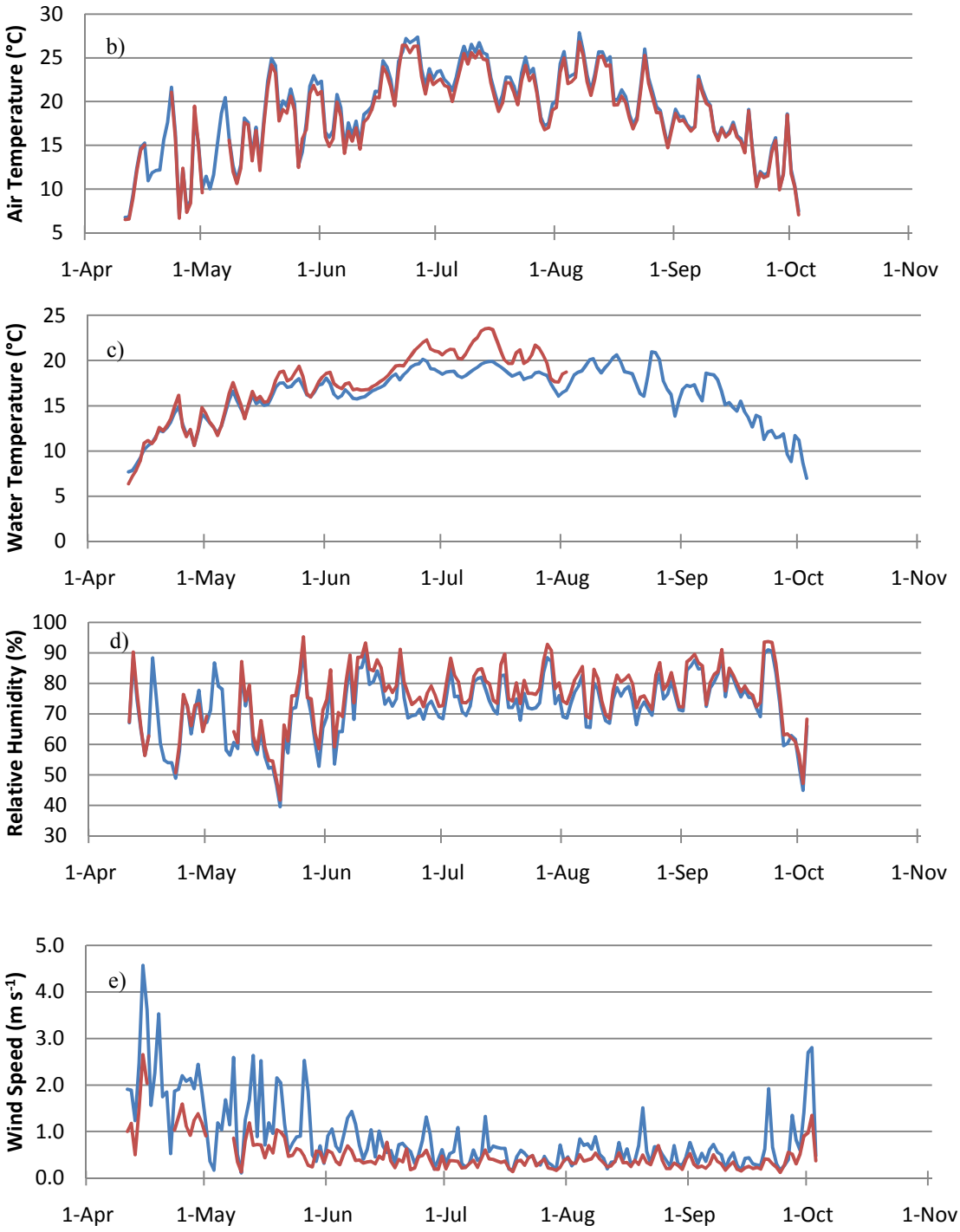

Figure 27. 2009 *P. australis* (blue line) and *T. latifolia* (red line) daily mean a) precipitation (green) and water level (cm), b) air temperature (°C), c) water temperature (°C), d) relative humidity (%), and e) wind speed (ms^{-1}) from the *P. australis* and *T. latifolia* meteorological stations.

3.3.3 *Surface Radiation Balance*

A general description of the surface radiation balance for the wetland throughout the growing season can be found in 2.6.3. The daily shortwave albedo, which is dependent on the angle of the sun, cloud cover, and surface characters (i.e. vegetation and water cover), varied throughout the year with *P. australis* and *T. latifolia* reaching a daily minimum of 0.16 (May 17) and 0.16 (July 14) and maximums of 0.24 (June 8) and 0.32 (April 11) (Figure 28). The growing season trend for *T. latifolia* shows decreasing albedo throughout vegetation growth, where after late July, the albedo begins to increases. The opposite occurs over *P. australis* where albedo increased during vegetation growth and decreased after late July. The albedo differences between the two vegetations could occur because of the later initial growth and earlier senescence of *T. latifolia*, allowing for greater reflectance from the dense brown vegetation rather than green vegetation. In addition, due to the dead *T. latifolia* being shorter and thicker than dead *P. australis* (from observations), less water is exposed, allowing less energy to be absorbed and reflected by the lower water albedo.

The monthly averages for each individual component of the radiation balance from the *P. australis* and *T. latifolia* stations are found in Table 3. July had the largest average incoming solar radiation, and while June's radiation would generally be higher than May (due to the earth-sun proximity), this was not the case due to frequent cloud cover decreasing the incoming solar radiation. The month of July received the most net radiation for both stations, and the daily and daytime averaged *Rn* reached a maximum on June 16 with fluxes of 248 W m^{-2} and 409 W m^{-2} at the *P. australis* station. From April to September there was less than 2% deviation between the longwave components at both

stations. The greatest difference occurred in April when the *T. latifolia* albedo was 5% higher in April, and along with higher outgoing longwave, resulted in *P. australis* April *Rn* being 9% higher. In terms of the total available energy from *Rn* during the growing season, there was less than a 1% difference, which is insignificant and could reside in instrument error.

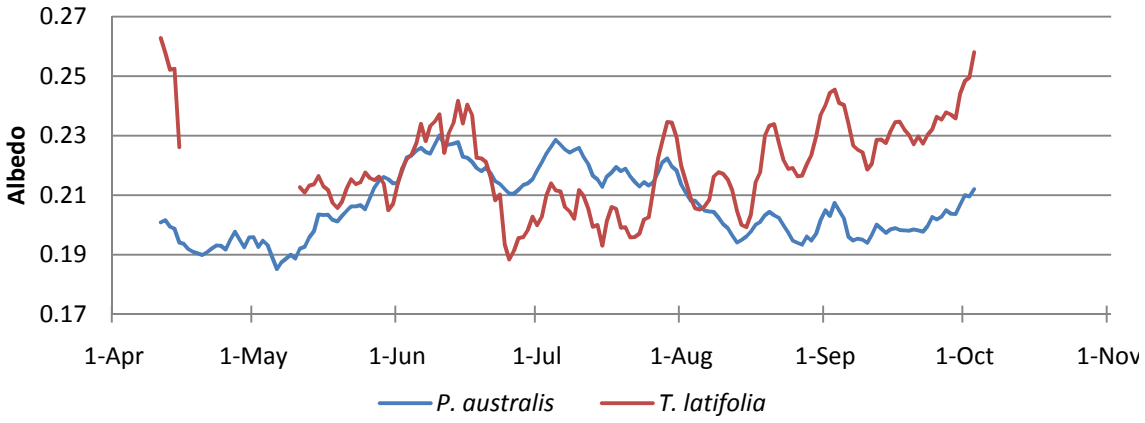

Figure 28. 2009 5-day running mean albedo comparison between *P. australis* and *T. latifolia*.

Month	Incoming Shortwave		Shortwave Albedo		Outgoing Longwave		Net Longwave		Net Radiation	
	P.aus	***T. lat***	***P.aus***	***T. lat***	***P.aus***	***T. lat***	***P.aus***	***T. lat***	***P.aus***	***T. lat***
April	*227*	-	*0.19*	*0.24**	*371*	*396**	*-51*	*-48**	*132*	*124**
May	*275*	-	*0.22*	*0.22**	*391*	*395**	*-53*	*-55**	*167*	*174**
June	*264*	-	*0.22*	*0.21*	*406*	*407*	*-37*	*-37*	*169*	*171*
July	*296*	-	*0.22*	*0.21*	*412*	*415*	*-39*	*-39*	*192*	*196*
August	*280*	-	*0.20*	*0.22*	*409*	*410*	*-41*	*-42*	*183*	*178*
September	*185*	-	*0.21*	*0.24*	*380*	*383*	*-37*	*-35*	*111*	*104*

Table 3. 2009 *P. australis* and *T. latifolia* average monthly radiational components from April 11 to October 3 (October was included in September's calculation). (*) indicates six days missing.

3.3.4 *Heat Storage Rate*

The heat storage rates for *P. australis* and *T. latifolia* were controlled by the available energy at the water surface, water temperature (Figure 27c), and water depth

(Figure 27a). Throughout the growing season, both heat storage rates exhibit similar fluctuations seen in (Figure 29) that are driven by the available energy. When comparing the individual portions of the $\Delta S/\Delta t$, the water storage of the *P. australis* was generally larger in magnitude than the *T. latifolia* (Table 4). The upper and deep soil storages were larger in magnitude throughout the year at the *T. latifolia* site. The $\Delta S/\Delta t$ between the two sites began to deviate in late July, where $\Delta S/\Delta t$ of *T. latifolia* began a trend to release more heat than sequester, of which did not occur until early September within *P. australis*. Although the total $\Delta S/\Delta t$ deviates between both locations during the growing season, both deep soil storage rates began to release energy into the water in mid-September. Since the water level in the *T. latifolia* was approximately 13 cm lower than at the *P. australis,* the water level was potentially a large driver for the differences between the soil and water storages of both sites.

The average diurnal heat storage rate throughout the growing season for both *P. australis* and *T. latifolia* were also unique from one another (Figure 30). The *P. australis* diurnal heat rate storage began to increase at sun rise along with the net radiation, where then it reaching a maximum shortly after net radiation. Before *Rn* becomes negative, $\Delta S/\Delta t$ began to release energy back into the atmosphere and does throughout the night at a constant rate until the air temperature becomes warmer than the water. The diurnal $\Delta S/\Delta t$ of *T. latifolia* increases and begins to absorb energy shortly after *P. australis* (which could be caused by tree shading in the morning in the area of the *T. latifolia*). Both vegetated areas reach a maximum storage approximately at the same time, but *T. latifolia* only reaches half the magnitude of *P. australis*. *T. latifolia* declines slowly and

does not begin to release energy until 21:00, where afterwards the *T. latifolia* $\Delta S/\Delta t$ continues to decline until sun rise.

Each month's average diurnal $\Delta S/\Delta t$ for *P. australis* and *T. latifolia* varied along with the percent of energy used from net radiation. In May during the early growth of vegetation, *P. australis* reached maximum $\Delta S/\Delta t$ for the growing season with 177 W m^{-2} of the available 570 W m^{-2} from net radiation at 13:00. *T. latifolia* reached an earlier maximum $\Delta S/\Delta t$ of 98 W m^{-2} of the available 387 W m^{-2} for 13:00 in April. Once vegetation reached a maximum in July, *P. australis* $\Delta S/\Delta t$ maximum was 40 W m^{-2} of 597 W m^{-2} at 13:00 and *T. latifolia* was 73 W m^{-2} of 623 W m^{-2} at 13:00. The percent of available *Rn* partitioned into the vegetation for these months changed from 33 to 7% for *P. australis* and 25 to 11% for *T. latifolia*. This decrease was due to a larger canopy, decreased temperature gradient between the water and air, decreased water level, and increased energy used by latent heat. Throughout the growing season, primary due to the soil storage difference, *T. latifolia* sequestered 7 W m^{-2} or 28% more energy than *P. australis*.

Month	**Deep Soil**		**Upper Soil**		**Water**		**Total**	
	P.aus	***T. lat***	***P.aus***	***T. lat***	***P.aus***	***T. lat***	***P.aus***	***T. lat***
April	*0.78*	*4.0*	*3.0*	*5.7*	*5.8*	*5.0*	*9.7*	*14.8*
May	*1.8*	*4.6*	*2.2*	*3.2*	*3.7*	*1.6*	*7.7*	*9.4*
June	*1.8*	*3.8*	*1.2*	*2.0*	*.72*	*2.1*	*3.7*	*7.9*
July	*2.1*	*3.9*	*0.83*	*0.03*	*-1.1*	*-0.44*	*1.7*	*3.5*
August	*1.7*	*2.4*	*-0.2*	*-0.13*	*0.83*	*-1.0*	*2.3*	*-2.5*
September	*0.24*	*-0.23*	*-2.4*	*-3.0*	*-0.22*	*-*	*-2.3*	*-2.8*

Table 4. Comparison of the lower and upper soil, water, and total storage (W m^{-2}) from April 11 to October 3 (October was included in September's calculation).

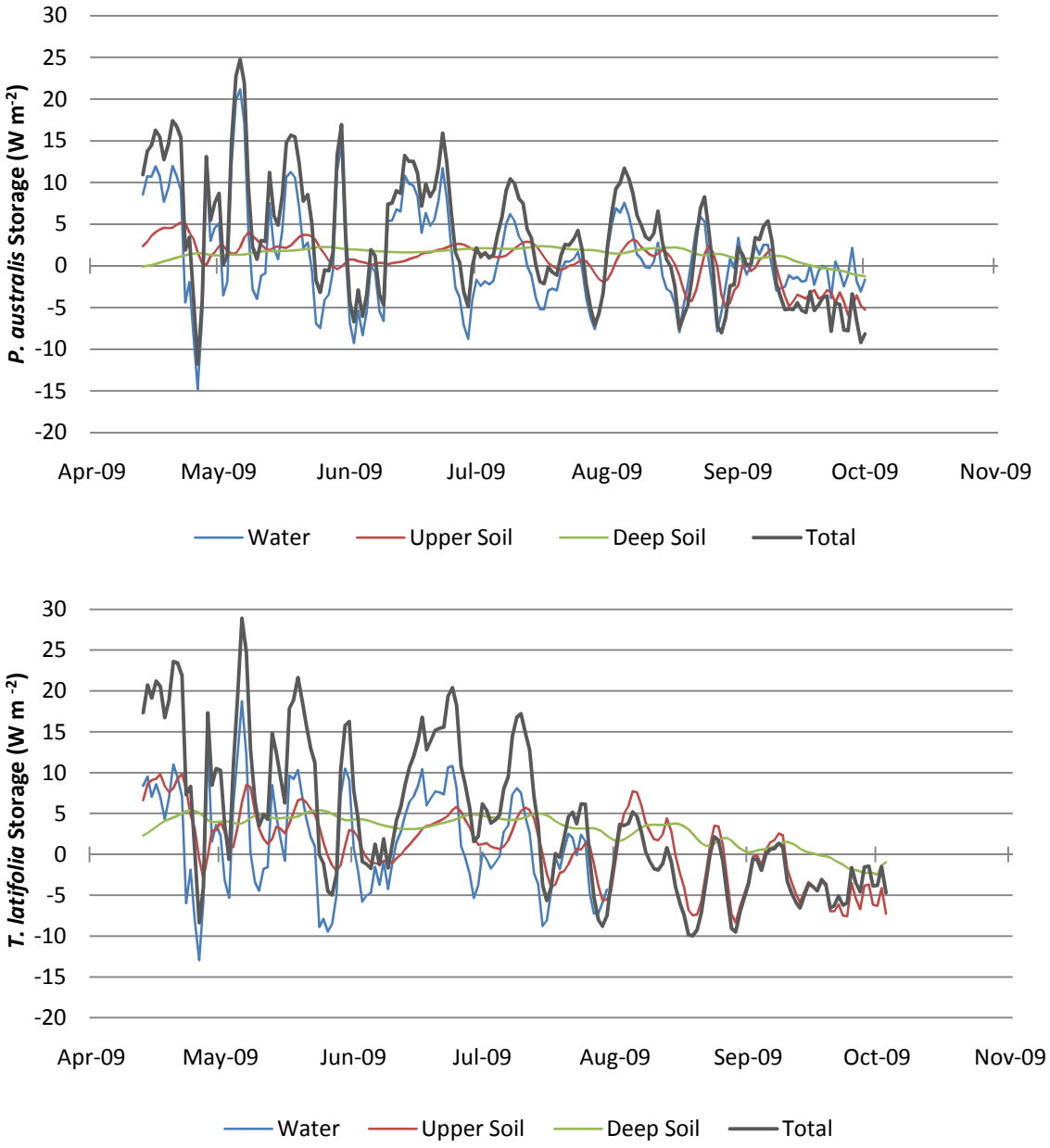

Figure 29. The growing season five day running mean heat storage (W m^{-2}) for water (blue large-dashed line), upper soil (red small-dashed line), lower "deep" soil (green cross-dashed line), and total storage (solid line) at the *P. australis* (top) *T. latifolia* (bottom) site.

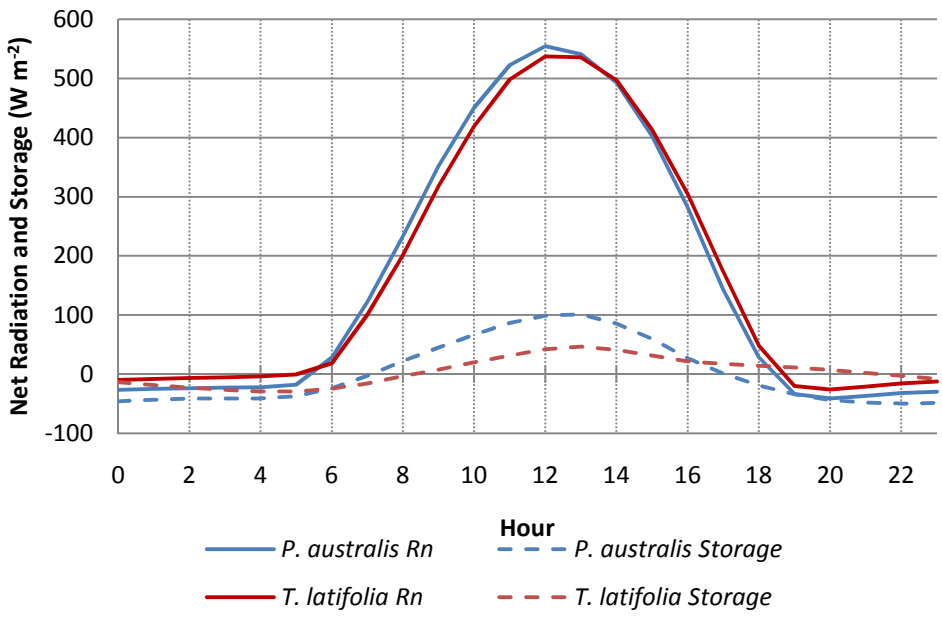

Figure 30. Diurnal averages of net radiation (solid line) and heat storage (dashed line) for *P. australis* (blue line) and *T. latifolia* (red line).

3.3.5 *Evapotranspiration*

The vegetated (green) and non-vegetated (red) surfaces is seen from the Landsat 5TM differences in ET rates in Figure 31. The outlined rectangles covering *P. australis* and *T. latifolia* in Figure 31a within the wetland were used to calculate an average ET for both surfaces on their respected DOY. The daily averaged ET rates from Landsat were then calibrated using a linear regression with the energy balance derived ET to account for the different methodologies. Using five days from Landsat ET and the energy balance ET, a linear regression fit through the x-y intercept yielded a 19% underestimation from Landsat ET (r^2=0.69). To account for the underestimation, the regression equation was used to calculate "new" ET rates from the initial Landsat *P. australis* and *T. latifolia* ET. The underestimated could be caused by the remote sensing methodology neglecting the local heat storage in the soil, water, and vegetation canopy.

The in-situ measurements also take into account evaporation from the water surface while the Landsat images only "looks" at vegetation. In addition, it is important to note that the reference ET used to calculate actual ET uses alfalfa as the vegetated surface, which is a different plant species than *P. australis* and *T. latifolia*.

Table 5 illustrates the Landsat daily-calibrated ET for both vegetated surfaces and the differences between both *P. australis* and *T. latifolia*. It can be seen that for each image, the *P. australis* area had higher ET rates than the *T. latifolia*, with differences ranging from 0.35-1.99 mm day^{-1} and over the five days *P. australis* averaged 28% (1.18 mm day^{-1}) greater daily ET. A study in a semi-arid wetland in Spain found that *P. australis* ET was 44% higher than *T. latifolia* over a 6 year study (Sánchez-C et al., 2004). Burba et al. (1999b) also concluded that *P. australis* averaged 11% higher daily ET than another small Nebraska native wetland species of *Scirpus acutus*.

A comparison of the calibrated Landsat values to the energy balance derived ET (with upper and lower error bounds) and Priestley-Taylor (P-T) daily ET averages are found in Figure 32. September 26 was the only day where the P-T equation and the energy balance had a significantly larger daily ET than the values calculated from Landsat. A disagreement between all three methodologies occurred on April 19, with the Landsat ET being greater than the upper ET bounds from the energy balance, but lower than the P-T ET. The high temperature advection, which occurred on April 19, has been found to cause errors for the P-T equation and may not have been accounted for by the Landsat methodology. The best agreement between all methodologies occurred during the period of full vegetation growth, where both Landsat and P-T ET rates were within the uncertainties of the energy balance ET. The three day ET averages during the full

growth period (June 22, July 8, July 24) for the Landsat, P-T, and energy balance were 7.23, 7.30, and 7.16 mm day^{-1}.

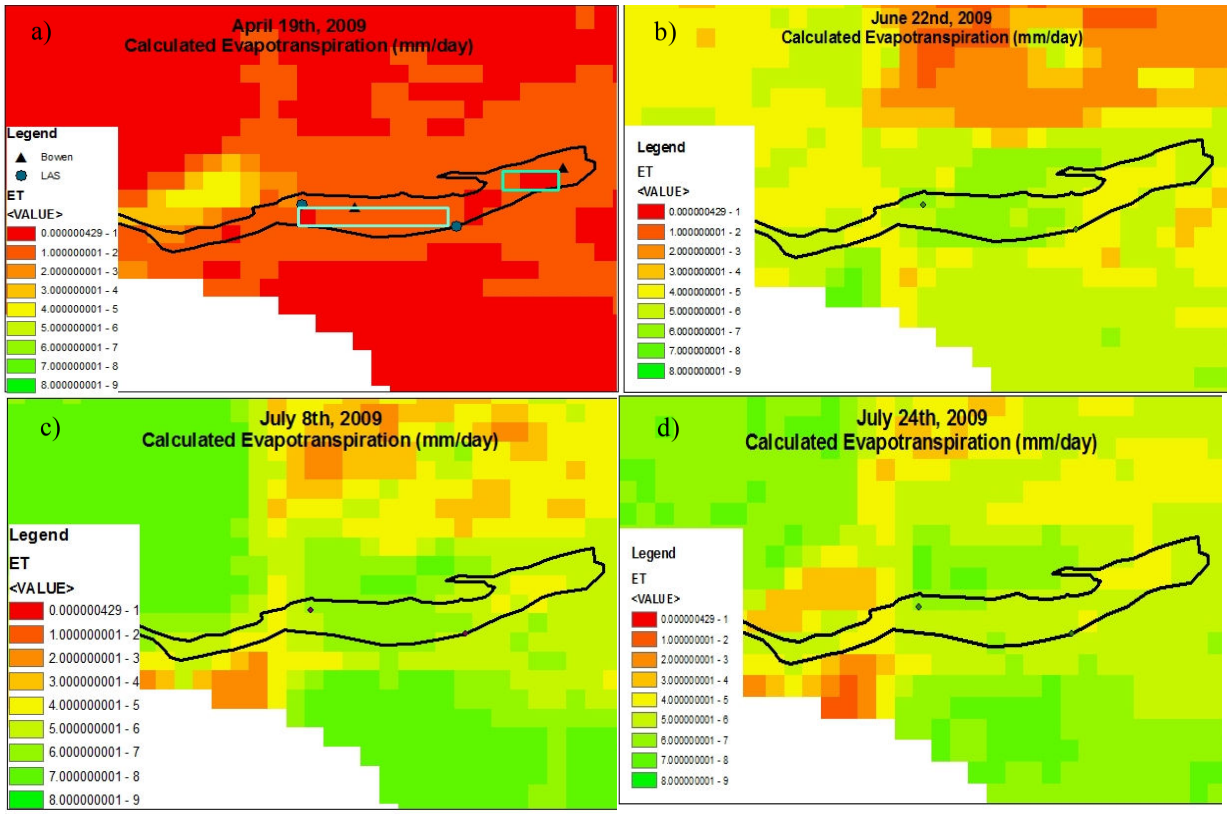

Figure 31. The daily evapotranspiration (mm day^{-1}) derived from Landsat, ranging from high (green) to low (red) for four respected days (pre-calibrated). The rectangles in (a.) represent the area used to average the daily ET. The wetland boundary (solid black line), LAS receiver and transmitter (circles), and *P. australis* and *T. latifolia* (triangles) are illustrated in the graphs above.

Day	*P. australis* ET (mm day^{-1})	*T. latifolia* ET (mm day^{-1})	Difference ET (mm day^{-1})	% Difference
April 19	1.39	1.04	0.35	28.6
June 22	7.35	5.36	1.99	31.2
July 8	7.57	5.77	1.80	27.0
July 24	6.78	5.42	1.36	22.3
September 26	1.72	1.29	0.43	28.6

Table 5. Daily average evapotranspiration (mm day^{-1}) and differences of *P. australis* and *T. latifolia* calculated from Landsat 5TM.

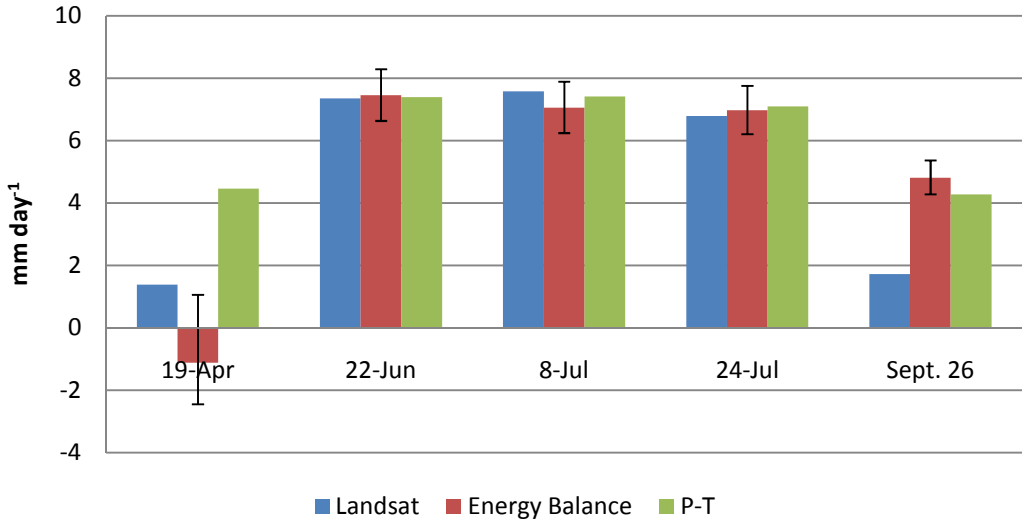

Figure 32. A comparison of daily average evapotranspiration rates (mm day^{-1}) for *P. australis* derived from Landsat 5TM, energy balance derived ET, and the Priestley-Taylor equation (P-T).

3.4 Discussion and Conclusions

An energy balance study was conducted in a wetland over *Phragmites australis* and *Typha latifolia* in southwest-central Nebraska in 2009. A Large Aperture Scintillometer (LAS) system was used to calculate sensible heat flux (*H*) and then calculate the residual of latent heat flux (*LE*) using the earth's energy budget. The measurements of net radiation (*Rn*) and heat storage rate $\Delta S/\Delta t$) were also directly measured at both the *P. australis* and *T. latifolia* locations. The Priestley-Taylor (P-T)

equation and the use of remote sensing were used as supplement methods to calculate and compared evapotranspiration (ET).

The water level at the *T. latifolia* location was approximately 13 cm lower than at the *P. australis* location, which resulted in the *T. latifolia* water level falling below the soil/water interface. The average air temperature and humidity was higher over the *T. latifolia* canopy, while the wind speed was normally greater over the *P. australis*. *P. australis* emerged from the water surface approximately two weeks before *T. latifolia*, where then *T. latifolia* reached a maximum height of 3.2 m a week before *P. australis* which grew to 4.2 m in early July. The *T. latifolia* leaf area index was only measured during the 2010 growing season, and assuming similar vegetation in 2009 and 2010, *T. latifolia* LAI would have been ~66% less than *P. australis* in late-May and ~34% less in mid-July. The albedo for *P. australis* varied between 19-22% and *T. latifolia* between 21-24% throughout the growing season. The total available energy from *Rn* during the growing season was less than a 1% different throughout the year, which is insignificant and could reside in the instrument error.

The *P. australis* and *T. latifolia* $\Delta S/\Delta t$ components varied throughout the year depending on the available energy at the water surface, water temperature, and water depth. Although the total $\Delta S/\Delta t$ deviates between both locations during the growing season, both deep soil storage rates began to release energy into the water in mid-September. The water storage in *P. australis* affected $\Delta S/\Delta t$ the greatest, while the deep and upper soil was the largest factor in *T. latifolia*. Since the water level in the *T. latifolia* was approximately 13 cm lower than at the *P. australis,* the water level was potentially a large driver for the differences between the soil and water storages of both

sites. The percent of available *Rn* partitioned into $\Delta S/\Delta t$ for May and July changed from 33 to 7% for *P. australis* and 25 to 11% for *T. latifolia*. Throughout the growing season, primary due to the soil and water storage differences, *T. latifolia* sequestered 7 W m^{-2} or 28% more energy than *P. australis*.

A linear regression was used to calibrate the two methodologies between the remote sensing and LAS derived energy balance ET. It was found using a linear regression fit through the x-y intercept that the Landsat ET was underestimated by 19%. To account for the underestimated, the regression equation was used to calculate "new" ET rates from the initial Landsat *P. australis* and *T. latifolia* ET. Some possible reasons for the underestimation were that remote sensing neglects evaporation from the water surface and heat storage of the wetland, as well as the underestimation of reference ET used in calculating ET from Landsat.

Using five days from the calibrated Landsat 5TM, *P. australis* had higher ET rates than *T. latifolia* with the differences ranging from 22-31% (0.35-1.99 mm day^{-1}) and over the five days *P. australis* averaged 28% (0.99 mm day^{-1}) greater daily ET. The P-T equation and the energy balance derived ET was larger than Landsat for September 26, while the P-T equation and Landsat had a higher ET on April 19 than the energy balance. The best agreement between Landsat and the other in-situ methods occurred on June 22 and July 8 (18%) when the vegetation was at full growth. The three day ET averages during the full growth period (June 22, July 8, July 24) for the Landsat, P-T, and LAS were 7.2, 7.3, and 7.2 mm day^{-1}. It can be concluded that the remote sensing methodology used is best applied over our wetland during a period when the vegetation is at full growth.

Chapter 4

Modeled Evaporation Rate of an Open Water Surface and Comparison with *Phragmites australis*

4.1 Introduction

One aspect of the vegetation removal campaign was to decrease consumptive use of water along the Republican River by reducing riparian evapotranspiration. The projects original plan was to have a control (*Typha latifolia*) and an experimental (*Phragmites australis*) site and compare the BREB derived ET rates between the two sites before and after the herbicide spraying, to evaluate the "water savings." There were two reasons this objective could not be accomplished: 1) the BREB method was not found to work well for our site due to the weak vertical vapor pressure gradients, 2) the herbicide spraying took longer than expected to kill the *P. australis* and no significant unnatural decrease in *LE* was found after the spraying. The development of a free water model enabled the estimation of the decreased consumptive use of water in the wetland after removing the non-native *P. australis* by comparing the model to 2009 *P. australis* energy balance and using atmospheric measurements from the wetland. The methodology for the energy balance and the Large Aperture Scintillometer are found in Chapter 2.4. Finally we can determine the "water saved" by estimating the total accumulated ET for both modeled and measured *P. australis* throughout the growing season.

4.2 Model Description

The model assumes a shallow, well-mixed water layer that is similar in area and depth to the existing wetland. To calculate the free water surface evaporation, an energy balance model was created with the inputs of air temperature (°C), relative humidity (%), wind speed (m s^{-1}), and downward shortwave and longwave radiation (W m^{-2}) measured from the *P. australis* station. The energy balance for the model is defined as

$$Rn - H - LE - G = \left(\frac{\Delta S}{\Delta t}\right)_{water}, \qquad (25)$$

where $\Delta S_w/\Delta t$ (W m^{-2}) is the water heat storage rate, G (W m^{-2}) is the ground heat flux which was calculated from the flux between the water temperature and the observed -75 cm temperature. The soil thermal conductivity of 0.98 W m^{-1}° C^{-1} was obtained from 15 *P. australis* and *T. latifolia* soil samples which yielded a standard deviation of 0.233 W m^{-1}° C^{-1}. Rn is calculated by

$$Rn = \left(1 + \tau_{\langle Sw \rangle}\right)Sw + \left(1 + \tau_{\langle Lw \rangle}\right)Lw + 0.97\sigma T^4, \qquad (26)$$

where $\tau_{\langle Sw \rangle}$ is the shortwave albedo, Sw is downward shortwave radiation, $\tau_{\langle l \rangle}$ is longwave albedo (0.03), Lw is downward longwave radiation, and σ is the Stephan Boltzmann constant (5.67x10^8 W m^{-2} K^{-4}). An albedo of 12% was used throughout the growing season to represent a shallow wetland in Nebraska (Burba et al., 1999b).

For simplicity H and LE were calculated by the mass and heat transfer equations similar to those of (dos Reis and Dias, 1998):

$$LE = \frac{0.622 l_{\langle v \rangle}}{p_{\langle a \rangle}} p_{\langle a \rangle} C_{\langle E \rangle} \cdot \overline{U\left[e_{\langle s \rangle}(T_{\langle w \rangle}) - RH \cdot e_{\langle s \rangle}(T_{\langle a \rangle})\right]} = 18.5 C_{\langle E \rangle}\left(\overline{U \cdot \Delta e}\right), \quad (27)$$

$$H = \rho_{\langle a \rangle} C p_{\langle a \rangle} C_{\langle H \rangle} \cdot \overline{U\left[T_{\langle w \rangle} - T_{\langle a \rangle}\right]} = 1170 (J m^{-3} °C^{-1}) \cdot C_{\langle H \rangle}\left(\overline{U \cdot \Delta T}\right), \quad (28)$$

where $C_{\langle E\rangle}$ and $C_{\langle H\rangle}$ are the transfer coefficients (both dimensionless), $l_{\langle v\rangle}$ is the latent heat of vaporization (MJ kg^{-1}), U is wind speed (m s^{-1}), $e_{\langle s\rangle}$ is the associated saturated vapor pressure (Pa), $\Delta e = e_{\langle s\rangle}\left(T_{\langle w\rangle} - RH \cdot e_{\langle s\rangle}\left(T_{\langle a\rangle}\right)\right)$ in Pa, and $\Delta T = T_{\langle w\rangle} - T_{\langle a\rangle}$ in °C. For the free water model, $C_{\langle E\rangle} = C_{\langle H\rangle}$, where $C_{\langle E\rangle}$ is found by an alternative form of the mass transfer equation (Sene et al., 1991; Sacks et al., 1994; dos Reis and Dias, 1998)

$$N = \frac{0.622\,\rho_{\langle a\rangle}}{p_{\langle a\rangle}\rho_{\langle w\rangle}} C_{\langle E\rangle}\,, \quad (29)$$

where written in units of cm day^{-1} s m^{-1} kPa^{-1}, $\rho_{\langle a\rangle}$ and $\rho_{\langle w\rangle}$ are the average densities for air and water for the 2009 growing season, $p_{\langle a\rangle}$ is the average pressure, and N is derived from the Harbeck area relationship ($N = 0.146 \cdot A^{-0.05}$), where A is the lake area in km^2 (Harbeck, 1962). The Harbeck area relationship was found to be 0.172 for the study site, which after calculating the Harbeck area relationship, Equation 29 was used to derive a mass transfer coefficient of 0.0027.

Once *Rn*, *LE*, and *H* have been estimated, the change in water temperature can be calculated by

$$\Delta T_{\langle w\rangle} = \frac{\Delta t * (Rn - LE - H - G)}{\rho_{\langle w\rangle} \cdot Cp_{\langle w\rangle} \cdot h_{\langle w\rangle}} \quad (30)$$

where afterwards, the final unknown variable in the energy balance ($\Delta S_w/dt$) can be calculated as

$$\left(\frac{\Delta S}{\Delta t}\right)_{water} = \rho_{\langle w\rangle} \cdot Cp_{\langle w\rangle} \cdot h_{\langle w\rangle} \cdot \frac{\Delta T_{\langle w\rangle}}{\Delta t} \quad (31)$$

where the initial water temperature of the model on April 11 was set to 8 °C (an approximate of the actual observed water temperature), and all variables were described previously. For direct comparison between the model and observations, the measured

hourly water level was used as the water depth in the open water model. To calculate the total evaporation from the open water surface (growing season and post-growing season), the model was run until the freezing point occurred on December 5 within the water temperature.

The uncertainties of water level, initial water temperature, wind speed, and the mass transfer coefficient were used to determine the error bounds for the accumulated ET throughout the growing season. A ±50% change in water level (0.3 m, 0.9m) resulted in an uncertainty of only ±0.35% and an initial temperature (4 °C, 12 °C) uncertainty of -0.88 and 1.1%. From this, it was concluded that the water level and initial temperature were negligible and only the wind speed and $C_{\langle E \rangle}$ uncertainties were needed. Since the variation of wind speed with height is one of multiple variables representing $C_{\langle E \rangle}$ (Harbeck, 1962) and wind speed is a significant component of latent and sensible heat, the wind speed itself is of main interest to determine the uncertainty. The wind speeds at our wetland site have been reduced by a "wind shading" effect of the nearby cottonwood trees, as well as the added wind resistance that occurred in conjunction with the growth of the *P. australis* (up to 4.2-m tall at the peak of the growing season). To understand the potential rate of free water evaporation, a non-sheltered wind speed that represented the regional climate must be used. The wind speeds for a non-sheltered area was obtained from the High Plains Regional Climate Center (HPRCC) from an Automated Weather Data Network (AWDN) station south of Holdrege, Nebraska. The AWDN station (number a253919) is located 31 km to the northeast of the wetland in an open grass field. The measured wind speed from the AWDN station was used to scale the *P. australis* wind speed measurements with a polynomial fit (r^2=0.65) using hourly data from April

11 – December 31 to represent a wetland with no shelter (Figure 33). The measured wind speeds over the wetland and scaled wind speeds were used to represent the lower and upper uncertainties for open water model.

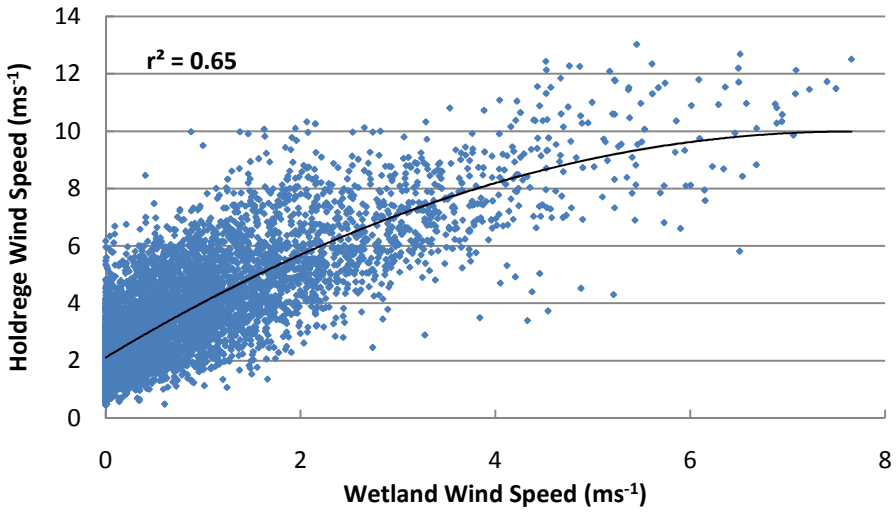

Figure 33. Comparison of the Holdrege and wetland hourly wind speed (m/s) from April 11- December 31 and fit with a 2nd order polynomial trend line.

4.3 Results

4.3.1 *Surface Radiation Balance*

The 5-day running means for April 11–December 5 for the modeled open water and observed (over *P. australis*) net radiation (*Rn*), net shortwave (SW_{net}), and net longwave (LW_{net}) are found in Figure 36b, Figure 35c, Figure 35d. The observed average *Rn* was 14% (17.5 W m^{-2}) greater than the modeled free water surface. Due to the uncertainties derived from the wind speed (measured vs. scaled) within the model, the modeled *Rn* upper and lower uncertainties yielded averages that were 32 % lower and 1%

greater than the observed averages. Daily average *Rn* between the model and observations began similarly, but started to deviate in June and continued throughout the growing season. While looking at the SW_{net} for the cause of the *Rn* deviation, the average SW_{net} over the open water (191.4 W m^{-2}) was higher than the observed measurement (172.3 W m^{-2}). Since the incoming solar radiation was the same for both environments, the ~10% difference in SW_{net} is due to the ~10% higher albedo over *P. australis* that was found in Chapter 2.6.3. LW_{net} , the other component of *Rn*, was driven by the longwave radiation emitted by the atmospheric and surface temperatures, where a warmer surface than atmosphere will yield a negative LW_{net}. The modeled average LW_{net} for the growing season was between 33% - 79% greater than the observed -41.7 W m^{-2}. This incongruence is due to a warmer modeled surface (Figure 36a), which led to more longwave radiation emitted from the water surface. As LW_{net} and *Rn* deviated between the modeled surface and observations, the differences in surface water temperature also increased between both as an effect of the energy stored.

From 8:00 to 16:00, the average diurnal *Rn* between the open water and observations show little change (Figure 38a); therefore, the nighttime *Rn* is the main cause of the daily differences described above. With SW_{net} being negligible from 17:00 to 7:00 and incoming longwave radiation the same for both environments, the nighttime difference in *Rn* can only be caused by outgoing longwave radiation. As seen in Figure 34, the average nighttime outgoing *LW* differences were as large as 17% (70.9 W m^{-2}) with the lower modeled uncertainties similar to the observed. Due to the water temperature lag (high specific heat) from the free water model, the observed outgoing longwave was greater than the modeled during 9:00 – 13:00. Since the emitted longwave

from observations is measured as the surface temperature (vegetation + water) and with vegetation (lower specific heat) being the majority of the surface, the surface temperature follows a similar daytime variation as air temperature (Figure 12a). It is also interesting to note the similarity between both modeled and observed diurnal daytime *Rn*. This comparison is due to the larger modeled LW_{net} that was offset by the higher albedo through much of the daylight hours.

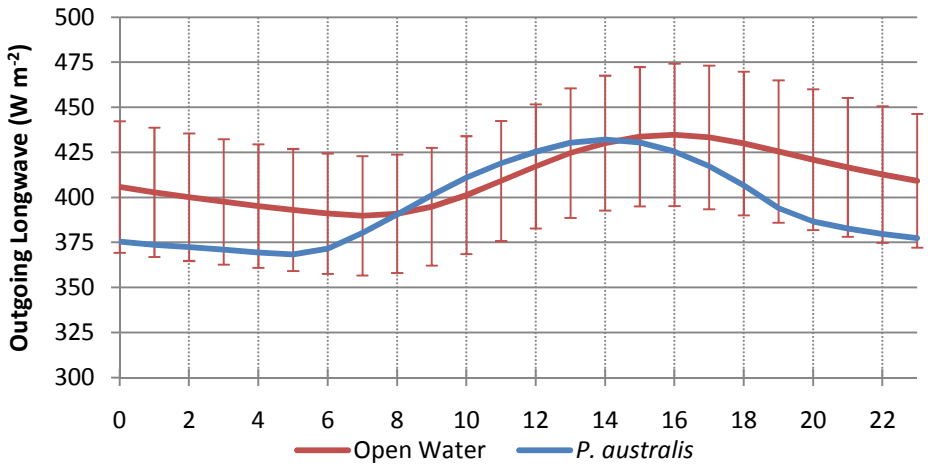

Figure 34. 2009 growing season average diurnal emitted longwave (W m^{-2}) for the open water model (red line) and *P. australis* (blue line).

4.3.2 *Heat Storage Rate*

An average of 121% (6.5 W m^{-2}) more observed *Rn* was sequestered from April 11 – November 3 in the free water surface than the modeled *Rn*. A reason for the lower heat storage rates within the *P. australis* was due to the incoming energy intercepted by *P. australis*, as well as a cooler surface. As a reflection of energy received and stored at the surface, the modeled water temperature through much of the year is greater than the measured air and *P. australis* water temperature (Figure 36a). The open water diurnal heat storage is up to six times greater in magnitude during the day and four times less at

night when compared to the observation. This is similar to Burba et al. (1999b), where they found the daytime open water storage to be about three times larger than *P. australis* and the nighttime open water energy sink was two to five times larger. A diurnal difference between the open water surface and *P. australis* heat storage are due in part to: 1) More incoming solar radiation is reaching the high density and high specific heat free water surface, rather than intercepted the *P. australis* canopy, 2) More energy is released in the free water surface during the nighttime hours due to the larger water/surface temperature gradients.

4.3.3 *Sensible Heat Flux*

The 5-day running mean of sensible heat flux for both modeled and observed is illustrated in Figure 37f. The observed average H from April 11 – November 3 (last day power was available to the LAS) was 120% (24.5 W m^{-2}) higher, but the average difference after June 1 decreased to only 64.0% (7.3 W m^{-2}). The early observation of a high H is due to little or no transpiration from the wetland during April and May, allowing energy to be available as H. Another reason for the early season deviation is most of the available energy ($Rn - \Delta S/\Delta t$) over the free water surface was portioned into latent heat flux, rather than H (Figure 35). The largest deviations between the open water surface and observed wetland conditions were during the period of little vegetation growth and after senesces. This deviation was due to how the partitioning of available energy in the model, with the average LE consuming over 100% of the available energy. The opposite from the model was measured over the *P. australis* where high sensible heat fluxes occurred over the wetland until the vegetation became dominate.

The observed *H* mean diurnal cycle for the growing season reveals that more available energy went into *H* than over the open water model during the daytime. The observed *H* is driven by *Rn* and wind speed that reaches a maximum around noon, but the free water *H* shows little influence by *Rn* with the greatest flux away from the surface occurring during the nighttime. As seen in Equation 28, the driver for the open water *H* is the product of magnitude for the wind and the temperature difference between the air and water surface. Even though the wind speed is lower during the night time hours (Figure 12b), the lag in water temperature with respect to the air temperature, and the amount of energy stored in the water causes large *H* fluxes from the water to the atmosphere. Since the average free water surface remained warmer at night (20:00 – 6:00), the nighttime *H* resulted in being 49% (7.5 W m^{-2}) higher than the observed.

4.3.4 *Latent Heat Flux and Evapotranspiration*

The latent heat flux that was derived from the energy balance and mass transfer equations were used to understand the difference in evapotranspiration ("water removed") from the modeled and observed wetland. The *LE* and ET 5-day running mean for the free water surface and observations are found in Figure 27g. From April 11 to around June 1, the free water surface *LE* was greater than observed, and afterwards, due to the dominance of vegetation, the observed *LE* becomes greater. During the growing season, the *P. australis* surface was cooler than the air temperature, which indicated *LE* (cooling process) was a significant sink of available energy. The average observed *LE* was 5% (4.9 W m^{-2} or 0.16 mm day^{-1}) larger when considering the period from April 11 – November 3, but from June 1 – November 3 the observed difference grew to 25% (32.4

W m^{-2} or 0.90 mm day^{-1}). During the early and late growing season, the free water *LE* consumed from 60% to over 100% of the available energy (Figure 35). The opposite is true for the *P. australis LE* where more energy was available to sensible heat. From early-June to mid-September, the daily observed available energy consumed by *LE* was on average 5% higher than over the open water. The main reason for the observed increase of *LE* and the available energy consumed by *LE* after early-June was due to the dominance of the high transpiring *P. australis*.

The daily LE to Rn-$\Delta S/\Delta t$ ratios can also help understand to what impact the herbicide spraying on July 22 of *P. australis* had on *LE*. Since the wetland measurements were used in the calculation of *LE* for the water model and over the *P. australis*, any climatic affect that would influence *LE* should be seen in both environments. We concluded since the daily and weekly trends are similar after July 22 until senescence (October 3), the herbicide spraying of *P. australis* had little or no impact on killing the vegetation during the 2009 growing season and decreasing the *LE*.

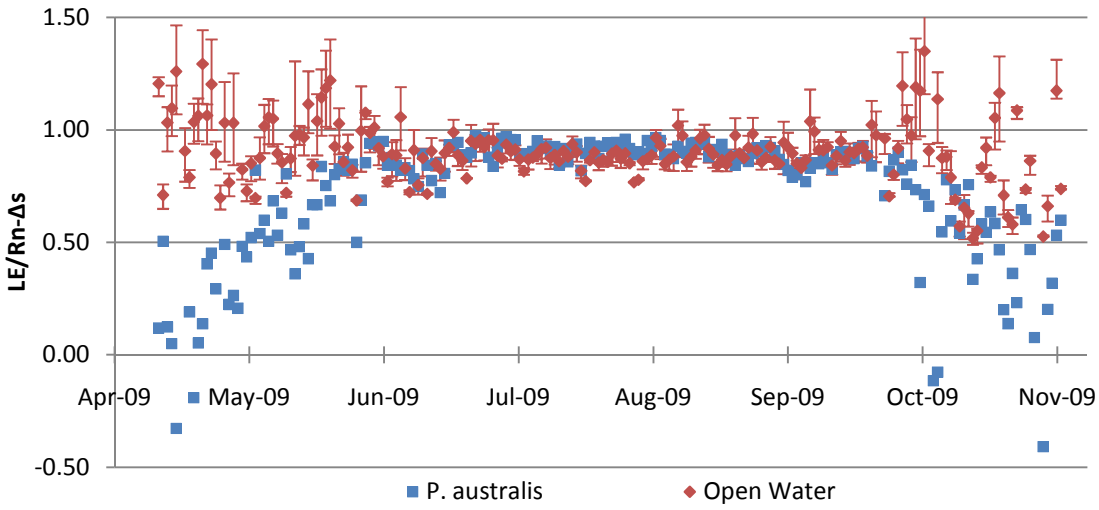

Figure 35. The ratio of latent heat flux and available energy (net radiation minus heat storage) from April 11 – November 3 for the *P. australis* (blue) and the free water model (red).

Similar to *H*, the average growing season diurnal *LE* between both environments have different atmospheric drivers. The increase, peak, and decrease of the observed *LE* are similar to that of *Rn*, illustrating the use of *Rn* by *P. australis* is strongly driven by the available energy of the surface. The maximum observed *LE* occurred at 12:00 (372.2 or 13.1 mm day-1), compared to the free water *LE* that occurred at 15:00 (218.4 W m^{-2} or 7.7 mm day^{-1}), where the later maximum is due a maximum vapor pressure gradient and wind speed in the late afternoon. The free water nighttime *LE* (20:00 – 6:00) averages were 142% (48.0 W m^{-2} or 1.7 mm day^{-1}) larger than the observed, which is due to the increased available energy from the larger heat storage over the free water and the vapor pressure gradient.

The average *LE* and ET from April 11 – November 3 over the observed wetland was 110.5 W m^{-2} and 3.9 mm day^{-1}, respectively. The average open water *LE* and ET over the same period was 105.6 W m^{-2} and 3.7 mm day^{-1}, respectively. The maximum daily ET for the free water was 11.2 mm day^{-1} on May 8 and 8.21 mm day^{-1} on June 29. The 31% higher maximum daily ET rates over the free water surface is similar to the ~24% found by Burba et al. (1999b). The earlier daily maximum ET date was due to the higher wind speeds and larger vapor pressure gradients during May, whereas high *Rn* and full growth vegetation yielded a later maximum ET over *P. australis*. The observed accumulated ET and precipitation throughout the observations were 807 mm and 470 mm, respectively, with a ratio of 1.7. Assuming all upper and lower uncertainties occurred over the *P. australis*; the accumulated ET maximum and minimums would range between 686 mm (1.5) to 936 mm (2.0). For the free water model, the average accumulated ET was 771 mm (1.2), and assuming the uncertainties would be within 553

mm (1.1) and 988 mm (2.1). As stated before, the open water model uncertainties reflect the measured wind speeds over the wetland and the scaled wind speeds that represents the potential ET in an open environment. Although the potential ET reaches 988 mm, it is unrealistic to assume that the all riparian regions are exposed to open terrain with higher wind speeds. Trees that create a "wind-shading" effect similar to the wetland generally surround much of the Republican River where the *P. australis* has been removed. Finally, to account for the extra energy that was stored in the open water model from April 11 – November 3 and may have been released through evaporation, the model was run until the water froze (December 5). The averaged modeled ET accumulated from April 11 – December 5 resulted in 810 mm with the uncertainty ranging between 573 mm and 1046 mm.

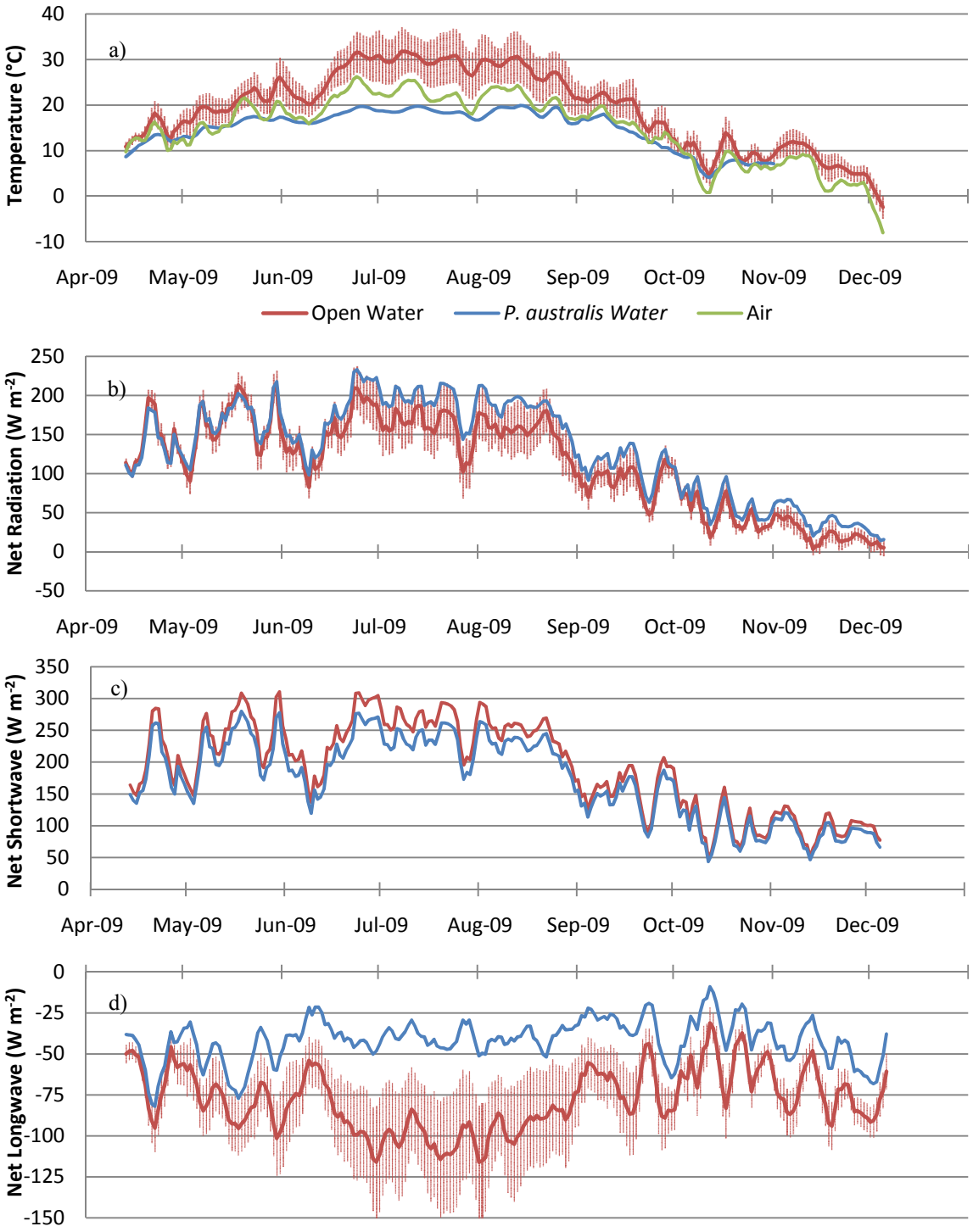

Figure 36. 2009 five-day running means of a) water and air temperature (°C), b) net radiation (W m^{-2}), c) net shortwave (W m^{-2}), and d) net longwave (W m^{-2}) from April 11 – December 5 for open water (red) and *P.australis* (blue). The vertical lines represent the upper and lower bounds.

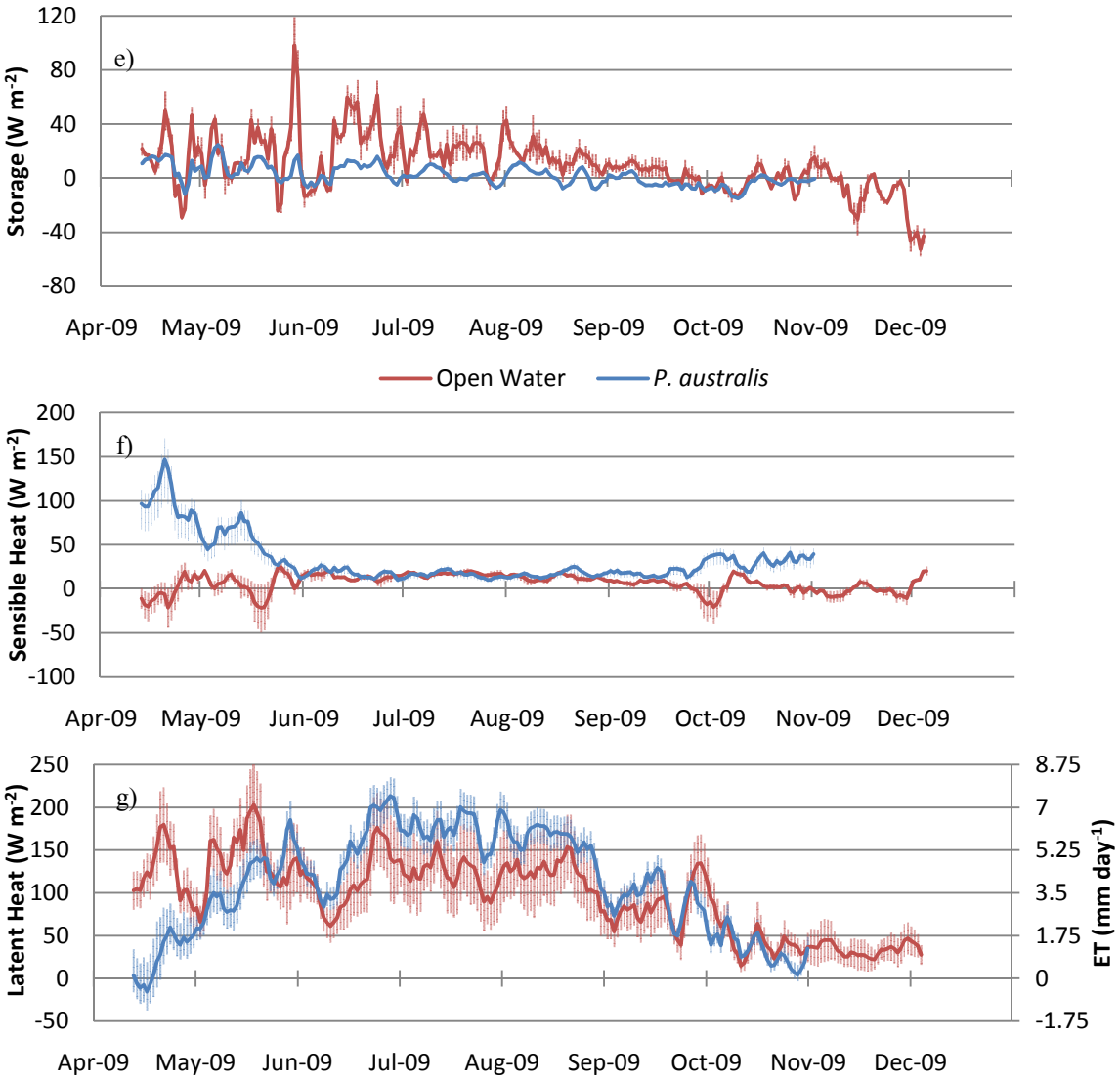

Figure 37. Same as

Figure **36**, but for e) heat storage, f) sensible heat flux, and g) latent heat flux.

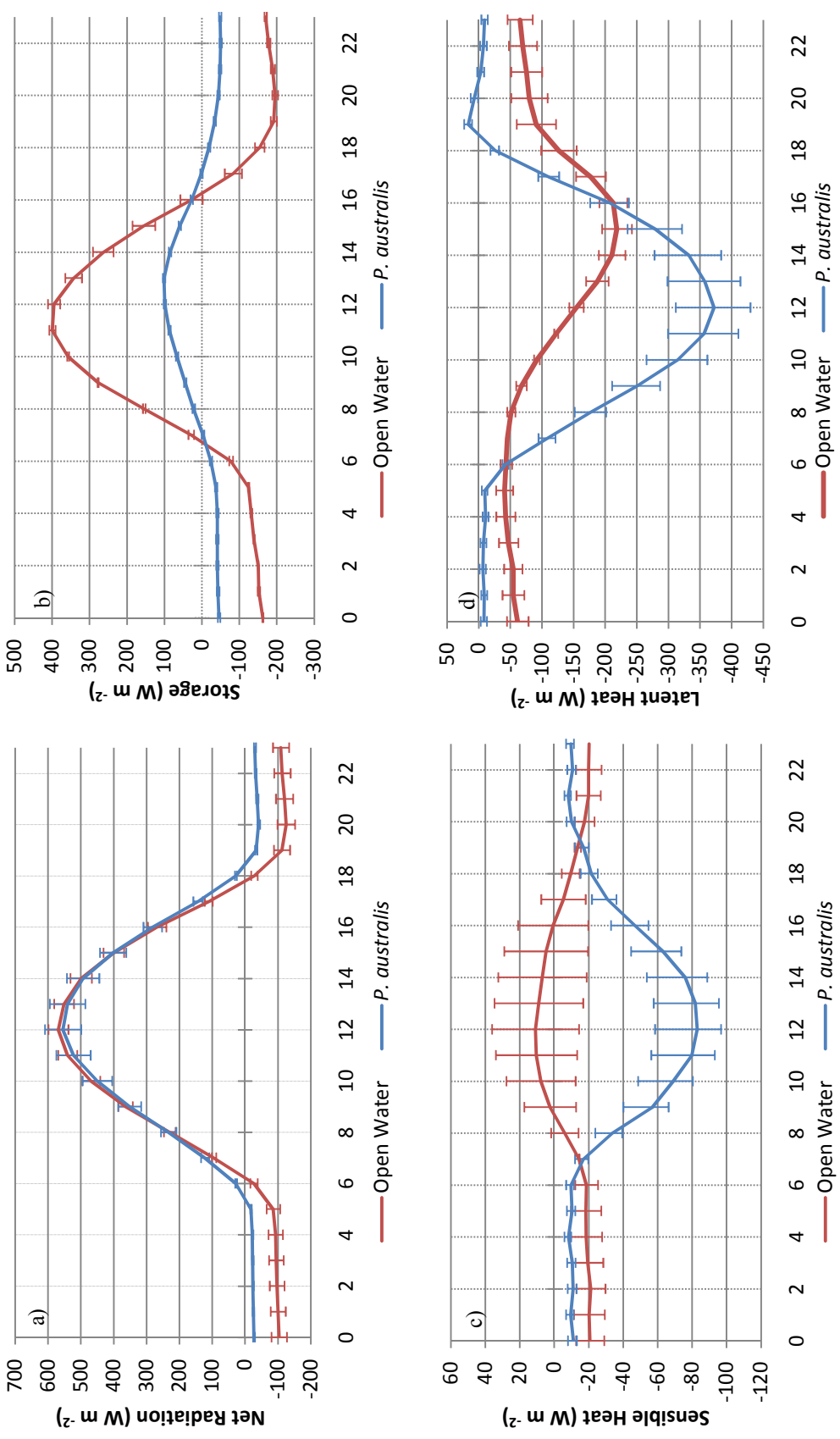

Figure 38. 2009 growing season average diurnal of a) net radiation (W m^{-2}), b) heat storage (W m^{-2}), c) latent heat flux (W m^{-2}), and d) sensible heat flux (W m^{-2}) for the free water model (red line) and the *P. australis* (blue line).

4.4 Discussion and Conclusions

The goal of this chapter is to determine how much water would be contained in the wetland if the invasive plant of *Phragmites australis* were removed. To do this, an energy balance comparison was conducted between the 2009 observations and a modeled free water wetland. An energy balance comparison also assisted in understanding to what impact the herbicide spraying had on *P. australis* on July 22. Using *LE* from the energy balance, a daily ET rate was integrated throughout the year to find the accumulated ET for both observed and modeled wetland.

The average *LE* and ET from April 11 – November 3 (last day the LAS was operational) over the observed wetland was 110.5 W m^{-2} and 3.9 mm day^{-1}, respectively. The average open water *LE* and ET over the same period was 105.6 W m^{-2} and 3.7 mm day^{-1}, respectively. The observed accumulated ET and precipitation throughout the observations were 807 mm and 470 mm, respectively, with a ratio of 1.7. Assuming all upper and lower uncertainty bounds occurred over the *P. australis*; the accumulated ET maximum and minimums would range between 686 mm (1.5) to 936 mm (2.0). For the free water model, the average accumulated ET was 771 mm (1.2), and the uncertainties would range from 553 mm (1.1) and 988 mm (2.1). To account for evaporation from excess heat storage in the water after November 3, the model ran until the first day the water froze (December 5). The averaged modeled accumulated ET from April 11 – December 5 resulted in 810 mm with the uncertainties ranging between 573 mm and 1046 mm. In conclusion, although on average the accumulated ET for both the *P. australis* and modeled free water surface was similar (~1 %), the wind speed is an important factor in determining how much energy is stored in the water and how much is

evaporated. It was also concluded that the "wind-shading" around the Republican River can significantly affect how much water *P. australis* and an open water surface can evapotranspire.

Comparing each environment's energy balance components allowed for a better understanding of the modeled and observed final accumulated ET. It was found that the *Rn* was the main driver for *H* and *LE* over the observed wetland, while in the model the wind speed had a strong influenced on *LE*, but only a small effect on *H*. The observed seasonal average *Rn* was 17.5 W m^{-2} (14%) larger than in the model, while open water surface heat storage sequestered 6.5 W m^{-2} (121%) more energy. The larger availability of energy ($Rn - \Delta S/\Delta t$) over the *P. australis* allowed for more energy to be partitioned into *LE* and *H* throughout the growing season. As a result, the average *H* and *LE* from the observations was 24.5 W m^{-2} (120%) and 4.9 W m^{-2} (5%) larger than in the model. The observed *LE was also found to* dominate during the daytime, but the open water nighttime *LE* (20:00 – 6:00) averages were 142% (48.0 W m^{-2} or 1.7 mm day^{-1}) larger than the observed. This was due to the increased available energy from the larger daytime heat storage and water/atmosphere vapor pressure gradient over the open water. Finally, during the daytime when *Rn* is at a maximum, the observed *LE* and modeled heat storage were discovered to be the main sinks of energy.

Chapter 5

Summary and Conclusions

Understanding the energy and water balance of *Phragmites australis* (Common Reed) in southwestern, Nebraska was the motivation for this thesis. Nebraska has spent $2 million a year removing the invasive species of *Phragmites australis* (Common Reed), *Tamarix* (Salt Cedar), and *Elaeagnus angustifolia* (Russian Olive) in hope to keep more water in the Republican River and alleviate legal tensions with Kansas. This study took place in a wetland with the surface occupied by 52% of the invasive *Phragmites australis* (Common Reed), 31% native *Typha latifolia* (Cattail), 8% native *Juncus effuses* (Common Rush), and 9% open water. The growing season was defined from April 11 to October 13, while both May and July of 2009 were characterized by well-above-normal precipitation and August-October was cooler than normal. A Large Aperture Scintillometer (LAS) and two Bowen ratio stations were installed within the wetland to measure the atmospheric conditions and energy balance over *P. australis* and native *T. latifolia*. This thesis was written in three main chapters:

- Energy and Water Balance Over *Phragmites Australis* **(Chapter 2)**
- Comparison of Energy Balance between *Phragmites Australis* and Native Vegetation (*Typha Latifolia*) **(Chapter 3)**
- Modeled Evaporation Rate of an Open Water Surface and Comparison with *Phragmites Australis* **(Chapter 4)**

In chapter two, to measure the energy and water balance within *P. australis*, the earth's energy budget was used to estimate latent heat (*LE*) and evapotranspiration (ET). The residual of *LE* was estimated from an LAS to calculate sensible heat (*H*), CNR2 to measure net radiation (*Rn*), and six temperature sensors to measure the wetland heat storage ($\Delta S/\Delta t$) within the soil, water, and vegetation canopy. Once ET was calculated, the measured precipitation and ET was used in the water balance to determine if the water storage of the wetland was controlled by only evaporation from the water surface and transpiration through the vegetation, or whether there were other forces that influenced the water storage and potentially evapotranspiration.

LE was calculated throughout the growing season for *P. australis* an increased(decreased) with vegetation growth(decay). A daily maximum of 233.0 W m^{-2} and 8.21 mm day^{-1} was measured on June 29. From April to mid-May, daily *LE* used less than 60% of the available energy ($Rn-\Delta S/\Delta t$), while the sensible heat sequestered the majority of energy. The daily *LE* utilized 80 to 97% of the available energy after May until mid-August while *H* became a minor component of the energy budget. The vegetation phonology and net radiation were found to be the two largest meteorological and environmental drivers for the seasonal variability in *LE*. It was found that the daily accumulated ET and precipitation (*P*) was 771 mm and 410 mm, giving a ratio of 1.6. Finally, we found although the *P. australis* was dead for the 2010 growing season, there was no strong evidence that the herbicide spraying on July 22 caused an unnatural decrease in *LE*.

The Priestley-Taylor (P-T) method has been used extensively in past literature to measure ET over open water and vegetation with abundant water. When comparing P-T

to the energy balance derived ET, it was found that that the P-T agreed well with the energy balance derived ET after June 1 (full vegetation), but during the beginning of the growing season the P-T method overestimated ET. The daily average *LE* for P-T was 139 W m^{-2} compared to 124 W m^{-2} from the energy balance derived ET, and the daily-accumulated ET from the P-T method was 861 mm, 11% higher than the LAS derived ET. It was concluded from this, that the P-T method (α=1.26) is a good approximation of ET once vegetation becomes dominate with low wind speeds.

Using only the water level, precipitation, and ET within the water balance, it was found that groundwater and overland flow was significant in the wetland throughout the growing season. Without the influx of groundwater and overland flow through the first half of the growing season the wetland could have completely lost the open water and thus affecting the ET from the wetland. It is believed that the groundwater flux was more significant than overland flow due to the low slopes for water drainage into the wetland, irrigation from groundwater, and groundwater peculation across the wetland towards the Republican River. To monitor the importance of groundwater, piezometers have been placed around the wetland to measure the groundwater influx and discharge, which will in turn be used to calculate ET from the water balance.

In chapter three, the measured atmospheric conditions, *Rn*, and $\Delta S/\Delta t$ were compared between *P. australis* and *T. latifolia*. A remote sensing method using Landsat 5TM was also used to compared ET rates between *P. australis* and *T. latifolia* for five days between April 19 and September 26. The Landsat ET rates were also compared to the LAS and P-T calculated from in-situ measurements. The daily averaged ET rates from Landsat weren calibrated using a linear regression with the LAS energy balance

derived ET to account for the different methodologies. A 19% underestimation from Landsat was found and to account for this, a regression equation was used to calculate "new" ET rates from the initial Landsat values.

It was found that the albedo of *T. latifolia* was 3-5% larger during April and September while the other months had a 0-2% difference between both vegetation's. The total available energy from *Rn* during the growing season was less than a 1% different throughout the year between the two vegetations, which is insignificant and is probably part of the instrument error. The *P. australis* and *T. latifolia Rn*-Δ*S/dt* components varied throughout the year and was found to be influenced by water temperature, water depth, and the water/atmospheric temperature gradient. The water heat storage in *P. australis* affected the total *Rn*-Δ*S/dt* the greatest, while the deep and upper soil was the largest factor in the *T. latifolia* total Δ*S/dt*. Throughout the growing season, primary due to the soil and water storage difference, *T. latifolia* sequestered 7 W m^{-2} or 28% more energy than *P. australis*. The primary reason for the heat storage difference was due to the water level within the *T. latifolia* being 13 cm lower than *P. australis*.

Using five days from the calibrated Landsat 5TM, the *P. australis* area had higher ET rates than the *T. latifolia* with the differences ranging from 22-31% (0.35-1.99 mm day^{-1}) and over the five days *P. australis* averaged 28% (0.99 mm day^{-1}) greater daily ET. The P-T equation and the energy balance derived ET was larger than Landsat for September 26, while the P-T equation and Landsat had a higher ET on April 19 than the energy balance. The 3-day ET averages during the full growth period (June 22, July 8, July 24) for the Landsat, P-T, and LAS were 7.2, 7.3, and 7.2 mm day^{-1}. It was

concluded that the remote sensing method used in this study is best applied over our wetland during the period of the vegetations full growth.

In chapter four, an energy balance comparison was conducted between the 2009 observations over *P. australis* and a modeled open water surface to determine the "water savings" for the wetland. The average *LE* and ET from April 11 – November 3 over the observed wetland was 110.5 W m^{-2} and 3.9 mm day^{-1}, with the accumulated ET being 807 mm and the uncertainties ranging from 686 to 936 mm. The accumulated ET for the free water model was 771 mm, but once the model was ran until no energy remained in the water (December 5), the accumulated ET was 810 mm. The uncertainty of the model (derived by wind speed) resulted in ET rates ranging from 573 mm to 1046 mm, which concluded that with a large range in ET, wind speed is important in determining how much water is evaporated from a free water body.

It was found that the *Rn* was the main driver for *H* and *LE* over the observed wetland, while wind speed strongly influenced *LE*, but had less of an impact on *H*. Higher available energy from *Rn* and $\Delta S/\Delta t$ at the surface from the wetland observations lead to more energy partitioned into *H* and *LE*. The large $\Delta S/\Delta t$ in the free water surface consumed a greater portion of daytime *Rn*, resulting in more energy warming the water temperature and a lower daytime ET. In comparison, the daytime *Rn* over the observed wetland was mostly partitioned into *LE*, leading to higher daytime ET rates. It was concluded from the model and observations that after comparing the ratio of daily available energy partitioned into *LE* after July 22, the herbicide spraying had little or no impact on the decrease in *LE* throughout the remaining of the growing season.

Results from this thesis suggest that the removal of *P. australis* from wetlands within the Republican River basin could potentially result in a growing season “water savings” of up to 28% if the native species of *T. latifolia* replaces the non-native *P. australis*. If a free water surface becomes dominant after the removal, we found that there could be either “water savings” or “water loss” depending on the amount of wind sheltering by trees. Presently, the existing wetland experiences significant wind sheltering, leading to lower wind speeds than other nearby meteorological stations. Model results suggest that such sheltering would lead to lower rates of evaporation from an open water surface than from the existing *P. australis* (i.e., "water savings"). The water surface, therefore, would be considerably warmer than the present wetland and would lose a significant amount energy to outgoing longwave radiation. Alternatively, if the wetland were less sheltered and had higher wind speeds more typical of other nearby meteorological stations, the open water evaporation rates would be considerably higher. This could potentially lead to "water loss" if *P. australis* were removed and replaced with open water. But since trees are generally present throughout the riparian corridor of the Republican River basin, we conclude that the more likely scenario would be that of the present wind sheltering, with removal of *P. australis* leading to a small, but tangible amount of "water savings" if replaced by open water.

References

Arasteh, P.D., Tajrishy, M., 2008. Calibrating Priestley-Taylor Model to Estimate Open Water Evaporation under Regional Advection Using Volume Balance Method-Case Study: Chahnimeh Reservoir, Iran. Journal of Applied Sciences 8(22), 4097-4104.

Burba, G.G., Verma, S.B., Kim, J., 1999a. Surface energy fluxes of *Phragmites australis* in a prairie wetland. Agricultural and Forest Meteorology 94, 31-51.

Burba, G.G., Verma., S.B., Kim, J., 1999b. A comparative study of surface energy fluxes of three communites (*Phragmites Australis, Scirpus Acutus,* and open water) in a prairie wetland ecosystem. Wetlands 19(2), 451-457.

Burt, O.R., Baker, M., Helmers, G.A., 2002. Statistical estimation of streamflow depletion from irrigation wells. Water Resources Research 38(12), 1296.

Chander, G., Markham, B., 2003. Revised Landsat-5 TM Radiometric Calibration Procedures and Postcalibration Dynamic Ranges. IEEE Transactions on Geosciences and Remote Sensing 41(11), 2674-2677.

Chehbouni, A., Watts, C., Lagouarde, J.-P., Kerr, Y.H., Rodriguez, J.-C., Bonnefond, J.-M., Santiago, F., Dedieu, G., Goodrich, D.C., Unkrich, C., 2000. Estimation of heat and momentum fluxes over complex terrain using a large aperture scintillometer. Agricultural and Forest Meteorology 150, 215-226.

Chen, B., Chen, J.M., Ju, W., 2007. Remote sensing-based ecosystem-atmosphere simulation scheme (EASS) – Model formulation and test with multiple-year data. Ecological Modelling 209, 277-300.

Clifford, S.F., Ochs, G.R., Lawrence, R.S., 1974. Saturation of optical scintillation by strong turbulence. Journal of Optical Society of America 64(2), 148-154.

De Bruin, H.A.R., Keijman, J.Q., 1979. The Priestley-Taylor Eevaporation Model Applied to a Large, Shallow Lake in the Netherlands. Journal of Applied Meteorology 18, 898-903.

Deering, D.W., Eck, T.F., 1987. Atmospheric optical depth effects on angular anisotropy of plant canopy reflectance. International Journal of Remote Sensing 8(6), 893-916.

dos Reis, R.J. and Dias, N.L., 1998. Multi-season lake evaporation: energy-budget estimates and CRLE model assessment with limited meteorological observations. Journal of Hydrology, 208(3-4), 135-147.

Dugas, W.A., Hicks, R.A., Wright, P., 1998. Effect of removal of *Juniperus ashei* on evapotranspiration and runoff in the Seco Creek watershed. Water Resources Research 34(6), 1499-1506.

Ezzahar, J., Chehbouni, A., Hoedjes, J.C.B., Er-Raki, S., Chehbouni, Ah., Boulet, G., Bonnefond, J.-M., De Bruin, H.A.R., 2007. The use of scintillation technique for monitoring season water consumption of olive orchards in a semi-arid region. Agricultural Water Management 89, 173-184.

Fermor, P.M., Hedges, P.D., Gilbert J.C., Gowing, D.J.G., 2001. Reedbed evapotranspiration rates in England. Hydrological Processes 15, 621-631.

Flowerday, C.A., Kuzelka, R.D., Pderson, D.T. compilers 1998 (seconded), The groundwater atlas of Nebraska, University of Nebraska-Lincoln Conservation and Survey Division Research Atlas 4a, 44p.

Fritschen, L.J., 1966. Accuracy of Evapotranspiration Determinations by the Bowen Ratio Method. Hydrological Sciences Journal 10(2), 38-48.

Gillies, R.R., Kustas, W.P., Humes, K.S., 1997. A verification of the 'triangle' method for obtaining surface soil water content and energy fluxes from remote measurements of the Normalized Difference Vegetation Index (NDVI) and surface e'. International Journal of Remote Sensing 18(35), 3145-3166.

Grothues, T.M., Able, K.W., 2003. Part B: Dedicated Issue: Phragmites australis: A Sheep in Wolf's Clothing? Coastal and Estuarine Research Federation 26(2), 563-573.

Guo, Y., Schuepp, P.H., 1994. On surface energy balance over the northern wetlands 2. The variability of the Bowen ratio. Journal of Geophysical Research 99(D1), 1613-1621.

Guyot, G., Gu, X.F., 1993 "Measurement of plant canopy reflectance". Crop Structure and Light Microclimate: Characterization and applications. Ed. Varlet-Grancher, C., Bonhomme, R., Sinoquet, H. INRA Editions, 323-335.

Harbeck, J., G.E., 1962. A practical field technique for measuring reservoir evaporation utilizing mass-transfer theory. 272-E, U.S. Geological Survey Professional Paper.

Hartogensis, O.K., De Bruin, H.A.R., Van de Wiel, B.J.H., 2002. Displaced-beam Small Aperture Scintillometer Test. Part II: Cases-99 stable boundary-layer experiment. Boundary-Layer Meteorology 105, 149-176.

Hartogensis, O.K., Watts C.J., Rodriguez, J.C., De Bruin, H.A.R, 2003. Derivation of an Effective Height for Scintillometers: La Poza Experiment in Northwest Mexico. Journal of Hydrometeorology 4, 915-928.

Herbst, M., Kappen, L., 1999. The ratio of transpiration versus evaporation in a reed belt as influenced by weather conditions. Aquatic Botany 63, 113-125.

Hermman, Kyle. Personal Interview. 8 July 2010.

Higuchi, A., Hiyama, T., Fukuta Y., Suzuki, R., Fukushima, Y., 2007. The behavior of a surface temperature/vegetation index (TVX) matrix derived from 10-day composite AVHRR images over monsoon Asia. Hydrological Processes 21, 1157-1166.

HPRCC, 2009. High Plains Regional Climate Center, Classic Online Services: Available from: <http://www.hprcc.unl.edu/services>, accessed in October 2009.

Hoedjes, J.C.B., Zuurmbier, R.M., Watts, C.J., 2002. Large Aperture Scintillometer used over homogenous irrigated area, partly affected by regional advection. Boundary-Layer Meteorology 105, 99-117.

Hovey, A., 2005. Nebraska drilling new wells, Lincoln Journal Star, Wednesday, January 12, 2005.

Jia, L., Xi G., Liu, S., Yan, Y., Liu, G., 2009. Regional estimation of daily to annual evapotranspiration with MODIS data in the Yellow River Delta wetland. Hydrology and Earth System Sciences Discussions 6, 2301-2335.

Jones, A.C., Gregory L. Effects of Brush Management on Water Resources. Texas Water Resources Institute Technical Report TR-338. November 2008.

Kansas Department of Agriculture, 2010. Fact Sheet: Republican River Compact Enforcement.

Kipp&Zonen, 2007. Large Aperture Scintillometer Manual.

Kiviat, E., 2006. *Phragmites* Management Sourcebook for the Tidal Hudson River and the Northeastern States. Hudsonia Ltd., Annandale NY. Available at hudsonia.org.

Kleissl, J., Gomez, J., Hong, S.-H., Hendrickx, J.M.H., Rahn, T., Defoor, W.L., 2008. Large Aperture Scintillometer Intercomparison Study. Boundary-Layer meteorology 128, 133-150.

Kohsiek, W., Meijninger, W.M.L., De Bruin, H.A.R., Beyrich, F., 2006. Saturation of the Large Aperture Scintillometer. Boundary-Layer Meteorology 121, 111-126.

Lenters, J.D., Kratz, T.K., Bowser, C.J., 2005. Effects of climate variability on lake evaporation: Results from a long-term energy budget study of Sparking Lake, northern Wisconsin (USA). Journal of Hydrology 308, 168-195.

Lord, D., Desjardins, R.L., Dube, P.A., Brach, E.J., 1985. Variations of Crop Canopy Spectral Reflectance Measurements Under Changing Sky Conditions. Photogrammetric Engineering and Remote Sensing 51(6), 689-695.

McAneney, K.J., Itier, B., 1996. Operational limits to the Priestley-Taylor formula. Irrigation Science, 17, 37-43.

Meijninger, W.M.L., Beyrich, F., Ludi, A., Kohsiek, W., De Bruin, H.A.R., 2006. Scintillometer-Based Turbulent Fluxes of Sensible and Latent heat over a Heterogeneous Land Surface – A Contribution to LITFASS-2003. Boundary-Layer Meteorology 121, 89-110.

Monteiro, A., Moreira, I., Sousa, E., 1999. Effect of Prior Common Read (*Phragmites australis*) Cutting on Herbicide Efficacy. Hydrobiologia 415, 305-308.

Moore, C.J., Fisch, G., 1986. Estimating the heat storage in Amazonian tropical forest. Agriculture Forest Meteorology 38, 147-168.

Moro, M. J., Domingo, F., Lopez G., 2004. Seasonal transpiration pattern of *Phragmites australis* in a wetland of semi-arid Spain. Hydrological Processes 18, 213-227.

NCDC, 2009. National Climatic Data Center: Available from: <http://www.ncdc.noaa.gov>, accessed in September 2009.

Peacock, C.E., Hess, T.M., 2004. Estimating evapotranspiration from a reed bed using the Bowen ratio energy balance method. Hydrological Processes 18, 247-260.

Pelleschi, S., Rocher J.-P., Prioul, J.-L., 1997. Effect of water restriction on carbohydrate metabolism photosynthesis in mature maize leaves. Plant, Cell and Environment 20, 493-503.

Randow, C.V., Kruijt, B., De Oliveira, M.B.L., 2008. Exploring eddy-covariance and large-aperture scintillometer measurements in an Amazonian rain forest. Agricultural and Forest Meteorology 148, 680-690.

Rosenberry, D.O., Stannard D.I., Winter, T.C., Martinez, M.L., 2004. Comparison of 13 Equations for Determining Evapotranspiration from a Prairie Wetland, Cottonwood Lake Area, North Dakota, USA. Wetlands 24(3), 483-497.

Saleh, A., Wu, H., Brown, C.S., Teagarden, F.M., McWilliams, S., M., Hauck, L.M., Millican, J.S., 2008. Effect of brush on evapotranspiration in the North Concho river watershed using eddy covariance technique. Journal of Soil and Water Conservation 64(5), 336-349.

Sánchez-C., S., Angeler, D.G., Sánchez-A, R., Alvarez-C., M., Garatuza-P., J., 2004. Evapotranspiration in semi-arid wetlands: relationships between inundation and

the macrophyte-cover:open-water ratio. Advances in Water Resources 27, 643-655.

Sene, K.J., Gash, J.H.C. and McNeil, D.D., 1991. Evaporation from a tropical lake: comparison of theory with direct measurements. Journal of Hydrology, 127, 193-217.

Sene, K.J., Gash, J.H.C. and McNeil, D.D., 1991. Evaporation from a tropical lake: comparison of theory with direct measurements. Journal of Hydrology 127, 193-217.

Smart, R.E., Bingham, G.E., 1974. Rapid Estimates of Relative Water Content. Plant Physiology 53, 258-260.

Smid, P., 1975. Evaporation from a Reedswamp. Journal of Ecology 31(1), 299-309.

Song, J., 1999. Phenological influences on the albedo of prairie grassland and crop fields. International Journal of Biometeorology 42, 153-157.

State of Kansas v. State of Nebraska and State of Colorado. No. 126. Supreme Ct. of the US. 28 January 2000.

Stewward, R.B., Rouse, W.R., 1976. A Simple Method for Determing the Evaporation From Shallow Lakes and Ponds. Water Resources Research 12(4), 623-628.

Szilagyi, J., 1999. Streamflow depletion investigations in the Republican River Basin: Colorado, Nebraska, and Kansas. Journal of Environmental Systems 27(3), 251-263.

Szilagyi, J., 2001. Identifying cause of declining flows in the Republican River. Journal of Water Resources Planning and Management July/August, 244-253.

Thom, A.S., 1976. Momentum, mass and heat exchange of plant communities. Vegetation and the Atmosphere Vol.1, Academic Press, New York, 57-109.

Twine, T.E., Kustas, W.P., Norman, J.M., Cook, D.R., Houser, P.R., Meyers, T.P., Prueger, J.H., Starks, P.J., Wesely, M.L., 2000. Correcting eddy-covariance flux underestimates over a grassland. Agricultural and Forest Meteorology 103, 279-300.

USGS. US Geological Services: USGS Global Visualization Viewer: Available from <http://glovis.usgs.gov/>

Utset, A., Imma, F., Martinez-Cob, A., Cavero, J., 2004. Comparing Penman-Monteith and Priestley-Taylor approaches as reference-evapotranspiration inputs for modeling maize water-use uner Mediterranean conditions. Agricultural Water Management 66, 205-219.

Virginia Department of Conservation and Recreation, 2007. Marsh Invader! How to identify and combat one of Virginia's most invasive plants: *Phragmites*.

Walters, S., 2010. Carbon Dynamics in a Phragmites Australis Invaded Riparian Wetland. Master's Thesis, University of Nebraska, Lincoln. 52 p.

Wang, T., Ochs G.R., Clifford S.F., 1978. Journal of Optical Society of America 68(3), 334-338.

Wen, F., Chen, X., 2006. Evaluation of the impact of groundwater irrigation on streamflow in Nebraska. Journal of Hydrology 327, 603-617.

Wesely, M.L., 1976. The Combined Effect of Temperature and Humidity Fluctuations on Refractive Index. Journal of Applied Meteorology 15, 43-49.

Wilcox, D.A., Whillans, T.H., 1999. Techniques for Restoration of Disturbed Coastal Wetlands of the Great Lakes. Wetlands 19(4), 835-857.

Wilson, K., Goldstein, A., Falge, E., Aubinet, M., Baldocchi, D., Berbigier, P., Bernhofer, C., Ceulemans, R., Dolman, H., Field, C., Grelle, A., Ibrom, A., Law, B.E., Kowalski, A., Meyers, T., Moncrieff, J., Monson, R., Oechel, W., Tenhunen, J., Valentini, R., Verma, S., 2002. Energy balance closure at FLUXNET sites. Agricultural and Forest Meteorology 113, 223-243.

Wyngaard, J.C., Izumi, Y., 1971. Behavior of the Refractive-Index-Structure Parameter near the Ground. Journal of the Optical Society of America 61(12), 1646-1650.

Zhou, L., Zhou, G., 2009. Measurement and modeling of evapotranspiration over a reed (*Phragmites australis*) marsh in Northeast China. Journal of Hydrology 372, 41-47.